GRAVITY MEASUREMENTS IN THE AREA OF MOUNT HOOD, OREGON

By

RICHARD COUCH
MICHAEL GEMPERLE

Geophysics Group

School of Oceanography

Oregon State University

May 1979

Final report of work carried out under OSU Grant No. 30-262-9117 from the Oregon Department of Geology and Mineral Industries; July 1977 through March 1979.

GTR 790517

TABLE OF CONTENTS

LIST OF FIGURES

LIST OF FIGURES (Con't.) Page

LIST OF TABLES

ABSTRACT

The analysis of gravity measurements at 337 stations on and about Mount Hood indicate lateral and vertical variations in the density of the flows and pyroclastics in and beneath Mount Hood. Complete Bouguer gravity anomalies indicate that the axis of Mount Hood is located on an elongate gravity high, oriented approximately N75E. Mount Hood is superimposed on a gravity low that extends from north of the mountain to the southern extent of the survey area. The gravity low suggests a north-south oriented graben-like structure. Prominent lineations in the gravity anomalies oriented approximately N23W occur both northwest and southwest of Mount Hood. A simple cone-on-a-cylinder model for the core of Mount Hood agrees with the gravity anomalies. Long wavelength anomalies suggest that undulations in the Columbia River Basalts beneath and about Mount Hood range from less than 500 m to over 1400 m above sea level. Porosities of the average rocks which comprise Mount Hood are estimated to be approximately 20 to 30 percent and the density is approximately 2.27 gm/cm^3.

GRAVITY ANOMALIES IN THE AREA OF MT. HOOD, OREGON

Gravity Measurements

Personnel of the Geophysics Group, Oregon State University (OSU) conducted a gravity survey in the High Cascade Mountains of northern Oregon during August and September, 1977 and August and September, 1978. The survey area which extends from 45°10' to 45°35'N lat. and from 121°25' to 122°00'W long. includes the picturesque 3424 m (11235 ft) high Mt. Hood stratovolcano and many surrounding foothills and mountains of the Cascade Range.

Figure 1 shows a topographic map of the area of and about Mt. Hood based on data contained on the U. S. Geological Survey (USGS) 1:250,000 quadrangle map, The Dalles NL 10-9. The map, contoured at an interval of 1000 ft (304.8 m), shows approximately 10,000 ft (3050 m) of topographic relief in the area of Mt. Hood. Mt. Hood, a relatively symmetric volcanic cone of Late Pleistocene to Holocene age, is surrounded by a north-south trending ridge over 6000 ft (1830 m) in elevation on the east and southeast side and isolated mountains and dissected ridges on the south, west, and northwest sides. Mt. Hood is composed almost entirely of pyroxene andesite and rises 8000 ft (2400 m) above a platform of Pliocene andesites and basalts (Wise, 1969). The high relief and few roads make access to the area difficult; consequently to achieve an approximately uniform grid of gravity stations most measurements were made by back-packing the meter to the station sites.

Mr. Kenneth Keeling, with the assistance of Messeurs.

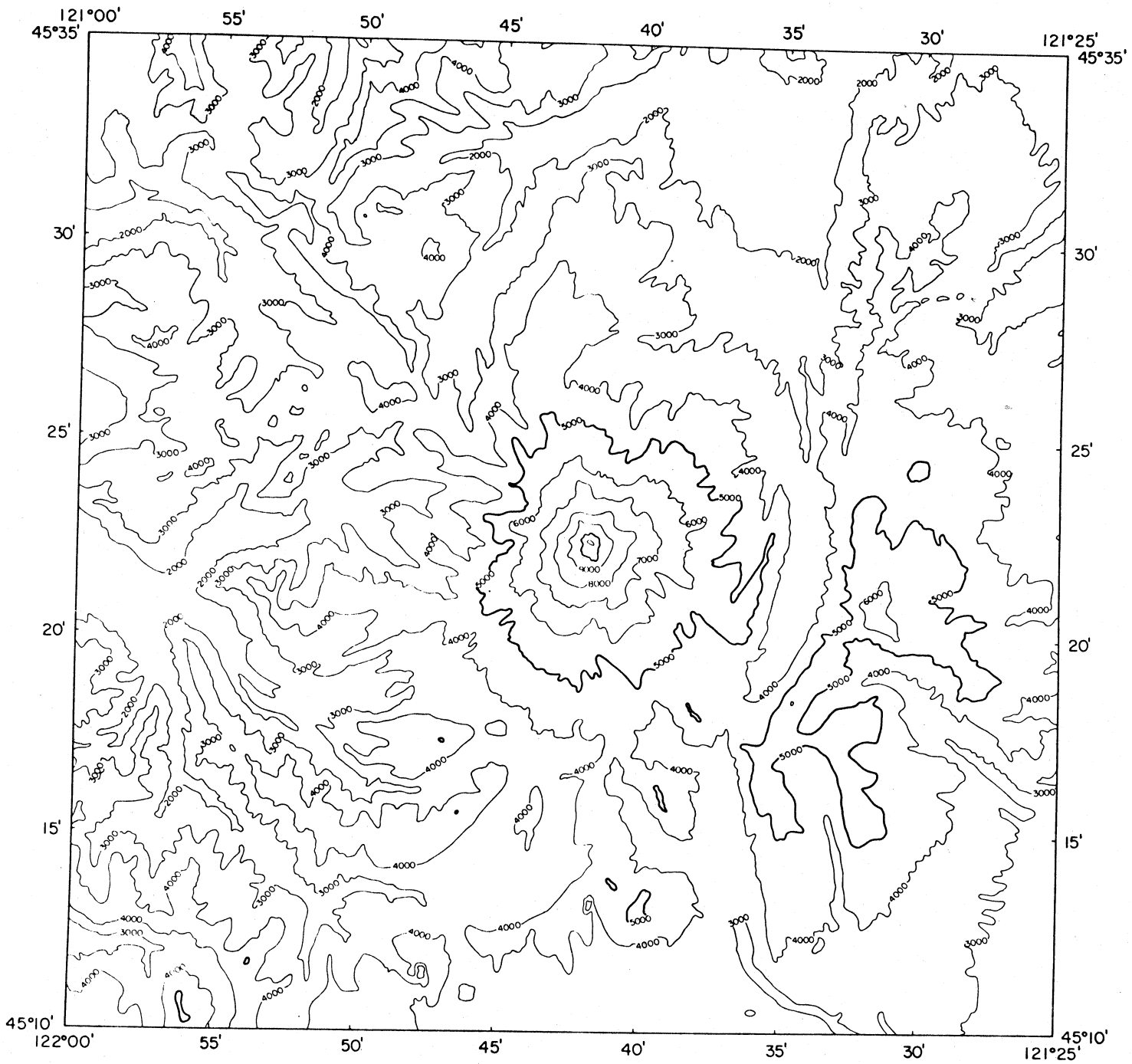

TOPOGRAPHIC MAP
MOUNT HOOD AREA, OREGON

DATA FROM USGS 1 250,000 QUADRANGLE MAP
THE DALLES NL 10-9

KILOMETERS
0 2 4 6 8
0 1 2 3 4 5
MILES

UNIVERSAL TRANSVERSE MERCATOR PROJECTION
CONTOUR INTERVAL 1000 FEET

OREGON STATE UNIVERSITY
DECEMBER, 1977

Figure 1

Terry Jones, William Plank, and Mark Brown obtained gravity measurements at 239 stations in the approximately 2000 km^2 area. Messeurs. Gordon Ness and John Bowers established 51 closely spaced gravity stations in the vicinity of the geothermal test hole south southeast of Timberline Lodge (3S/9E-7ca) on the south slope of Mt. Hood and added an additional 33 stations to the area survey. These stations, combined with station data from the Oregon State University Library (Thiruvathukal, 1968), total 337 and yield an approximate spatial density of one station per 6 km^2.

Figure 2 shows the locations of the 337 gravity stations in the Mt. Hood survey area. In addition to the approximately uniform scatter of stations in the area, a high concentration of stations which form a plus sign near the middle of the map, occur along lines which extend north, south, east and west from a point near the site of the geothermal test hole. Gravity stations are concentrated also toward the south and west along Highway U. S. 26 on the south flank of Mt. Hood. A solitary gravity station is located on the summit of Mt. Hood.

Base stations for the measurements were established at Zigzag Ranger Station, Government Camp, White Bridge Park, Parkdale, and near Cooper Spur. The Zigzag Ranger Station gravity base station (980,489.14 mgl) was tied to the USAF gravity base station WA-142A (Woollard and Rose, 1963) located at Portland International Airport (980,648.3 mgl) by personnel of the USGS (personnel comm. D. G. Barnes, 1969) and by the personnel of the OSU Geophysics Group (unpublished data, OSU Gravity Library, 1975). The detailed survey near Timberline

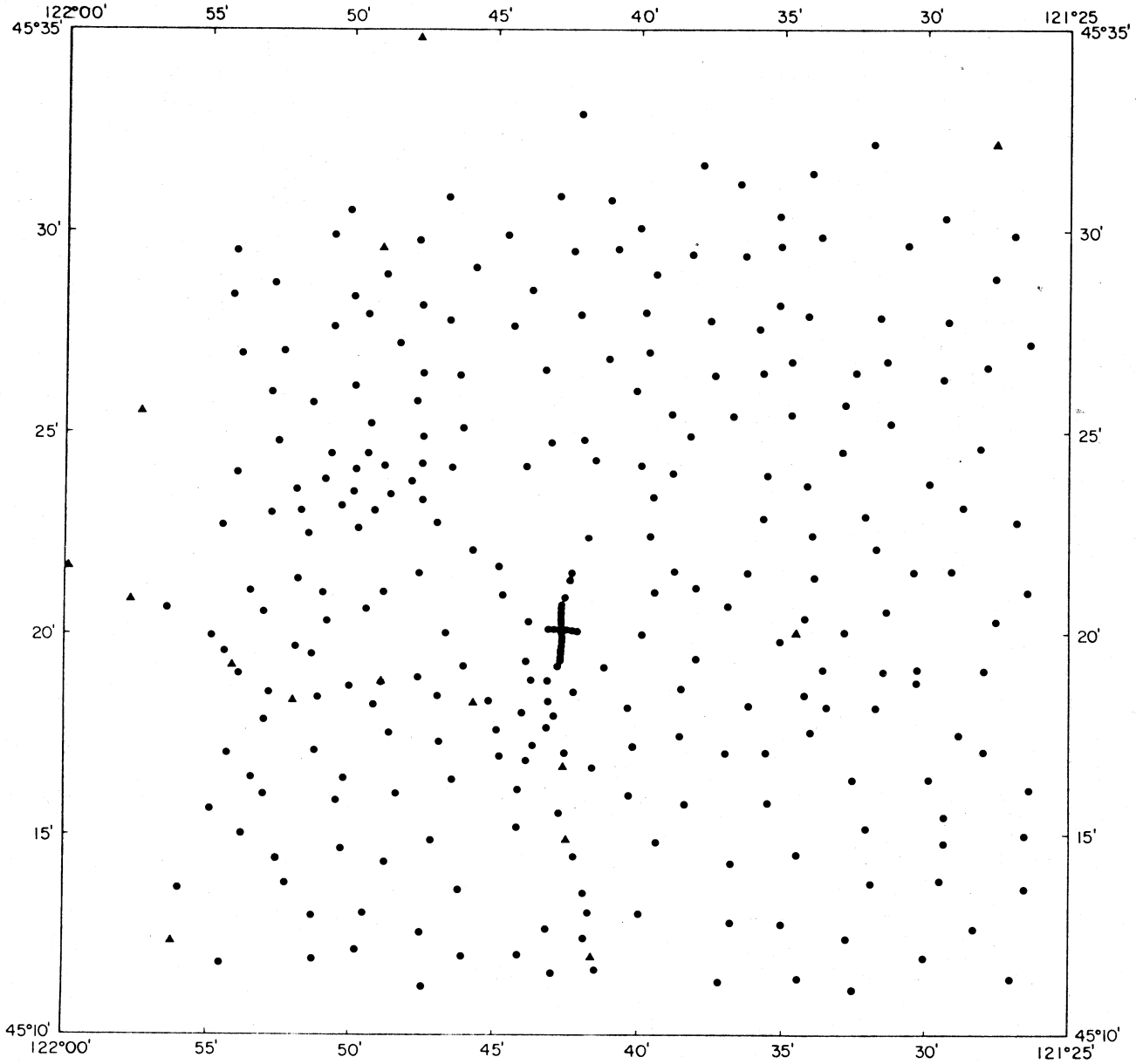

GRAVITY STATIONS
MOUNT HOOD AREA, OREGON

GRAVITY STATIONS
▲ J. THIRUVATHUKAL 1969 OSU
● K. KEELING 1977 OSU
G. NESS & J. BOWERS 1978 OSU

KILOMETERS
0 2 4 6 8
0 1 2 3 4 5
MILES

UNIVERSAL TRANSVERSE MERCATOR PROJECTION

OREGON STATE UNIVERSITY
DECEMBER, 1978

Figure 2

Lodge is referenced to the gravity base station at Zigzag Ranger Station. The measurements were made with a LaCoste and Romberg Model G Geodetic Gravity Meter #126.

USGS benchmarks, spot elevations on USGS 7.5 minute and 15 minute topographic maps and barometric altimetry provided vertical control for the gravity stations. The estimated uncertainties in the vertical control associated with these methods of elevation determination are $\pm$ 1, $\pm$ 5, and $\pm$ 10 feet respectively. A recording barometer base station, used to monitor barometric changes during the survey, provided data to ascertain the validity and accuracy of altitudes determined by barometric altimetry.

USGS 7.5 minute and 15 minute topographic maps were used to determine horizontal position. The estimated uncertainty in horizontal position is $\pm$ 0.02 minutes of latitude and longitude. MSS Inc., Corvallis, established reference points for the gravity stations near the geothermal drill site. The positions and elevations of the detailed gravity survey, determined by triangulation and leveling techniques, were established with reference to a USGS benchmark at Timberline Lodge. The estimated uncertainty is less than $\pm$ 0.3 meters in the horizontal position of each station and less than $\pm$ 0.3 meters in the vertical elevation of each station with respect to the USGS benchmark.

The observed gravity was corrected for earth tides using the formulation of Longman (1959) and for meter drift by linear interpolation between values observed at reoccupied base stations. The mean drift of the gravity meter observed during

reoccupation of base stations at the end of a gravity traverse or loop was $\pm$ 0.04 mgl and the standard deviation was 0.09 mgl. The maximum observed drift was 0.47 mgl. The uncertainties in the measurements caused by the drift of the meter is generally much less than caused by the uncertainties in the corresponding station elevations.

Reduction of the Gravity Measurements

The gravity measurements were reduced to free-air and complete Bouguer gravity anomalies with standard techniques. The following equation from Scheibie and Howard (1964) and Oliver (1973), used in this study, yields the free-air gravity anomaly:

$$FAA = OG - THG + (0.09411549 - 0.000137789 \sin^2\theta)h - 0.67 \times 10^{-8} h^2$$

where,

FAA = Free-air anomaly in milligals

OG = Observed gravity in milligals

THG = Theoretical gravity in milligals

θ = Latitude

h = Elevation in feet

The International Gravity Formula (IGF), yields theoretical gravity (THG) values at designated latitudes. The IGF of 1930 (Swick, 1942), used in this study, is:

$$THG = 978049.0 \ (1 + .0052884 \sin^2 \phi - 0.0000059 \sin^2 2\phi)$$

The following equation yields the complete Bouguer gravity anomaly (CBA).

$$CBA = FAA - 2\pi Gph + TCC - CC$$

where,

CBA = Complete Bouguer gravity anomaly in milligals

FAA = Free-air gravity anomaly in milligals

and G = Universal gravitational constant (6.67×10^{-8}cgs)

p = Reduction density in gm/cm^3

h = Elevation in feet

TTC = Total terrain correction in milligals

CC = Curvature correction = $hp\,(1.671 \times 10^{-8} + h[-1.229 \times 10^{-8} + h(4.76 \times 10^{-16})]$ milligals (Oliver, 1973)

Terrain corrections for each station account for the change in gravity caused by topography about the station. Total terrain corrections, (TTC) for each station were computed for topography within a distance of 166.7 km of the station. This distance is equivalent to Hayford-Bowie zone "0" (Swick, 1942). A computer program written by D. L. Plouff (1977a) of the USGS which uses digital terrain data was used to compute terrain corrections. The program also incorporated a modification of the program developed by Plouff (1977b) which permitted the calculation of the terrain correction for the distance interval zero to 0.895 km, Hammer's zone F (Hammer, 1939). The digital terrain data was based on the National Cartographic and Information Center 0.01 inch digitization of 1:250,000 scale topographic maps. These data provide the average elevation in 0.5, 1.0 and 3.0 minute square areas. The gravitational effects of the topography were calculated for radial distances from zero to 2.29 km using topography digitzied at 0.5 minute increments, from 2.29 km to 15 km using 1.0 minute data, and 15 km

to 166.7 km using 3 minute data. The terrain effect calculated for the area between 0 and 2.29 km of the station exceeded 5.0 mgls for 40 stations. Subsequently these stations were recalculated by hand, utilizing a method outlined by Oliver and others (1969).

Table 1 (Appendix) lists the principal facts for each gravity station in the Mount Hood study area. The table heading explains the column designations. The table does not list the parameters or values of special reductions or analyses described in this report, however, these can be calculated from the principal facts and the relations described in the appropriate text of this report.

Free-Air Gravity Anomalies

Figure 3 shows a free-air gravity anomaly map of the Mount Hood area based on measurements at the station locations shown in Figure 2. The map contours are at intervals of 10 mgl and heavy contours occur at 0, 50, 100 and 150 mgl levels. The free-air anomalies reflect the very irregular topography of the area and the 0 mgl contour of the gravity map coincides approximately with the 3000 foot topographic contour in Figure 1. The summit of Mount Hood, approximately in the center of the map, exhibits a free-air anomaly of greater than +150 mgls. Elongate gravity anomaly lows near 45°30'N lat and 121°35' and 121°45'W long are oriented approximately north-south. The easternmost gravity anomaly low extends southward past Mount Hood at least to the southern limit of the survey area. The westernmost gravity low extends to just west of Mount Hood where it appears

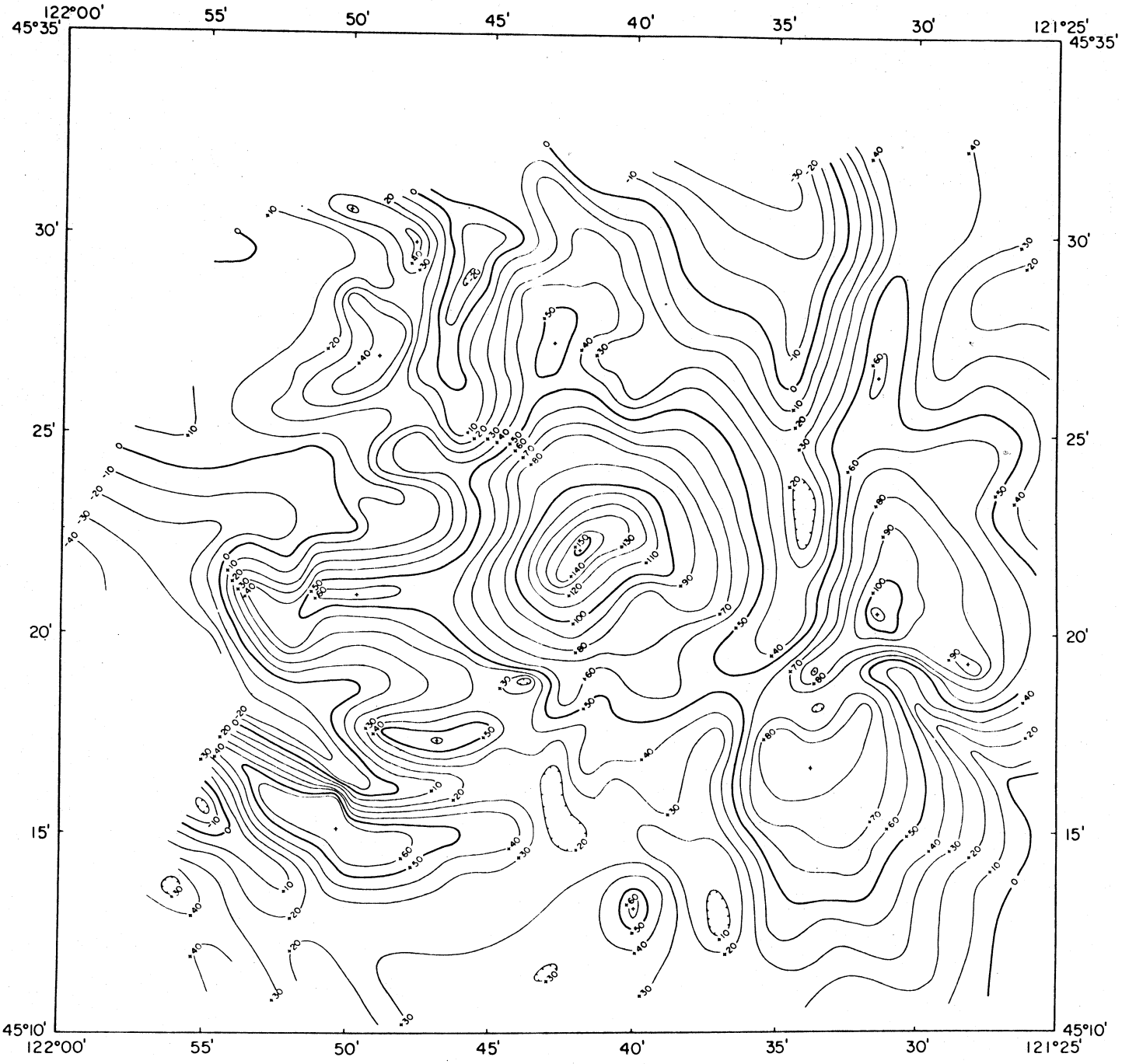

FREE-AIR GRAVITY MAP
MOUNT HOOD AREA, OREGON

AREA OF THIS MAP

GRAVITY DATA FROM
J THIRUVATHUKAL 1969 OSU
K KEELING 1977 OSU

KILOMETERS
0 2 4 6 8
0 1 2 3 4 5
MILES

OREGON STATE UNIVERSITY
DECEMBER, 1977

UNIVERSAL TRANSVERSE MERCATOR PROJECTION
CONTOUR INTERVAL 10 MGALS
ESTIMATED STATION UNCERTAINTY ±2 MGAL

Figure 3

to be interrupted by a series of gravity highs oriented approximately east-west. The two north-south trending lows suggest a major structural offset in the basement rocks beneath the post-Miocene rocks which form Mount Hood. The relatively short wavelength, positive anomalies associated with Mount Hood and the surrounding mountains suggest the mountains are not locally compensated to any significant extent and consequently are interpreted as localized loads imposed on a relatively rigid crust or lithosphere.

Bouguer Gravity Anomalies

Figure 4 shows a complete Bouguer gravity anomaly map of the Mount Hood area. The map, prepared using a standard reduction density of 2.67 gm/cm^3, exhibits contours at intervals of 2 mgls and heavy contours at 10 mgl intervals. A marked gravity low of less than -108 mgls occurs on Mount Hood. This gravity low is the most negative part of a larger gravity low which extends north of Mount Hood to about 45°30' and extends south of Mount Hood at least to the limit of the survey area. The negative anomaly, closed north of Mount Hood, is open to the south and suggests a large geologic feature on which Mount Hood is superimposed that begins in the vicinity of Mount Hood and extends southward. The anomalies east of Mount Hood near 45°20-25'N lat and 121°30-34' W long show only a small correlation with topography; hence, the average density of the near-surface rocks which form the topographic features is near 2.67 gm/cm^3. The negative correlation between the topography and gravity anomaly of Mount Hood and the mountains west and south

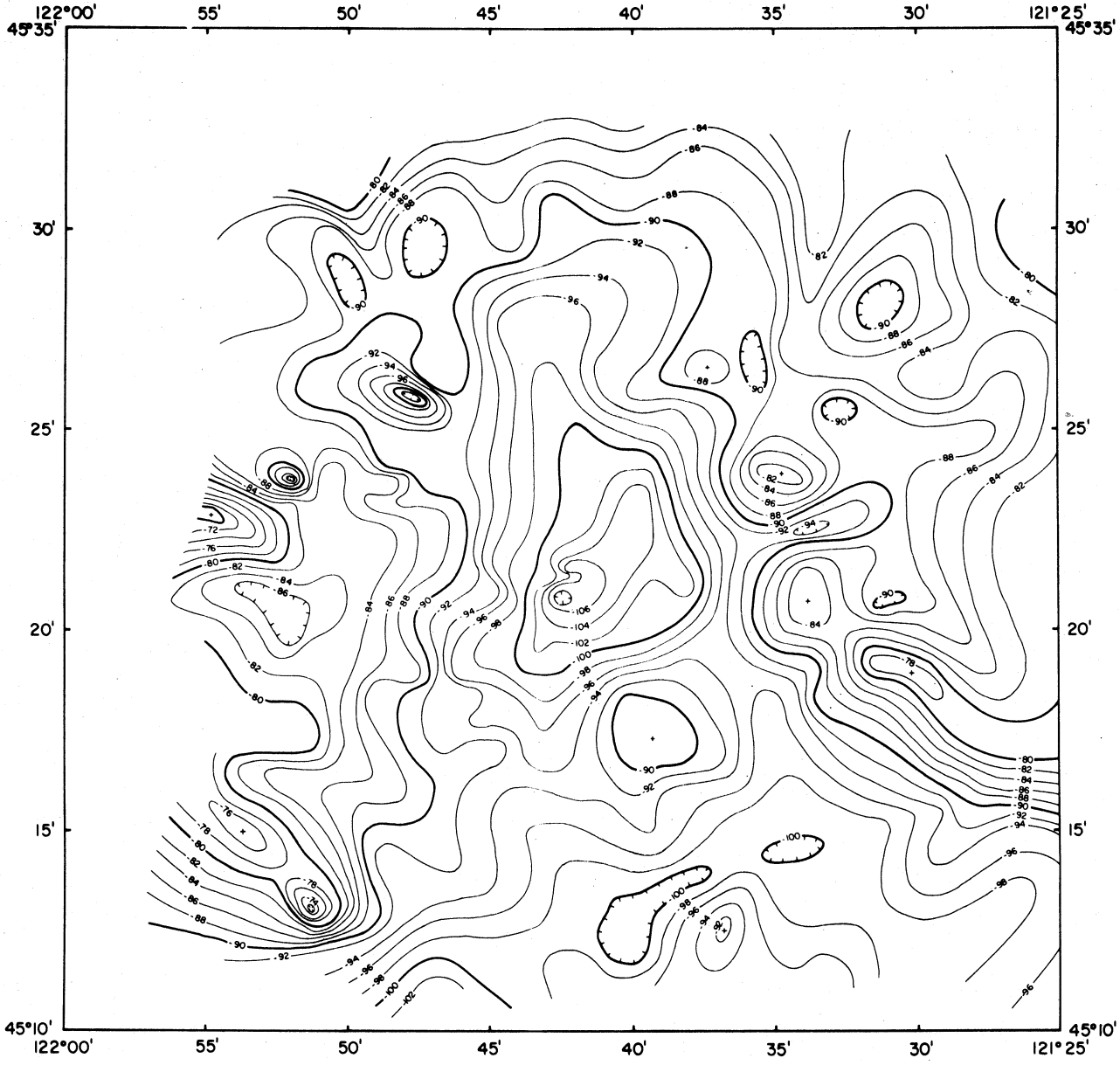

COMPLETE BOUGUER GRAVITY ANOMALY MAP

MOUNT HOOD AREA, OREGON

AREA OF THIS MAP

GRAVITY DATA FROM

J. THIRUVATHUKAL	1969	O.S.U.
K. KEELING	1977	O.S.U.
G. NESS & J. BOWERS	1978	O.S.U.

KILOMETERS

0 2 4 6 8

0 1 2 3 4 5

MILES

OREGON STATE UNIVERSITY

DECEMBER, 1978

UNIVERSAL TRANSVERSE MERCATOR PROJECTION

CONTOUR INTERVAL 2 MGALS

ESTIMATED STATION UNCERTAINTY ±2 MGAL

REDUCTION DENSITY 2.67 gm/cm³

Figure 4

of Mount Hood suggest the standard reduction density (2.67 gm/cm^3) is greater than the average density of the rocks which form the mountains.

Computation of the standard deviation of the complete Bouguer anomalies of a region yields an indication of the correlation of the anomalies and the topography of the region. Figure 5 shows a graph of the standard deviation of the complete Bouguer gravity anomaly as a function of density for the Mount Hood area. The curve shows a minimum when the density equals 2.27 gm/cm^3. To determine a regional density for Mount Hood the gravity station data were separated into a set which included all the stations and a subset which included only the stations located on Mount Hood proper. Both sets of data indicate approximately the same density, 2.27 gm/cm^3, when the standard deviation of the computed anomalies is a minimum. Although the density of 2.27 gm/cm^3 yields anomalies with a minimum correlation with the topography of the area, the curve in Figure 5 is relatively flat near the minimum and suggests the actual densities of the topographic features have a broad range. For example, the Bouguer gravity anomalies in Figure 4 suggest the average density of the mountains immediately east of Mount Hood is greater than 2.27 gm/cm^3 and may be as high as 2.7 gm/cm^3.

Figure 6 shows a complete Bouguer anomaly map of the Mount Hood area based on a reduction density of 2.27 gm/cm^3. The Bouguer anomaly associated with Mount Hood is less than -64 mgls; however, it is actually an anomaly high with respect to the surrounding anomalies. The anomaly high associated with

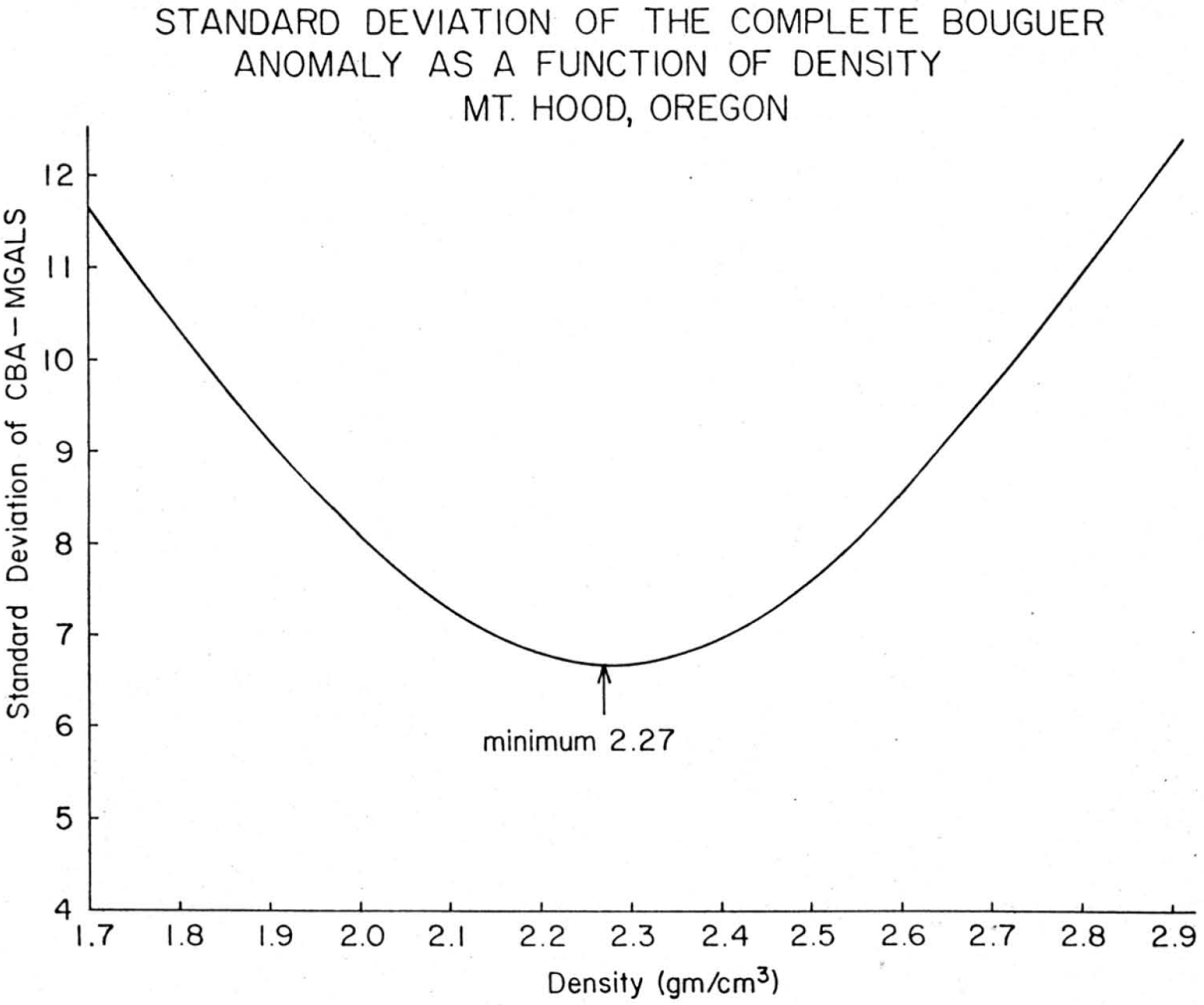
STANDARD DEVIATION OF THE COMPLETE BOUGUER ANOMALY AS A FUNCTION OF DENSITY
MT. HOOD, OREGON
Standard Deviation of CBA – MGALS
12
11
10
9
8
7
6
5
4
minimum 2.27
1.7
1.8
1.9
2.0
2.1
2.2
2.3
2.4
2.5
2.6
2.7
2.8
2.9
Density (gm/cm3)

Figure 5

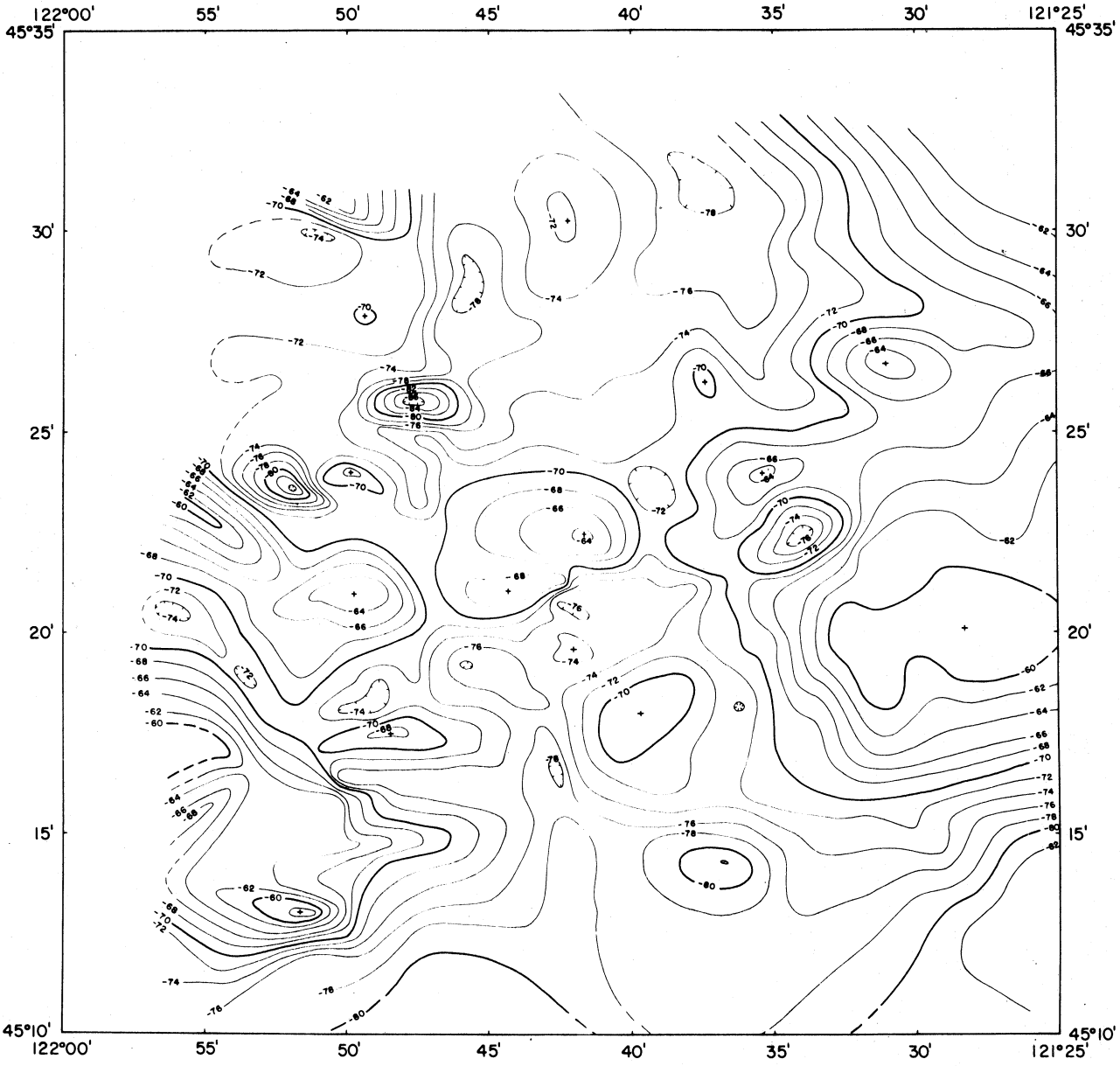

COMPLETE BOUGUER GRAVITY ANOMALY MAP
MOUNT HOOD AREA, OREGON

AREA OF THIS MAP

GRAVITY DATA FROM
J. THIRUVATHUKAL 1969 O.S.U.
K. KEELING 1977 O.S.U.
G. NESS & J. BOWERS 1978 O.S.U.

KILOMETERS
0 2 4 6 8
0 1 2 3 4 5
MILES

OREGON STATE UNIVERSITY
DECEMBER, 1978

UNIVERSAL TRANSVERSE MERCATOR PROJECTION
CONTOUR INTERVAL 2 MGALS
ESTIMATED STATION UNCERTAINTY ±2 MGAL
REDUCTION DENSITY 2.27 gm/cm³

Figure 6

Mount Hood is flanked on the northeast and southwest by Bouguer anomaly highs. Together, these contiguous highs suggest a structural high, oriented approximately N75E, beneath the Plio-Pleistocene rocks which form Mount Hood and the surrounding mountains. The gravity high transects at an angle what appears to be an extensive north-south oriented gravity low. The east side of the gravity low exhibits higher gradients and is generally better delineated than the west side. The low suggests a graben-like structure with the east farther down and/or bounded by more prominent faults than the west side.

This interpretation of the gravity anomalies suggests Mount Hood sets in and covers to some extent a north-south oriented graben. The gravity high near the center of Mount Hood suggests its location may be structurally controlled in that the central vent lies along a structural ridge indicated by the contiguous gravity highs which cross the north-south gravity low. An alternative explanation of the gravity high associated with Mount Hood is that it reflects the internal structure of the mountain and may indicate the main vent or core of the mountain. Because of the sparcity of stations, gravity anomalies are not well delineated near the summit.

South of Mount Hood, near 45°15'N lat., gravity gradients suggest a structural lineation oriented approximately N85 E. The senior author has speculated, on the basis of the alignment of earthquake epicenters and SLAR imagery, that a fault - possibly a thrust fault - may extend along the base of Mount Hood on the south side. The gravity anomalies are consistent

with this hypothesis but do not strongly support it.

Prominent lineations in the gravity anomalies oriented approximately N23°W occur both northeast and southwest of Mount Hood. Two lineations northeast and two southeast of Mount Hood appear to extend completely across the area mapped in the gravity survey and may be complementary to the east northeast-south southwest lineations described above.

Many closed short-wavelength anomalies occur also in the area and are very likely associated with surface or very near surface structural and/or compositional features.

Closely spaced gravity stations occur along lines which extend north, south, east and west from gravity station GS 33 which is located 70 feet west of the geothermal drill hole south of Timberline Lodge. To obtain accurate gravity measurements differential leveling was used to determine the station elevations. The initial elevation, 5936', was stamped in the USDA, Bureau of Public Roads BM 50-1, located in the front steps of Timberline Lodge. A stadia survey connected all gravity stations to an X-Y coordinate system. The initial azimuth, 190°, was scaled from the Pucci chairlift as shown on 7.5 minute USGS Topographic Map, Mount Hood. Poor weather prevented additional ties. Longitudes and Latitudes of the stations were computed based on:

a) The initial station MHL 8 latitude (45° 19.87') and longitude (121° 42.61')

b) The scale 1" of latitude = 101.27 feet at 45°20' N lat. as per Oregon Plane Coordinate Projection Tables SP 270

c) And a scale ratio at 45°20' of 1" long/1" lat = 0.708 and 1" long = 71.699 feet.

Table 1 in the back of this report lists the latitude, longitude and gravity anomaly values for the gravity survey near the Timberline drill site.

Figure 7a shows a complete Bouguer gravity anomaly, based on a reduction density of 2.67 gm/cm^3, around the Timberline geothermal drill site at approximately 45°19.7'N lat, 121°42.6'W long. The map indicates a general east-west trend to the anomaly contours and decreasing anomalies towards the north away from the drill site. The gravity anomalies contoured at an interval of 2 mgls suggest a relatively uniform structure in the vicinity of the drill site and rock layers of a relatively low density.

Figure 7b shows a complete Bouguer anomaly of the same area as Figure 7a but based on a reduction density of 2.27 gm/cm^3. This density as discussed previously, is more representative of the average density of the rocks of Mount Hood. Figure 7b indicates that the drill site is located on a relative gravity high. The Bouguer anomaly high is of low amplitude and closed. The anomaly suggests a thickening of the more dense layers which form this sector of Mount Hood, an intrusive body, or a doming of the layers. A density contrast of 0.6 gm/cm^3 between massive andesite (2.6 gm/cm^3) and andesitic ash containing water (2.0 gm/cm^3) suggests a flow or intrusive thickness of approximately 80 m. A relatively steep gradient in the gravity anomalies which trends approximately east northeast-west southwest occurs north of the drill site near 45°21'N

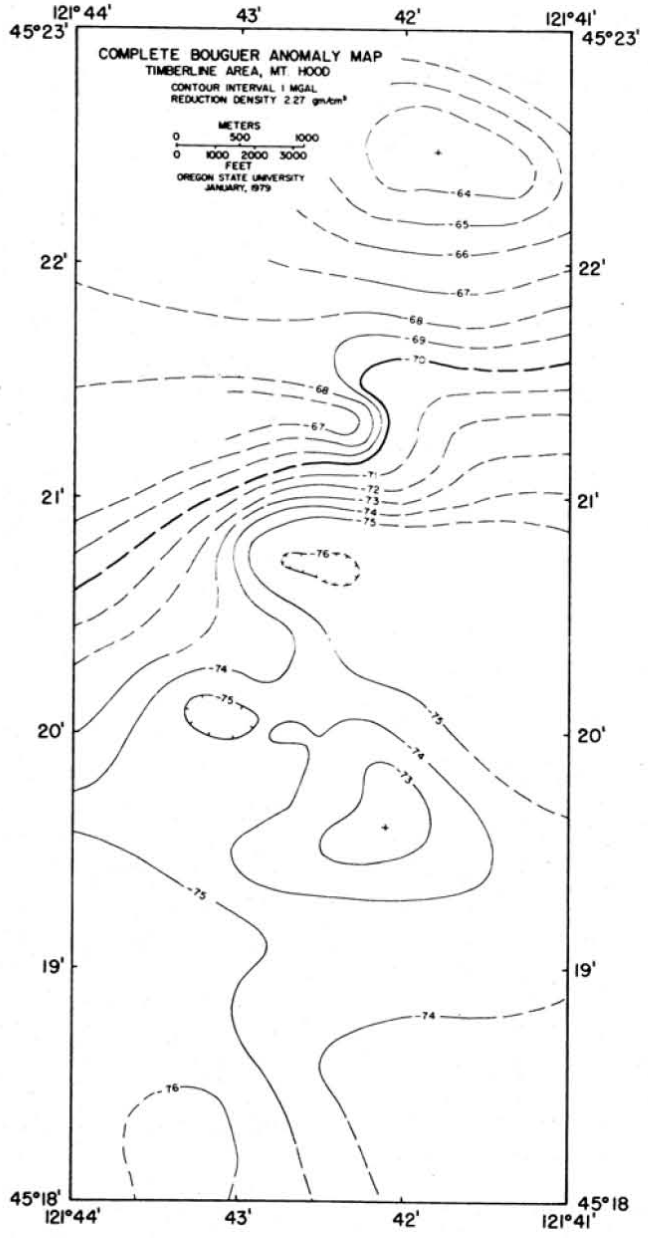

Figure 7b

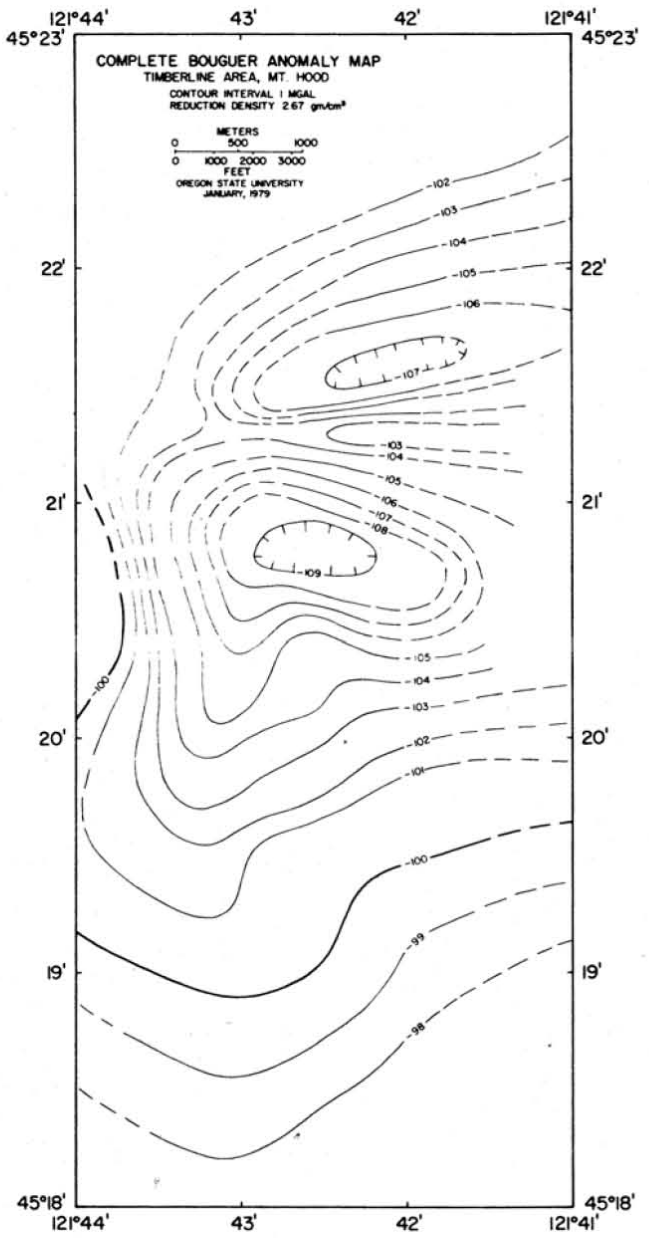

Figure 7a

lat. The anomaly is positive to the north and suggests that either a higher density layer (or flow) extends southward beneath the surface ash and cinder to approximately 45°21' or that a structural break (or fault) occurs in the subsurface layers with the southside down about one mile north of the drill site. Other interpretations are also possible, however, the gravity measurements do not indicate any marked lateral variations in structure or density in the immediate vicinity of the drill site.

Regional Gravity Anomalies

Spectral separation of the short and long wavelength components of the complete Bouguer anomalies of the Mount Hood area yields "regional gravity anomalies" and "residual gravity anomalies". Estimates of the frequency at which the spectral separation should occur were based initially on the wavelengths of the topography of the region. The authors postulated that, because of a relatively high density contrast, the long wavelength gravity anomalies more likely would be associated with the pre-Pliocene rocks of the region such as the Columbia River Basalts and the short wavelength anomalies would reflect shallow sources caused by lateral and vertical variations in the Pliocene and Holocene rock and ash which form Mount Hood and the surrounding mountains of the High Cascades. The initial spatial frequency separating the long and short wavelength parts of the gravity anomaly spectrum was 5 cycles per 65 kilometers or 13 km per cycle. Later iterations based on attempts to determine a "surface" for the Columbia River Basalts from the gravity

measurements as described below indicated a better separation of the anomaly wavelengths occurred at 8 cycles per 65 km or 8.1 km/cycle. Subsequently regional and residual anomalies separated spectrally at 8.1 km/cycle, were recomputed from the complete Bouguer anomalies shown in Figure 6.

Figure 8 shows a map of the regional gravity anomaly of the Mount Hood area with wavelengths longer than 13 km. The map shows gravity highs which trend generally north-south on the east and west sides of the map. Between the gravity highs a north-south trending gravity low suggests a depression or graben-like structure in the upper crustal rocks beneath the post-Miocene rocks of the High Cascades. A gravity high oriented approximately east-west transects the large north-south gravity low. The center of Mount Hood is located approximately on the east-west gravity high and the mountain's "core" may contribute to the positive anomaly.

Figure 9 shows a map of the residual gravity anomalies of the Mount Hood area shorter than 13 km. The map shows a large number of closed gravity highs and lows. These anomalies suggest density variations in the post-Miocene rocks of the area and may relate to individual flows or intrusions. No attempt was made to correlate these anomalies with the surface or near-surface geology.

Figure 10 shows a map of the regional gravity anomaly of the Mount Hood area with wavelengths longer than 8.1 km. The map includes shorter wavelength components than the map shown in Figure 8 and therefore shows more irregularity or character in the anomaly contours and steeper anomaly gradients.

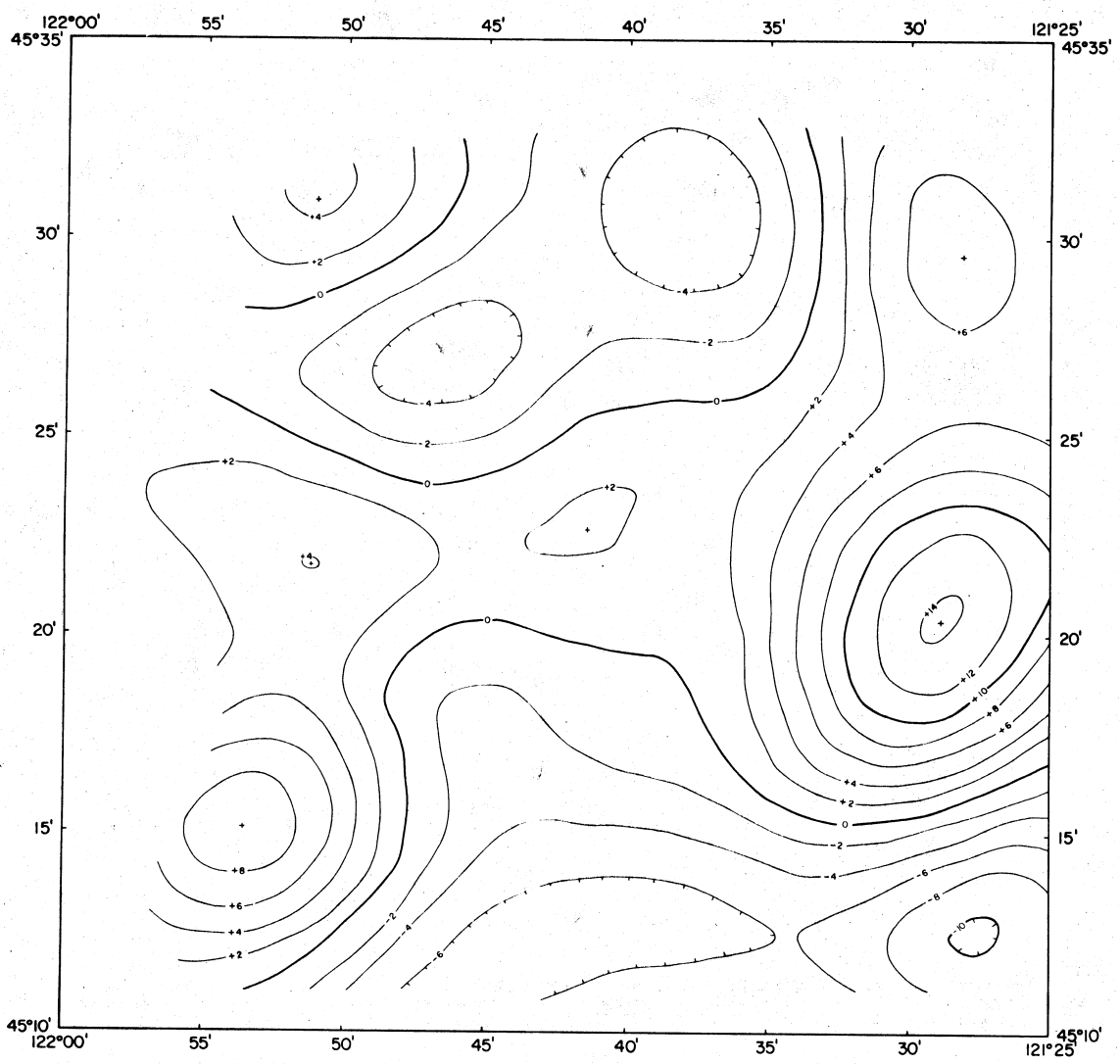

REGIONAL GRAVITY MAP
MOUNT HOOD AREA, OREGON

CONTOUR INTERVAL 2 MGALS

KILOMETERS
0 2 4 6 8
0 1 2 3 4 5
MILES

UNIVERSAL TRANSVERSE MERCATOR PROJECTION

OREGON STATE UNIVERSITY
DECEMBER, 1978

Figure 8

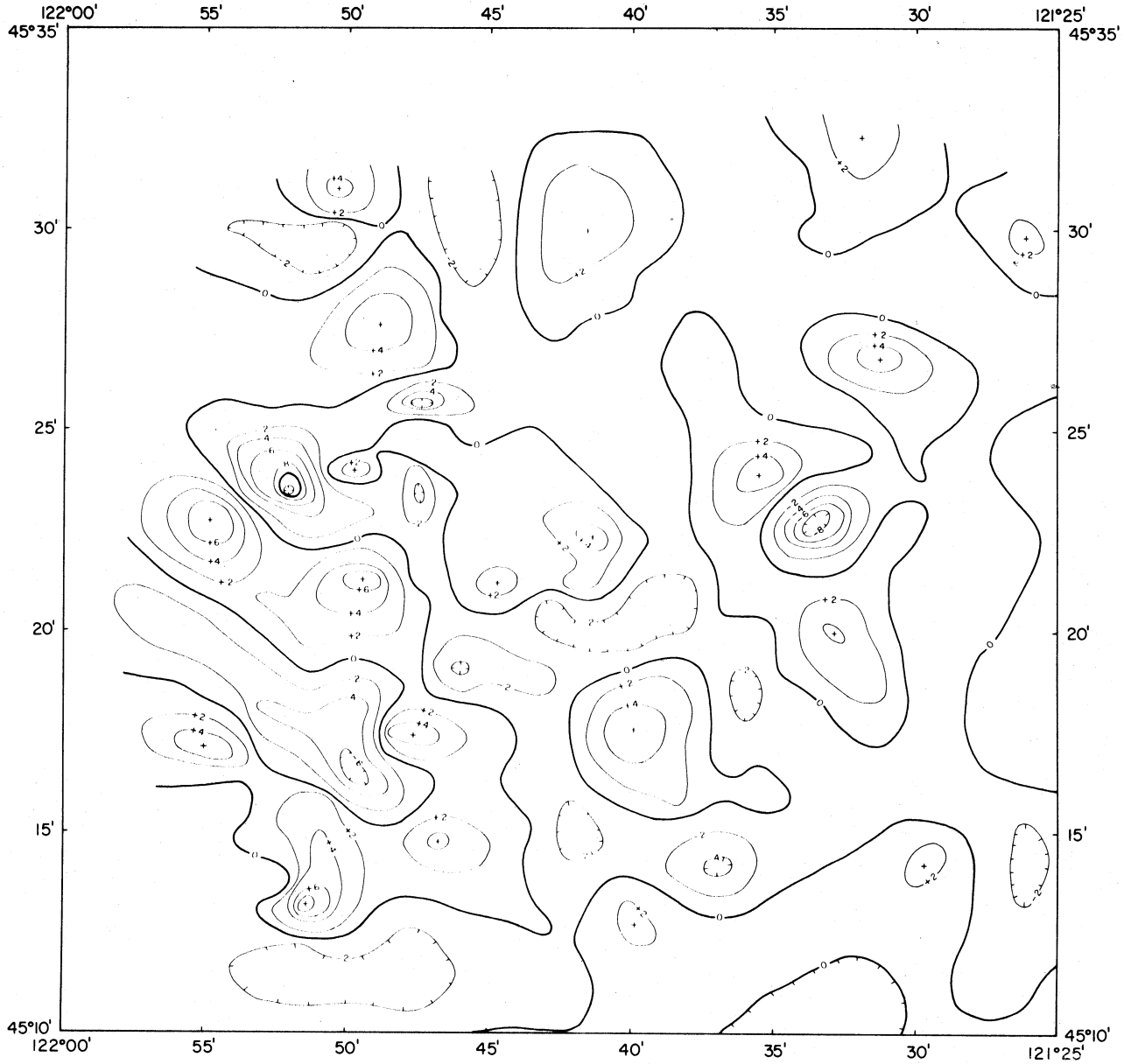

RESIDUAL GRAVITY MAP
MOUNT HOOD AREA, OREGON

AREA OF THIS MAP

CONTOUR INTERVAL 2 MGALS

KILOMETERS
0 2 4 6 8
0 1 2 3 4 5
MILES

UNIVERSAL TRANSVERSE MERCATOR PROJECTION

OREGON STATE UNIVERSITY
DECEMBER, 1978

Figure 9

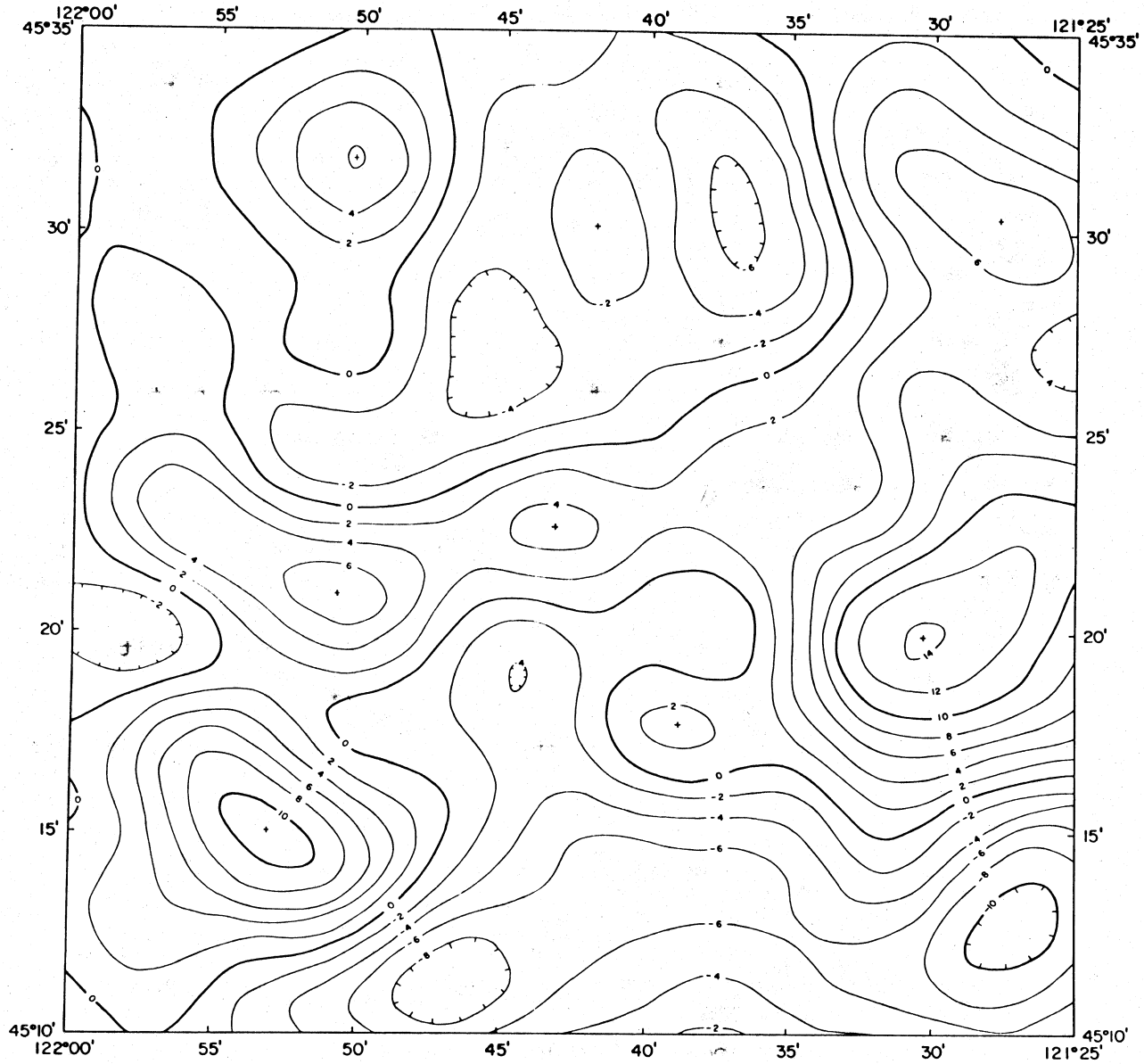

REGIONAL GRAVITY ANOMALY MAP
MOUNT HOOD AREA, OREGON

CONTOUR INTERVAL 2 MGALS

KILOMETERS
0 2 4 6 8
0 1 2 3 4 5
MILES

UNIVERSAL TRANSVERSE MERCATOR PROJECTION

OREGON STATE UNIVERSITY
FEBRUARY, 1979

Figure 10

Contiguous gravity highs, aligned north and south, occur east and northeast as well as west and southwest of Mount Hood. These highs together with a high northwest of Mount Hood flank a north-south oriented low. A relatively narrow high oriented approximately N75E, connects the highs on the western side with the highs on the eastern side and suggests a linear structure or an offset in structure beneath Mount Hood. A gravity low, south of Mount Hood, approximately parallels the N75E gravity high and intersects or truncates the north-south oriented highs east and west of Mount Hood. Hence two dominant anomaly lineations are evident; approximately north-south and approximately N75E. The north-south lineations suggest a graben-like structure in which Mount Hood is located and the east-northeast lineations that suggest folds and/or faults which cross the graben-like structure. The anomalies are relatively long wavelengths and are likely associated with the more dense pre-Pliocene rocks beneath Mount Hood and the surrounding mountains.

Figure 11 shows a map of the residual gravity anomalies of the Mount Hood area shorter than 8.1 km. The map shows a large number of closed gravity highs and lows of small areal extent. These anomalies suggest local density variations in the post-Miocene rocks of the area and may relate to individual flows or intrusions or relatively thick ash deposits. The station location density and the smoothing inherent in the computations and subsequent contouring of the data limit the resolution of the individual anomalies and consequently the anomaly causing bodies. No attempt was made to correlate

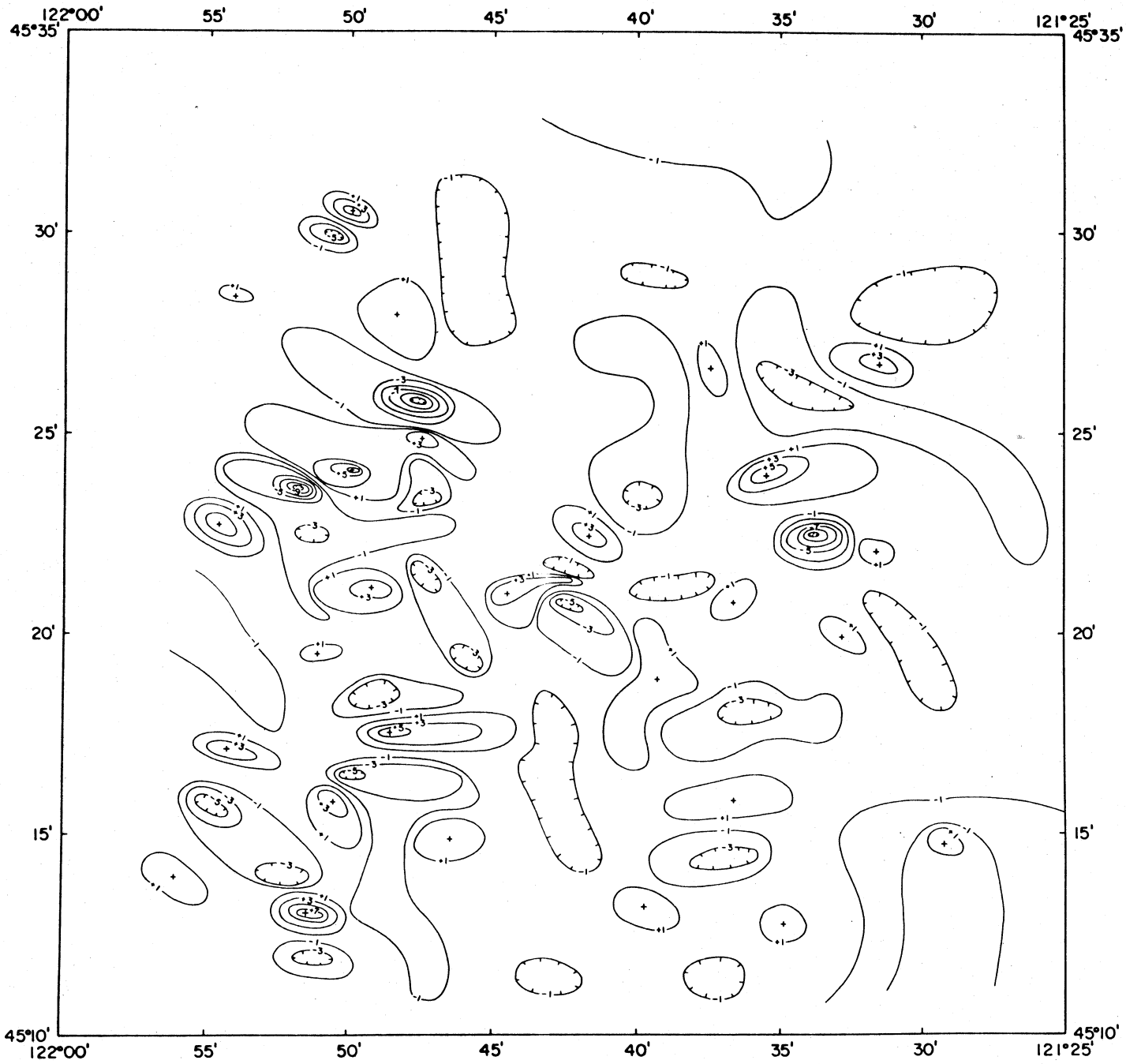

RESIDUAL GRAVITY ANOMALY MAP

MOUNT HOOD AREA, OREGON

AREA OF THIS MAP

CONTOUR INTERVAL 2 MGALS

KILOMETERS

0 2 4 6 8

0 1 2 3 4 5

MILES

UNIVERSAL TRANSVERSE MERCATOR PROJECTION

OREGON STATE UNIVERSITY

FEBRUARY, 1979

Figure 11

these anomalies with the surface or near-surface geology.

MODELS OF MOUNT HOOD

A large number of geological, geophysical, and geochemical studies contemporary with the gravity study described in this report will provide data with which to constrain future models of the internal and substructure of Mount Hood. Simple models, based on only a few gravity values, are offered and described below which may suggest limits or directions to other investigators studying Mount Hood. Topographic elevations, a Bouguer gravity anomaly based on a measurement on the summit of Mount Hood of 7.6 mgls, and an anomaly wavelength based on gravity measurements on the flanks of Mount Hood constrain the simple models.

Figure 12 shows a sphere model of Mount Hood that agrees with the observed Bouguer gravity anomaly and anomaly wavelength. The model assumes a density contrast, $\Delta \rho$, of 0.6 gm/cm^3 between mountain and "core". Because the average density associated with the topography of the region is approximately 2.3 gm/cm^3 the density of the spherical core would be approximately 2.9 gm/cm^3. A density of 2.9 gm/cm^3 would be near the maximum density expected for a volcanic core particularly if it were warm, altered and/or fractured. The size of core required to satisfy the observations and assumptions suggests the model is unrealistic.

Figure 13 shows a graph of a family of curves which describe the height and radius of a cylinderical core which satisfies the observed gravity anomaly on the summit of Mount Hood. The heavy curve which crosses the family of curves of different

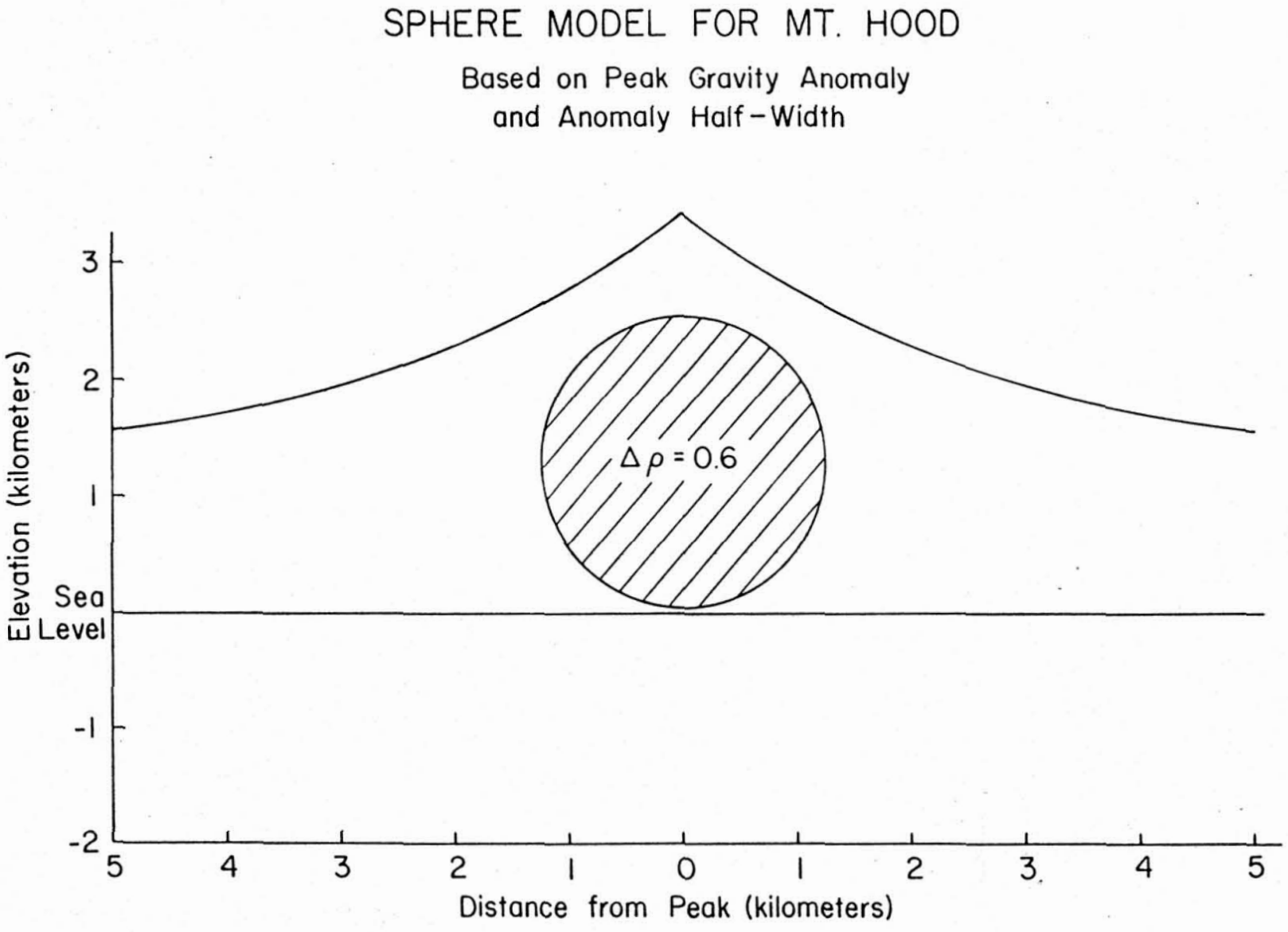
SPHERE MODEL FOR MT. HOOD
Based on Peak Gravity Anomaly
and Anomaly Half-Width
Elevation (kilometers)
3
2
1
Sea Level
-1
-2
Δρ = 0.6
5
4
3
2
1
0
1
2
3
4
5
Distance from Peak (kilometers)

Figure 12

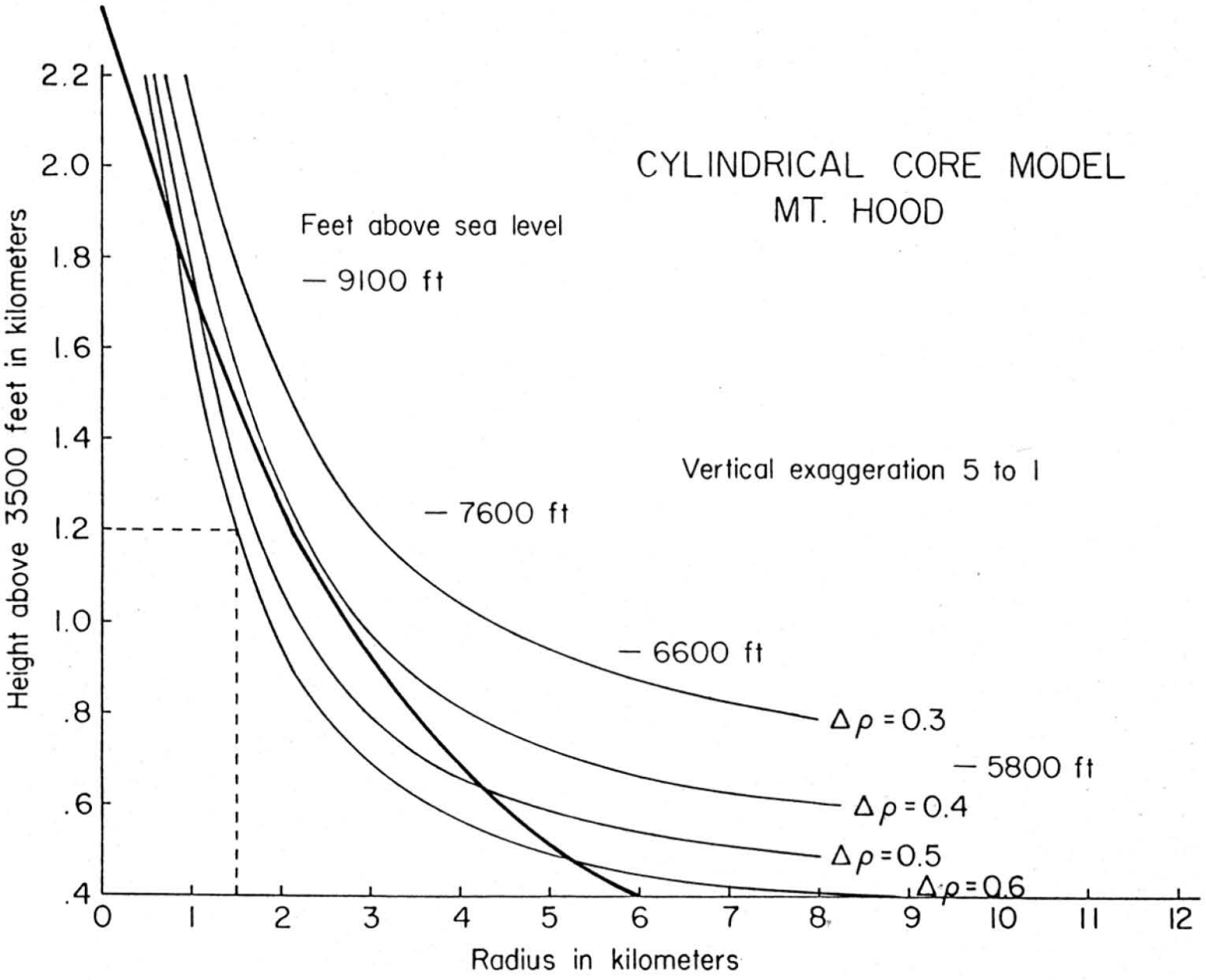
CYLINDRICAL CORE MODEL
MT. HOOD
Feet above sea level
— 9100 ft
— 7600 ft
— 6600 ft
— 5800 ft
Vertical exaggeration 5 to 1
Δρ = 0.3
Δρ = 0.4
Δρ = 0.5
Δρ = 0.6
Height above 3500 feet in kilometers
Radius in kilometers
2.2
2.0
1.8
1.6
1.4
1.2
1.0
.8
.6
.4
0
1
2
3
4
5
6
7
8
9
10
11
12

Figure 13

density contrasts is the smoothed topography of Mount Hood; therefore, any cylinderical model postulated is limited in radius and/or height by the topography. The dotted line illustrates one possible model: the cylinder has a radius of 1.5 km, a height of 1.2 km (above an assumed base for Mount Hood of 3500 ft), and a density contrast of 0.6 gm/cm^3. Smaller density contrasts yield larger cylinders but the minimum density contrast, limited by the topography, is slightly greater than 0.4 gm/cm^3.

Figure 14 shows a cylinder plus cone model of Mount Hood which satisfies the observed gravity anomaly, and topography. This model implies that the higher density rock of the volcanic core extends to the surface at the summit of the mountain. This is consistent with the resistant rocks which are visible near the summit and which are probably more dense than most of the rock on the flanks of the mountain. Figure 12 illustrates the size of the core when a density contrast of 0.5 gm/cm^3 is assumed. In this model the base of the cylindrical core rests on Columbia River Basalt at an elevation of 3500 ft; however, it could extend much deeper without significantly altering the gravitational effect of the model. Changes in the dimensions of the model near the summit cause the larger changes in the gravitational attraction of the cylinder and cone model. Figure 15 shows a graph of the changes in radius of the cylinder and core models versus the density contrast between the cylinder and core and the surrounding mountain. The curve assumes the density of the surrounding rock is 2.27 gm/cm^3 and the observed Complete Bouguer anomaly is 7.6 mgls. A large

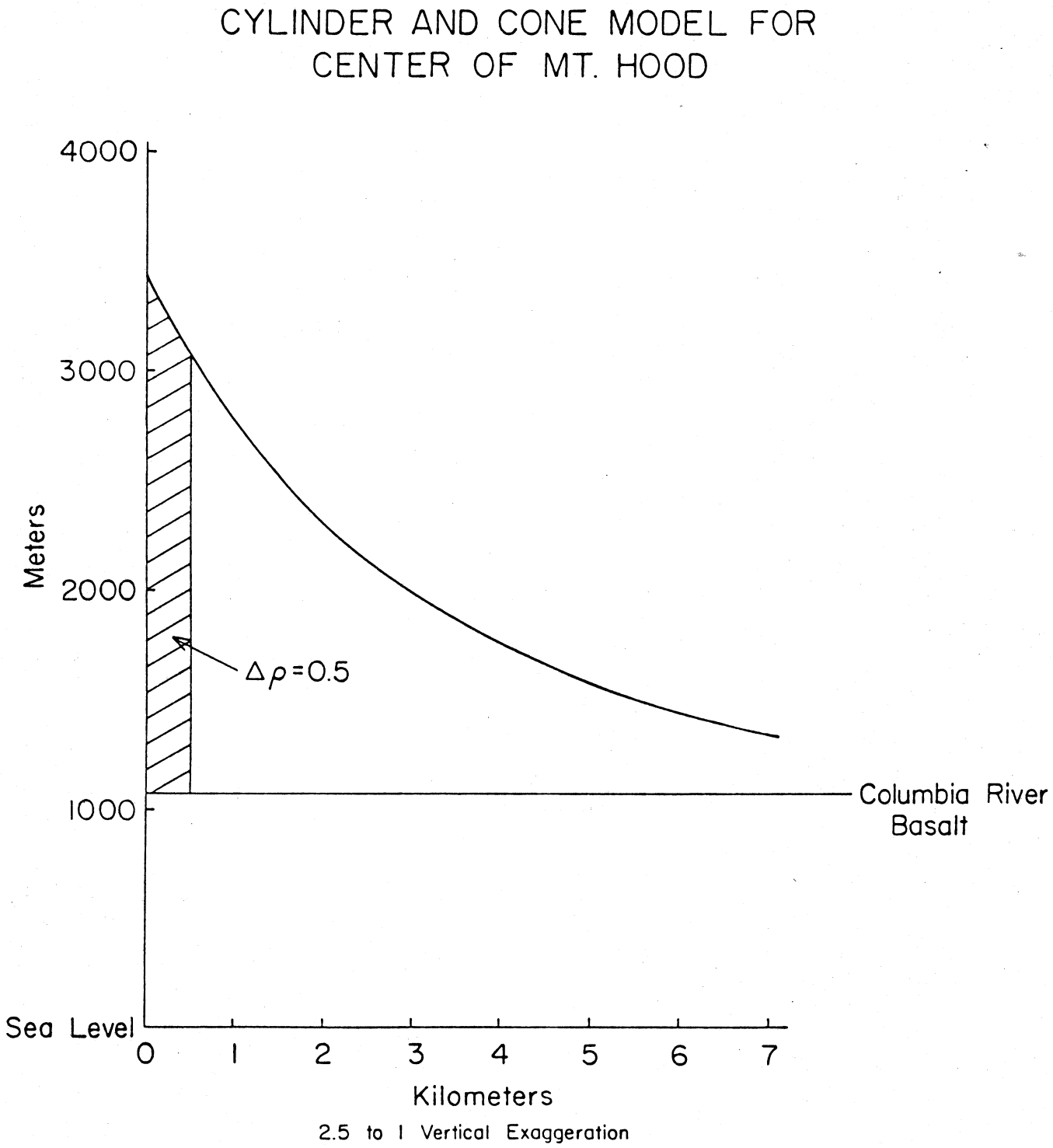
CYLINDER AND CONE MODEL FOR
CENTER OF MT. HOOD
4000
3000
2000
1000
Meters
Δρ=0.5
Columbia River
Basalt
Sea Level
0
1
2
3
4
5
6
7
Kilometers
2.5 to 1 Vertical Exaggeration

Figure 14

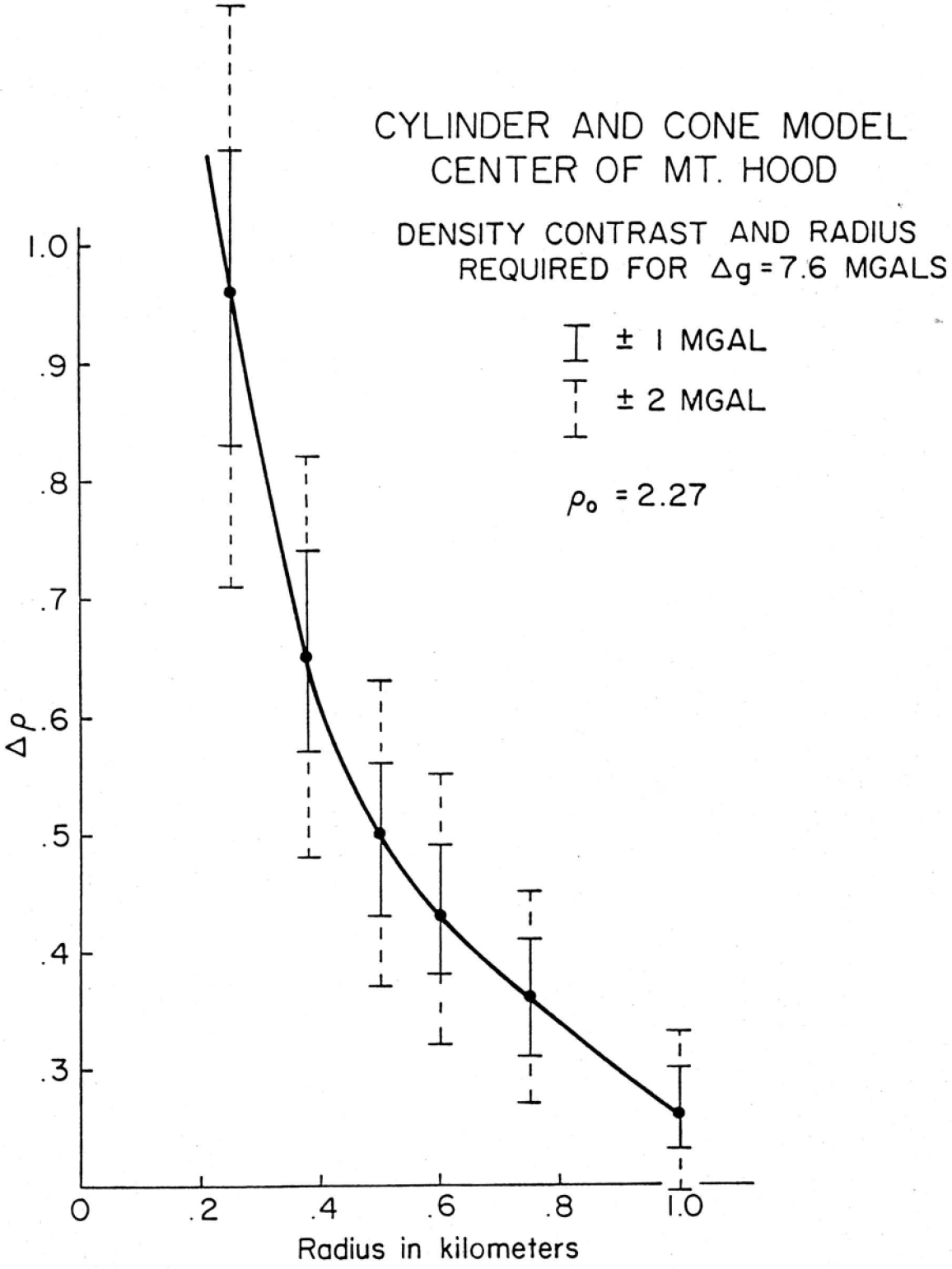
CYLINDER AND CONE MODEL
CENTER OF MT. HOOD
DENSITY CONTRAST AND RADIUS
REQUIRED FOR Δg = 7.6 MGALS
± 1 MGAL
± 2 MGAL
ρo = 2.27
Δρ
1.0
.9
.8
.7
.6
.5
.4
.3
0
.2
.4
.6
.8
1.0
Radius in kilometers

Figure 15

uncertainty is associated with the terrain correction of the summit anomaly on Mount Hood; hence, error bars of $\pm$ and $\pm$ 2 mgls are shown on the curve to indicate the uncertainties in the resulting models.

ELEVATION OF THE COLUMBIA RIVER BASALT

The 2.27 gm/cm^3 density of the rocks which form the topography of and about Mount Hood is considerably less dense than the density of 2.7 to 2.9 gm/cm^3 generally associated with the Columbia River Basalts. Therefore, the gravity anomalies of the area contain information on the structure or the shape of the interface between the Columbia River Basalts and the overlying rocks. To estimate the elevation of the Columbia River Basalt (Yakima Basalt) the complete Bouguer gravity anomalies, computed with a reduction density of 2.27 gm/cm^3, were spectrally separated into regional and residual components. The regional components that represent the anomaly field caused by the Columbia River Basalts were determined, after several interactions, to be best approximated by anomaly wavelengths longer than 8.1 km. The geologic map of the area indicates the Columbia River Basalts outcrop in several areas about Mount Hood. The elevations of the outcrops and the corresponding gravity anomalies provide a reference point for computations of the elevation of the Columbia River Basalt. The reference point selected was an elevation of 1040 meters and a gravity anomaly of +4 mgls. The equation to compute the elevation at other gravity stations was then

$$H = \left(\frac{RCBA_{2.27} - 4}{41.92\,\Delta\rho}\right) 1000 + 1040$$

where

H = is the elevation in meters of the Columbia River Basalt above sea level

$RCBA_{2.27}$ = is the complete regional Bouguer anomaly at a reduction density of 2.27 gm/cm^3

= is the assumed density contrast between the Columbia River Basalt and the overlying flows and pyroclastics.

Elevations were computed for density contrasts of 0.4 and 0.6 gm/cm^3. A density contrast of 0.6 gm/cm^3 yields the best fit to the mapped outcrops of the Columbia River Basalt. Figure 16 shows the estimated elevations of the top of the Columbia River Basalt (Yakima Basalt) based on computations that used a regional gravity field with spatial anomaly wavelengths greater than 8.1 km. The contour interval is 100 m with heavy contours shown at an elevation of 1000 m. Undulations in the surface range from less than 500 to greater than 1400 m above sea level. The highest elevations occur on the east, northeast and southwest sides of Mount Hood. The axis of Mount Hood is located approximately on an elevated ridge, oriented approximately N75E, that extends from the high elevations of the Columbia River Basalts on the east side of Mount Hood to the high on the southwest side.

Elevation estimates of the Columbia River Basalt is based on gravity measurements, an assumed density contrast between the Columbia River Basalts and the post-Miocene pyroclastics and flows of the High Cascade Mountains, and a reference elevation and gravity anomaly on an outcrop of the Columbia River Basalts in the study area. Inherent in these estimates are limits on the resolution of the surface configuration and elevation imposed by the position and spacing of the primary data grid and the continuity or smoothness of potential fields. Further, the elevations are computed independently for each station. Because of the limitations inherent in the method of

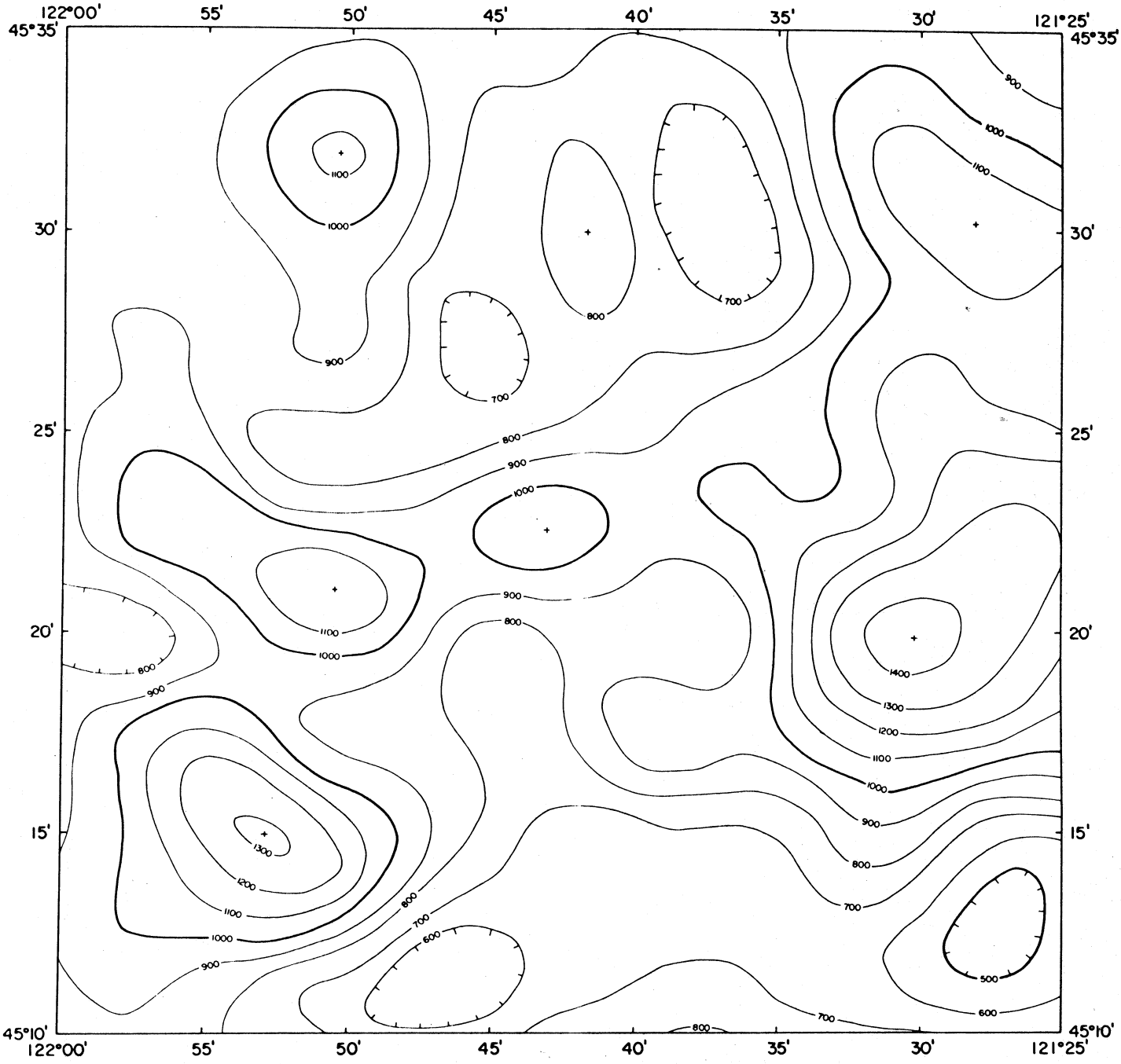

ESTIMATED ELEVATION OF THE COLUMBIA RIVER BASALTS
MOUNT HOOD AREA, OREGON

AREA OF THIS MAP

CONTOUR INTERVAL 100 METERS

KILOMETERS
0 2 4 6 8
0 1 2 3 4 5
MILES

UNIVERSAL TRANSVERSE MERCATOR PROJECTION

OREGON STATE UNIVERSITY
FEBRUARY, 1979

Figure 16

estimating the elevations many features cannot be resolved. For example, features with edges, such as faults or lava flows, are smoothed and included in the undulations of the estimated topography. The method also cannot differentiate between flows or changes in the Columbia River Basalt and other high density flows in the area, hence their surface is mapped as Columbia River Basalt. High density intrusions in the material above the Columbia River Basalt may be reflected or included in the undulations of the basalt.

To assess the effectiveness of the elevation estimates the computed elevations were compared to topographic elevations to generate a map of the "computed outcrops" of the Columbia River Basalts. Figure 17 shows a map of both the observed and computed outcrops of the Columbia River Basalts. The agreement between computation and observation is reasonable but generally more Columbia River Basalt is expected to outcrop than is actually observed. This discrepancy may be caused by a wrong reference elevation for the computations, erosion of the basalt in the area of expected outcrops, insufficient geologic mapping, or broadening of the surface during computation and contouring. West of Mount Hood relatively high density rocks are associated with Pliocene volcanism.

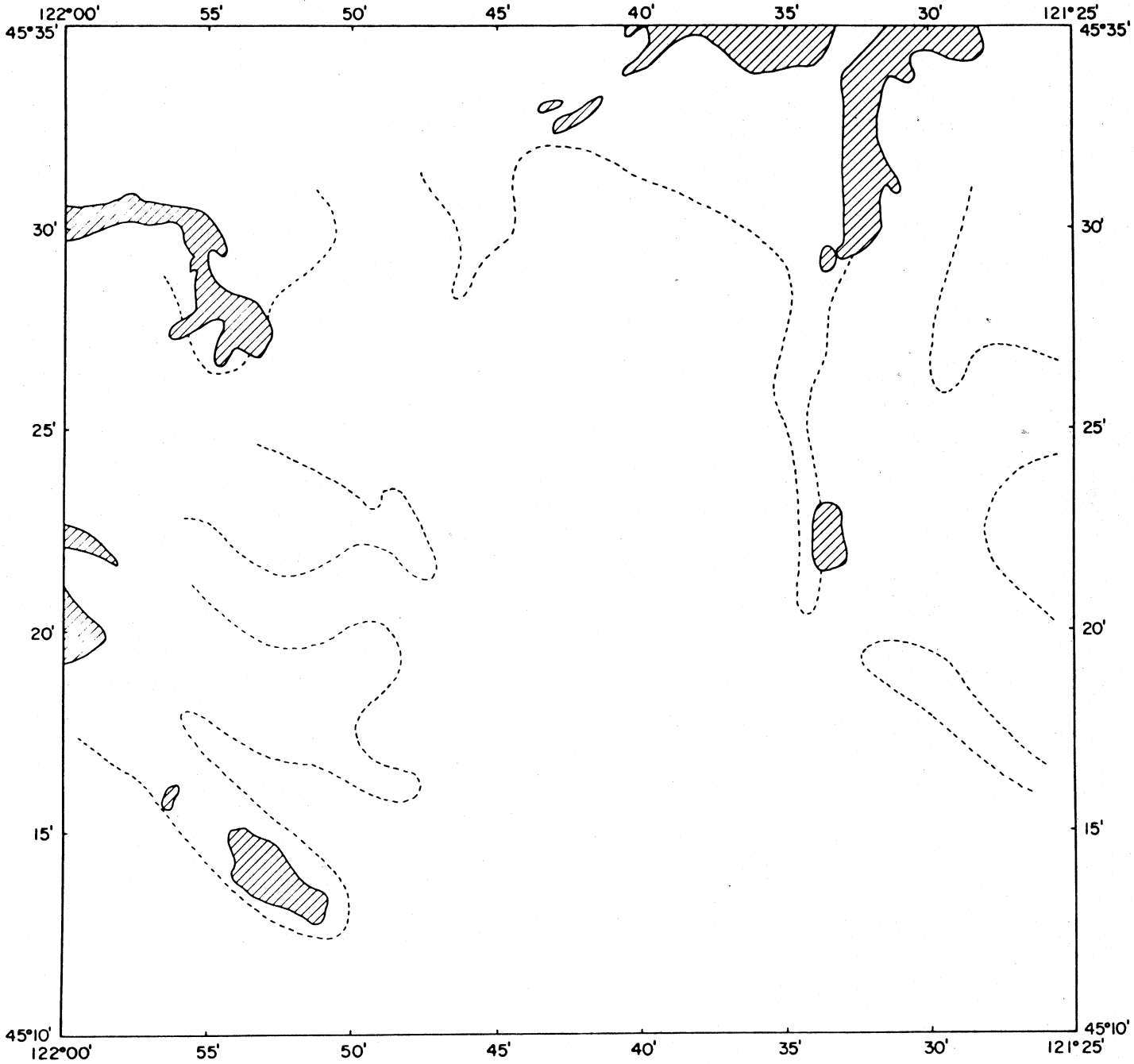

TOPOGRAPHIC SURFACE OF PRE-PLIOCENE ROCKS
MOUNT HOOD AREA, OREGON

COLUMBIA RIVER BASALT
OBSERVED OUTCROP
COMPUTED OUTCROP

KILOMETERS
0 2 4 6 8
0 1 2 3 4 5
MILES

UNIVERSAL TRANSVERSE MERCATOR PROJECTION

OREGON STATE UNIVERSITY
FEBRUARY, 1979

Figure 17

POROSITY ESTIMATES

Laboratory measurements on rocks from Mount Hood by Dr. N. Christianson (University of Washington, personal communication, 1978) show porosities of 6 to 7 percent in samples of fresh massive andesite. The measured samples have densities and p-wave velocities listed in Table 2.

TABLE 2

Sample	Density (gm/cm^3)	Velocity (km/sec)
1	2.56	4.49
2	2.58	4.52
3	2.60	4.65
4	2.62	4.52
5	2.62	4.97
6	2.59	4.84

The average density of the samples is 2.60 gm/cm^3 and the average velocity is 4.67 km/sec. If $p_{2.6}$ is the density of andesite at 7 percent porosity, then p_{max}, the density at 0 percent porosity is 2.80 gm/cm^3. Recognizing that the rocks which form Mount Hood are believed to be more than 90 percent andesite (Wise, 1969) the value, p_{max}, provides a reference point to compute average porosities for the rocks of Mount Hood above the Columbia River Basalts. The elevation difference, h, between the estimated elevation of the Columbia River Basalt and the topographic surface, the residual gravity anomalies (RGA), obtained as the difference between the complete Bouguer anomalies and the regional anomalies and the reduction density $p_{2.27}$, provide the parameters used to compute an average density

for the mass column between the Columbia River Basalts and the topographic surface. The equation is,

$$p_{avg} = p_{2.27} + \frac{RGA}{2\pi\sigma h}$$

where σ is the gravitational constant. The estimated porosity is given by the equation:

$$\text{Porosity (\%)} = 100 \left(\frac{2.8 - p_{avg}}{2.8}\right)$$

Because the rocks are porous they can contain water, consequently the equation above yields a porosity for dry rocks. The equation for 100 percent water saturated rocks is:

$$\text{Porosity (\%)} = 100 \left(\frac{2.8 - p_{avg}}{1.8}\right)$$

Figure 18 shows a map of the estimated average porosities of the rocks in the Mount Hood area above the Columbia River Basalts based on the assumption that the rocks are water saturated. Because the computed values have large inherent uncertainties and show a large scatter or range in values they result in numerous "one-point" anomalies. Consequently, the computed values were smoothed and the contours only separate areas of porosities greater than or less than the average porosity, 30 percent, of water saturated rocks. The map shows an area east of Mount Hood with porosities less than 30 percent that corresponds reasonably well to the area where the complete Bouguer anomalies suggest the presence of higher density rocks. These observations of course, are not independent. A contour line that separates porosities of greater than 30 percent on the east side from porosities of less than 30 percent on the west side crosses the summit of Mount Hood from approximately south southwest to north northeast. The difference in the

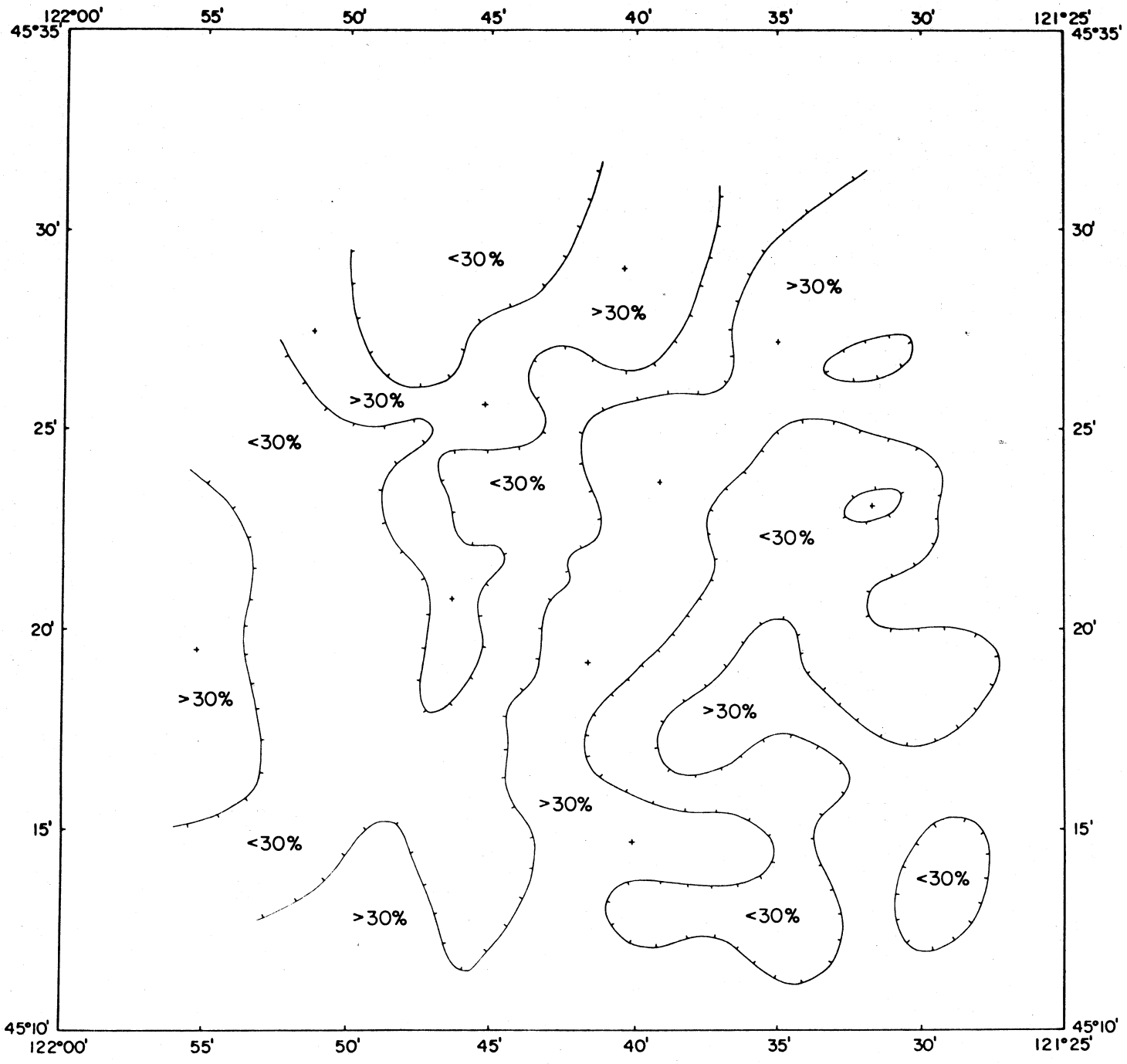

ESTIMATED REGIONAL POROSITY
MOUNT HOOD AREA, OREGON

KILOMETERS
0 2 4 6 8
0 1 2 3 4 5
MILES

UNIVERSAL TRANSVERSE MERCATOR PROJECTION

OREGON STATE UNIVERSITY
FEBRUARY, 1979

Figure 18

porosities indicated by the map suggests an asymmetry in the average rock, a composite of flows and pyroclastics, that forms Mount Hood. Alternatively, the average porosity of the rock materials may be the same about the summit and flanks of Mount Hood but the porous rocks may contain more water on the west side than on the east side.

TRAVEL TIME RESIDUALS

Empirical relations between rock density and compressional wave velocity (Ludwig, Nafe, and Drake, 1970) provide a means to estimate p-wave travel time residuals for the Mount Hood area based on gravity measurements. The empirical curves of Ludwig and others (1970) indicate a compressional wave velocity of approximately 3.3 km/sec for rock of density 2.27 gm/cm^3. Recognizing that the average complete Bouguer anomaly for the Mount Hood area is -71.7 mgl then the approximate travel time vertically through the material above sea level is given by the equation:

$$\Delta T = \frac{h}{1.45\ (2.27 + \Delta \rho)}$$

where h is the elevation in kilometers and

$$\Delta \rho = \frac{CBA + 71.7}{2 \pi \gamma h}$$

Figure 19 shows estimated travel time residuals for the Mount Hood area. The travel time residuals are the time of travel from sea level to the surface and the differences are caused by variations in topographic elevation and rock density along the ray path. The computed travel time residuals are estimates only and do not allow for irregular travel paths caused by refraction and diffraction of the seismic waves. The map does indicate, however, that significant travel time differences caused by near-surface effects can be expected.

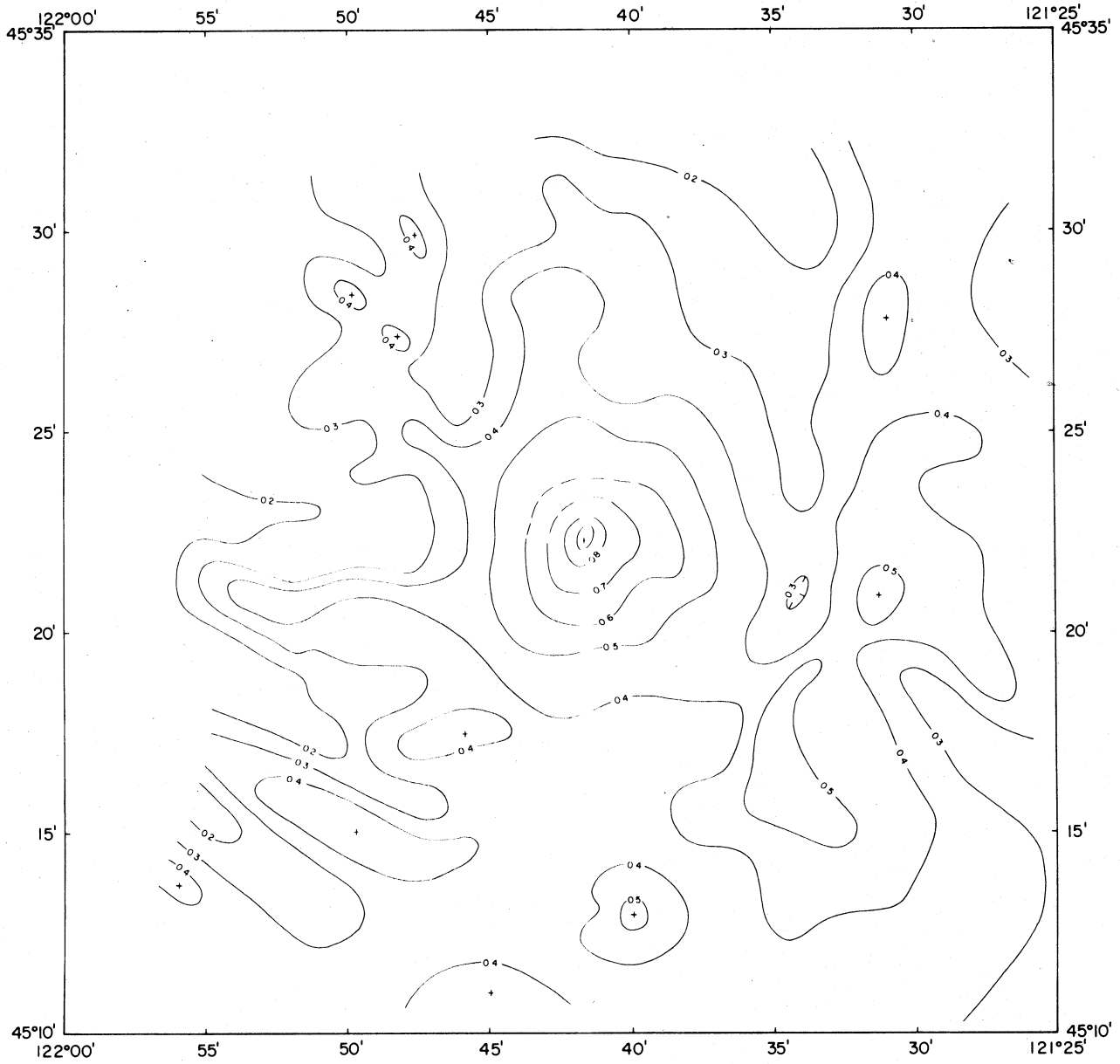

ESTIMATED TRAVEL-TIME RESIDUALS
MOUNT HOOD AREA, OREGON

AREA OF THIS MAP

CONTOUR INTERVAL 0.1 SEC

KILOMETERS
0 2 4 6 8
0 1 2 3 4 5
MILES

UNIVERSAL TRANSVERSE MERCATOR PROJECTION

OREGON STATE UNIVERSITY
JANUARY, 1979

Figure 19

ACKNOWLEDGEMENTS

Messuers. K. Keeling, T. Jones, W. Plant, G. Ness, M. Brown, and J. Bowers made the gravity measurements in the Mount Hood area. S. Pitts, K. Keeling, D. Braman, J. Cook, G. Axelsson and W. Avera assisted in the data reduction. P. Pitts, B. Priest, D. Burt, and S. Troseth prepared the maps and illustrations, J. Brenneman and N. Kneisel helped prepare the report. This work was supported by the Oregon State Department of Geology and Mineral Industries through a grant from the U. S. Department of Energy.

REFERENCES

Hammer, Sigmond, 1939, Terrain Corrections for Gravimeter Stations, Geophysics, v. 4, p. 184-194.

Longman, I. M., 1959, Formulas for computing the tidal accelerations due to the moon and the sun: J. of Geophys. Res., v. 64, n. 12, p. 2351-2355.

Ludwig, W., Nafe, J. E., and Drake, C. L., 1970, Seismic refraction, In: The Sea, A. E. Maxwell (editor), vol. 4, Part I, New York, Wiley-Interscience, p. 53-84.

Oliver, H. W., 1973, Principal facts, plots, and reduction for 1753 gravity stations in the Southern Sierra Nevada and Vicinity, California: NTIS pub #PB 231 185, U. S. Dept. of Commerce, Washington, D. C.

Oliver, H. W., Griscom, A., Robbins, S. L., Hanna, W. F., 1969, U. S. Geological Survey Gravity data in California, part IV: U. S. Geol. Survey, Internal report, Menlo Park, California.

Plouff, D., 1977a, Preliminary documentation for a FORTRAN program to compute gravity terrain corrections based on topography digitized on a geographic grid: U. S. Geol. Survey, Open-file report, no. 77-535, U. S. Govt. Printing Office, Washington, D. C.

Plouff, D., 1977b, Gravity observations near McDermitt, Nevada during 1976: U. S. Geol. Survey, open-file report, no. 77-536, 13 p., U. S. Govt. Printing Office, Washington, D. C.

Scheibe, D. M., and Howard, H. W., 1964, Classical methods for reduction of gravity observation: U. S. Air Force, Aeronautical Chart and Information Center Ref., Pub. 12, 65 p.

Swick, C. H., 1942, Pendulum gravity measurements and isostatic reductions: U. S. Coast and Geod. Survey, Spec. Pub., no. 232, 82 p.

Thiruvathukal, J. T., 1968, Regional Gravity of Oregon: unpub. Ph.D. Dissertation, Oregon State University, Corvallis, Oregon, 92 p.

Wise, W. S., 1969, Geology and Petrology of the Mt. Hood Area: A study of High Cascade Volcanism, Geo. Soc. of Am. Bull., v. 80, p. 969-1006.

Woollard, G. P., Rose, J. C., 1963, International gravity measurements: Society of Exploration Geophysics, Tulsa, OK, 518 p.

APPENDIX

THEORETICAL GRAVITY : IUGG 1930 INTERNATIONAL GRAVITY FORMULA

EXPLANATION OF SYMBOLS: ID - STATION IDENTIFICATION, LAT - LATITUDE, LONG - LONGITUDE, ELEV - ELEVATION (FEET), OG - OBSERVED GRAVITY, THG - THEORETICAL GRAVITY, HTC - HAND TERRAIN CORRECTION, TTC - TOTAL TERRAIN CORRECTION, CC - CURVATURE CORRECTION, FAA - FREEAIR ANOMALY, CBA1, CBA2 - VARIABLE DENSITY COMPLETE BOUGUER ANOMALIES. GRAVITY DATA, ANOMALIES, AND CORRECTIONS IN MGALS. ESTIMATED UNCERTAINTIES, FAA +- 1.0 MGL, CBA +- 1.5 MGL.
CBA1 REDUCTION DENSITY = 2.67 GM / CC CBA2 REDUCTION DENSITY = 2.27 GM / CC

ID	LAT	LONG	ELEV	OG	THG	HTC	TTC	CC	FAA	CBA1	CBA2	ID
MHL 3	45 20.61	-121 56.46	1425.0	980489.14	980660.39	0.00	4.85	0.57	-37.25	-81.57	-74.93	MHL 3
MHL 6	45 18.28	-121 45.27	3880.0	980328.18	980656.89	0.00	3.39	1.24	36.09	-94.09	-74.59	MHL 6
MHL 7	45 18.58	-121 42.29	4900.0	980260.54	980657.22	0.00	6.64	1.40	63.99	-97.93	-73.64	MHL 7
MHL 8	45 19.87	-121 42.16	5950.0	980190.14	980659.20	0.00	12.46	1.49	90.19	-101.77	-73.01	MHL 8
MHS01	45 17.04	-121 42.53	3652.0	980339.79	980655.03	0.00	3.11	1.19	28.13	-94.51	-76.14	MHS01
MHS02	45 25.46	-121 34.69	3860.0	980393.11	980667.69	0.00	5.51	1.06	13.14	-86.77	-71.81	MHS02
MHS03	45 30.39	-121 35.14	1831.0	980476.90	980675.10	0.02	2.77	0.71	-25.03	-86.41	-77.37	MHS03
MHS05	45 32.90	-121 42.03	1279.0	980513.34	980678.88	0.00	8.12	0.52	-45.27	-81.29	-75.89	MHS05
MHS06	45 13.07	-121 41.69	3874.0	980316.61	980649.06	0.00	3.47	1.24	31.79	-98.11	-78.65	MHS06
MH 01	45 19.96	-121 54.87	1577.0	980478.54	980659.42	0.00	6.71	0.62	-32.59	-80.28	-73.14	MH 01
MH 02	45 19.57	-121 54.42	1672.0	980472.62	980658.84	0.01	6.48	0.65	-28.99	-80.19	-72.52	MH 02
MH 03	45 19.01	-121 53.93	1804.0	980463.43	980657.99	0.00	6.49	0.78	-24.92	-80.66	-72.31	MH 03
MH 04	45 18.55	-121 52.88	1990.0	980451.92	980657.29	0.00	6.34	0.76	-18.24	-80.53	-71.28	MH 04
MH 05	45 18.43	-121 51.15	2294.0	980433.58	980657.12	0.00	5.41	0.85	-7.91	-81.59	-70.56	MH 05
MH 06	45 18.78	-121 50.04	2547.0	980416.69	980657.52	0.00	5.25	0.92	-1.34	-83.88	-71.52	MH 06
MH 07	45 18.85	-121 47.78	3120.0	980376.58	980657.75	2.38	9.06	1.07	12.19	-86.24	-71.49	MH 07
MH 08	45 18.80	-121 48.91	2806.0	980397.83	980657.67	0.61	4.85	0.99	4.80	-87.85	-74.09	MH 08
MH 09	45 18.46	-121 46.95	3581.0	980347.95	980657.15	0.00	3.30	1.18	27.49	-92.52	-74.54	MH 09
MH 10	45 15.55	-121 42.71	3420.0	980350.56	980652.78	0.00	3.60	1.14	19.34	-94.85	-77.74	MH 10
MH 11	45 14.48	-121 42.23	3550.0	980338.63	980651.16	0.20	3.21	1.17	21.25	-97.79	-79.96	MH 11
MH 12	45 13.55	-121 41.86	3952.0	980312.85	980649.77	0.02	2.82	1.25	34.65	-98.57	-78.62	MH 12
MH 13	45 11.65	-121 41.45	3826.0	980319.63	980646.91	0.01	1.64	1.23	32.44	-97.64	-78.15	MH 13
MH 14	45 17.33	-121 46.91	5027.0	980248.31	980655.46	7.77	14.33	1.41	65.45	-93.08	-69.33	MH 14
MH 15	45 17.63	-121 44.91	4656.0	980269.59	980655.91	10.32	14.23	1.37	51.41	-94.52	-72.66	MH 15
MH 16	45 18.04	-121 44.02	3925.0	980323.23	980656.53	0.00	4.89	1.25	35.73	-95.29	-75.66	MH 16
MH 17	45 17.24	-121 43.67	3838.0	980329.37	980655.32	0.00	2.94	1.23	34.15	-94.77	-75.45	MH 17
MH 18	45 16.13	-121 44.15	3608.0	980342.11	980653.65	0.00	2.69	1.18	27.69	-93.86	-75.65	MH 18
MH 19	45 15.19	-121 44.21	4145.0	980305.66	980652.24	0.04	4.27	1.29	43.13	-95.26	-74.53	MH 19
MH 20	45 14.34	-121 48.79	4705.0	980270.47	980650.96	1.88	6.94	1.37	61.85	-93.05	-69.85	MH 20
MH 21	45 15.87	-121 50.48	5041.0	980243.93	980653.26	14.02	22.61	1.42	64.58	-96.16	-63.57	MH 21
MH 22	45 16.02	-121 53.06	4770.0	980265.45	980653.49	11.64	19.78	1.38	68.40	-83.83	-62.27	MH 22
MH 23	45 16.45	-121 53.49	4226.0	980307.14	980654.13	5.83	11.44	1.30	50.33	-83.66	-63.59	MH 23
MH 24	45 17.84	-121 54.33	4118.0	980317.37	980655.83	9.35	14.61	1.28	48.76	-78.89	-59.89	MH 24
MH 25	45 14.66	-121 50.30	4689.0	980276.16	980651.43	0.29	10.46	1.37	63.56	-85.28	-62.68	MH 25
MH 26	45 17.87	-121 53.85	1846.0	980458.28	980656.27	0.00	8.62	0.71	-24.48	-79.46	-71.21	MH 26

ID	LAT	LONG	ELEV	OG	THG	HTC	TTC	CC	FAA	CBA1	CBA2	ID
MH 27	45 17.11	-121 51.25	2114.0	980436.04	980655.13	9.35	14.19	0.80	-20.30	-79.02	-70.23	MH 27
MH 28	45 16.41	-121 50.23	2380.0	980412.29	980654.00	10.31	14.42	0.80	-18.00	-85.63	-75.50	MH 28
MH 29	45 16.04	-121 48.40	2893.0	980381.40	980653.51	9.69	12.76	1.02	-0.09	-87.02	-74.00	MH 29
MH 30	45 16.38	-121 46.46	3188.0	980366.94	980654.03	9.02	6.00	1.09	12.66	-91.00	-75.54	MH 30
MH 31	45 16.96	-121 44.80	3531.0	980348.86	980654.90	0.03	4.70	1.17	25.95	-90.94	-73.43	MH 31
MH 32	45 14.80	-121 47.17	4457.0	980290.04	980651.78	0.05	4.60	1.34	50.09	-90.66	-68.38	MH 32
MH 33	45 13.64	-121 46.21	3467.0	980349.19	980649.90	0.03	1.84	1.15	25.26	-92.30	-74.69	MH 33
MH 34	45 12.43	-121 41.86	4024.0	980306.68	980648.09	0.18	2.39	1.26	36.92	-99.19	-78.80	MH 34
MH 35	45 11.56	-121 42.97	3573.6	980333.20	980646.77	0.04	2.87	1.18	22.37	-97.80	-79.79	MH 35
MH36A	45 19.16	-121 41.15	4799.0	980266.89	980658.22	0.02	7.08	1.39	59.84	-98.14	-74.47	MH36A
MH 37	45 17.53	-121 48.63	4414.0	980296.28	980655.76	0.10	7.64	1.33	55.51	-88.73	-67.12	MH 37
MH 38	45 12.82	-121 44.12	3879.0	980314.95	980647.47	0.02	1.98	1.24	32.19	-99.37	-79.66	MH 38
MH 39	45 12.66	-121 43.17	3931.0	980311.77	980648.44	0.03	4.24	1.25	32.93	-98.15	-78.52	MH 39
MH 40	45 11.99	-121 46.07	3844.0	980316.91	980647.42	0.00	1.79	1.23	30.91	-99.64	-80.00	MH 40
MH 41	45 11.22	-121 47.44	3969.0	980305.82	980646.27	0.01	1.82	1.25	32.72	-102.09	-81.09	MH 41
MH 42	45 12.13	-121 49.75	3588.0	980337.61	980647.63	0.04	3.79	1.18	27.33	-92.44	-74.49	MH 42
MH 43	45 11.92	-121 51.26	3223.0	980359.28	980647.31	0.49	3.42	1.10	15.01	-92.59	-76.47	MH 43
MH 44	45 11.81	-121 54.54	4088.0	980308.14	980647.15	0.01	3.66	1.28	45.34	-91.70	-71.17	MH 44
MH 45	45 13.69	-121 56.01	4877.0	980246.39	980649.99	19.49	27.61	1.40	54.91	-83.22	-64.22	MH 45
MH 46	45 12.58	-121 47.54	3586.0	980335.40	980648.31	0.42	3.05	1.18	24.25	-96.10	-78.14	MH 46
MH 47	45 13.06	-121 49.51	3236.0	980366.97	980649.04	0.11	2.22	1.10	22.19	-87.06	-70.69	MH 47
MH 48	45 13.00	-121 51.31	2867.0	980403.41	980648.95	0.19	3.22	1.01	24.04	-71.54	-57.22	MH 48
MH 49	45 13.80	-121 52.26	2710.0	980405.10	980650.15	0.46	4.50	0.97	9.84	-79.05	-65.74	MH 49
MH 50	45 14.40	-121 52.63	2655.0	980411.70	980651.05	0.03	4.69	0.95	10.30	-76.52	-63.51	MH 50
MH 51	45 15.01	-121 53.85	2492.0	980424.10	980651.97	0.62	5.23	0.91	6.46	-74.22	-62.13	MH 51
MH 52	45 15.65	-121 54.93	1773.0	980461.83	980652.93	0.00	9.54	0.69	-24.38	-76.00	-69.27	MH 52
MH 53	45 13.03	-121 39.95	5294.0	980219.99	980648.99	0.01	11.68	1.44	68.69	-101.64	-76.12	MH 53
MH 54	45 17.04	-121 35.57	5724.0	980196.95	980655.02	11.33	19.71	1.48	80.03	-96.96	-70.45	MH 54
MH 55	45 18.18	-121 33.47	4465.0	980294.61	980656.73	0.00	7.07	1.34	57.66	-88.89	-66.94	MH 55
MH 56	45 18.17	-121 31.74	5125.0	980259.31	980656.73	0.01	6.13	1.42	84.39	-85.78	-60.22	MH 56
MH 57	45 15.79	-121 35.52	5600.0	980202.62	980653.15	10.26	18.55	1.47	75.92	-98.00	-71.34	MH 57
MH 58	45 14.50	-121 34.50	4865.0	980256.01	980651.23	0.01	4.90	1.39	62.18	-100.24	-75.91	MH 58
MH 59	45 12.77	-121 35.02	4342.0	980286.34	980648.59	0.00	5.66	1.32	45.97	-97.78	-76.24	MH 59
MH 60	45 11.40	-121 34.43	3705.0	980327.55	980646.53	0.00	2.41	1.20	29.36	-95.79	-77.04	MH 60
MH 61	45 11.13	-121 32.51	3326.0	980350.38	980646.13	0.01	1.73	1.12	16.97	-95.86	-78.96	MH 61
MH 62	45 11.93	-121 30.04	3702.0	980325.37	980647.34	0.04	2.69	1.20	26.10	-98.60	-79.98	MH 62
MH 63	45 12.40	-121 32.76	3849.0	980319.26	980648.05	0.01	2.25	1.23	33.10	-97.16	-77.65	MH 63
MH 64	45 13.79	-121 31.91	4584.0	980274.10	980650.13	0.01	4.36	1.36	54.94	-98.40	-75.43	MH 64
MH 65	45 15.15	-121 32.88	5305.0	980222.00	980652.17	0.01	9.53	1.45	76.07	-99.51	-73.21	MH 65
MH 66	45 16.35	-121 32.55	5279.0	980237.08	980653.98	0.00	7.55	1.44	79.38	-94.56	-68.50	MH 66
MH 67	45 12.66	-121 28.29	3333.0	980348.95	980648.44	0.03	2.04	1.12	13.89	-98.87	-81.97	MH 67
MH 68	45 13.86	-121 29.49	3611.0	980337.17	980650.23	0.02	2.94	1.18	26.45	-94.95	-76.77	MH 68
MH 69	45 14.78	-121 29.34	4011.0	980316.18	980651.62	0.02	3.39	1.26	41.67	-93.00	-72.83	MH 69

ID	LAT	LONG	ELEV	OG	THG	HTC	TTC	CC	FAA	CBA1	CBA2	ID
MH 70	45 14.97	-121 26.52	3803.0	980375.78	980651.91	0.01	2.29	1.04	6.23	-94.94	-79.79	MH 70
MH 71	45 13.66	-121 26.51	2905.0	980376.97	980649.94	0.01	1.80	1.02	0.18	-98.12	-83.39	MH 71
MH 72	45 11.40	-121 27.01	2783.0	980382.91	980646.55	0.01	1.37	0.99	-1.96	-96.49	-82.33	MH 72
MH 73	45 16.68	-121 41.57	4067.0	980315.79	980654.47	0.10	2.90	1.27	43.69	-93.39	-72.86	MH 73
MH 74	45 16.17	-121 40.35	4250.0	980309.57	980656.72	0.01	4.07	1.30	52.43	-89.76	-68.46	MH 74
MH 75	45 18.63	-121 38.51	4674.0	980282.32	980657.41	0.03	4.55	1.37	64.34	-91.90	-68.49	MH 75
MH 76	45 19.80	-121 35.08	3793.0	980340.42	980659.18	0.00	5.22	1.22	37.86	-87.50	-68.72	MH 76
MH 78	45 17.47	-121 38.55	3856.0	980332.19	980655.67	0.28	4.15	1.23	39.06	-89.54	-78.27	MH 78
MH 79	45 17.03	-121 36.97	3585.0	980344.10	980655.01	0.16	6.58	1.18	26.16	-90.71	-73.20	MH 79
MH 80	45 14.38	-121 36.79	3449.0	980342.58	980650.90	0.01	3.15	1.15	15.96	-99.67	-82.35	MH 80
MH 81	45 12.81	-121 36.78	2970.0	980373.34	980648.66	0.00	6.36	1.04	3.94	-92.03	-77.65	MH 81
MH 82	45 11.32	-121 37.18	3452.0	980344.27	980646.42	0.03	2.81	1.15	22.42	-94.46	-76.95	MH 82
MH 83	45 14.82	-121 39.37	3283.0	980356.31	980651.68	0.01	5.62	1.11	13.31	-94.15	-78.86	MH 83
MH 84	45 15.98	-121 40.31	3639.0	980339.89	980653.43	0.00	4.68	1.19	28.68	-92.82	-73.95	MH 84
MH 85	45 20.13	-121 42.69	6277.0	980166.97	980659.68	0.01	13.85	1.51	97.36	-104.39	-74.17	MH 85
MH 86	45 20.48	-121 42.67	6635.0	980148.19	980660.19	0.09	17.93	1.52	103.78	-106.19	-74.74	MH 86
MH 87	45 20.71	-121 42.64	6980.0	980114.93	980660.55	0.05	19.83	1.52	110.49	-109.26	-76.34	MH 87
MH 88	45 20.91	-121 42.53	7282.0	980093.72	980660.85	0.13	23.46	1.51	117.35	-109.86	-75.14	MH 88
MH 90	45 21.32	-121 42.36	8068.0	980043.72	980661.46	7.55	33.61	1.46	140.58	-102.45	-66.84	MH 90
MH 91	45 21.51	-121 42.28	8484.0	980007.86	980661.76	0.19	39.68	1.42	143.51	-107.68	-70.85	MH 91
MH 92	45 22.70	-121 54.58	1947.0	980474.22	980663.54	0.01	4.48	0.74	-6.24	-68.91	-59.52	MH 92
MH 93	45 23.02	-121 52.79	2055.0	980453.72	980664.02	0.08	7.68	0.78	-17.06	-80.33	-78.85	MH 93
MH 94	45 23.61	-121 51.90	2389.0	980419.59	980664.90	0.22	6.73	0.88	-28.67	-96.38	-84.97	MH 94
MH 95	45 24.49	-121 50.78	2657.0	980416.55	980666.23	0.27	5.35	0.95	0.15	-86.88	-73.16	MH 95
MH 96	45 25.24	-121 49.32	3118.0	980387.61	980667.37	0.13	3.49	1.07	13.41	-90.51	-74.94	MH 96
MH 97	45 25.80	-121 47.73	3225.0	980367.87	980668.20	0.09	4.45	1.10	2.90	-103.75	-87.77	MH 97
MH 98	45 22.60	-121 49.75	2582.0	980421.09	980663.39	0.03	5.23	0.93	0.48	-83.29	-78.74	MH 98
MH 99	45 24.19	-121 48.84	3811.0	980340.60	980665.77	0.02	7.45	1.22	33.14	-90.62	-72.08	MH 99
MH100	45 26.47	-121 47.52	2909.0	980401.24	980669.21	2.77	6.57	1.02	5.55	-88.11	-74.00	MH100
MH101	45 27.01	-121 46.60	2399.0	980434.24	980671.22	0.88	4.66	0.88	-11.40	-89.45	-77.75	MH101
MH102	45 29.10	-121 45.72	2156.0	980449.63	980673.16	0.06	6.28	0.81	-28.60	-80.66	-78.47	MH102
MH103	45 29.91	-121 44.61	2323.0	980444.34	980674.39	0.13	4.83	0.86	-11.62	-86.88	-75.61	MH103
MH105	45 20.55	-121 53.03	4460.0	980285.53	980660.30	14.19	22.29	1.34	45.29	-86.15	-66.46	MH105
MH106	45 21.86	-121 53.53	4564.0	980274.74	980661.07	16.79	27.42	1.35	42.76	-86.84	-67.42	MH106
MH107	45 19.67	-121 51.93	4017.0	980324.87	980658.99	0.84	8.80	1.26	42.76	-86.71	-67.31	MH107
MH108	45 19.50	-121 51.36	3306.0	980374.48	980658.73	0.04	4.12	1.12	26.59	-83.16	-66.72	MH108
MH109	45 20.34	-121 50.82	3753.0	980346.88	980659.99	0.87	4.74	1.21	39.75	-84.72	-66.87	MH109
MH110	45 20.63	-121 49.47	3995.0	980333.41	980660.42	0.86	5.54	1.26	48.59	-83.30	-63.61	MH110
MH111	45 21.02	-121 50.98	4877.0	980265.86	980661.01	9.86	18.92	1.40	63.35	-85.46	-63.17	MH111
MH112	45 21.05	-121 48.86	4971.0	980260.32	980661.05	11.80	19.84	1.41	66.60	-84.51	-61.87	MH112
MH113	45 20.29	-121 43.80	5744.0	980206.00	980659.92	0.05	11.41	1.48	86.06	-99.92	-72.85	MH113
MH114	45 20.98	-121 44.70	5764.0	980208.90	980660.95	0.08	14.45	1.48	89.81	-93.82	-66.31	MH114
MH115	45 21.69	-121 44.85	5686.0	980211.57	980662.02	0.14	14.73	1.48	84.08	-96.59	-69.53	MH115

ID	LAT	LONG	ELEV	OG	THG	HTC	TTC	CC	FAA	CBA1	CBA2	ID
MH116	45 22.87	-121 45.78	4451.0	980297.07	980662.59	0.22	10.20	1.34	52.94	-90.00	-60.59	MH116
MH117	45 22.77	-121 47.01	3299.0	980373.29	980663.64	0.06	7.09	1.11	19.75	-86.80	-70.84	MH117
MH118	45 23.48	-121 48.63	2739.0	980412.88	980664.71	0.01	5.17	0.98	5.71	-83.51	-70.14	MH118
MH119	45 19.28	-121 46.86	3806.9	980329.67	980658.27	0.02	4.48	1.22	29.24	-97.31	-70.35	MH119
MH120	45 19.30	-121 43.89	4997.0	980252.68	980658.43	0.09	7.26	1.41	64.03	-100.55	-75.90	MH120
MH121	45 26.47	-121 35.66	3169.0	980386.00	980669.22	0.02	4.13	1.08	14.75	-90.29	-74.56	MH121
MH122	45 27.57	-121 35.83	2787.0	980411.89	980670.07	0.01	3.08	0.99	3.07	-89.89	-75.96	MH122
MH123	45 28.16	-121 35.13	2510.0	980430.47	980671.76	0.01	2.79	0.91	-5.28	-89.01	-76.46	MH123
MH124	45 29.63	-121 35.12	2026.0	980464.33	980673.97	0.01	2.74	0.77	-19.13	-86.26	-76.20	MH124
MH125	45 32.18	-121 31.87	3779.0	980358.57	980677.79	4.75	10.66	1.22	36.08	-83.37	-65.47	MH125
MH126	45 30.32	-121 29.34	3954.0	980350.01	980675.00	0.00	3.96	1.25	46.76	-85.39	-65.60	MH126
MH127	45 29.88	-121 26.90	3370.0	980390.35	980674.34	0.04	3.68	1.13	32.86	-79.53	-62.69	MH127
MH128	45 29.66	-121 30.65	3986.0	980344.91	980674.01	0.00	4.34	1.26	45.66	-87.20	-67.30	MH128
MH129	45 27.87	-121 31.60	4444.0	980303.51	980671.31	0.53	11.07	1.33	50.01	-91.83	-70.50	MH129
MH130	45 25.24	-121 31.22	4316.0	980316.84	980667.35	0.00	3.74	1.31	55.26	-89.52	-67.83	MH130
MH131	45 24.55	-121 32.91	4230.0	980321.00	980666.32	0.02	4.07	1.30	53.18	-88.32	-67.12	MH131
MH132	45 27.77	-121 37.52	2845.0	980409.29	980671.17	0.00	3.43	1.00	5.63	-88.98	-74.80	MH132
MH133	45 26.05	-121 40.07	3589.0	980356.46	980668.58	0.26	8.04	1.18	25.33	-90.22	-72.91	MH133
MH134	45 27.01	-121 39.64	3590.0	980357.46	980670.02	0.22	5.18	1.18	24.97	-93.47	-75.72	MH134
MH135	45 26.85	-121 41.01	3670.0	980352.84	980669.78	0.01	4.46	1.20	28.11	-93.79	-75.53	MH135
MH136	45 26.56	-121 43.25	4747.0	980279.89	980669.35	0.30	8.47	1.38	56.82	-97.99	-74.80	MH136
MH137	45 26.79	-121 31.36	4912.0	980274.62	980669.69	9.21	16.50	1.40	66.72	-85.71	-62.87	MH137
MH138	45 26.65	-121 27.81	3632.0	980364.48	980669.47	0.01	2.75	1.19	36.49	-85.82	-67.50	MH138
MH139	45 26.34	-121 29.37	3449.0	980376.63	980669.01	0.08	4.79	1.15	31.98	-82.89	-65.82	MH139
MH140	45 27.77	-121 29.21	3448.0	980376.33	980671.16	0.03	2.81	1.15	29.36	-86.58	-69.21	MH140
MH141	45 28.83	-121 27.57	3830.0	980487.71	980672.77	0.07	2.95	1.05	19.84	-81.69	-66.41	MH141
MH142	45 27.20	-121 26.34	3258.0	980389.53	980670.31	0.02	2.03	1.11	25.55	-84.64	-68.13	MH142
MH143	45 24.63	-121 28.05	4627.0	980295.56	980666.44	0.02	6.37	1.36	64.12	-88.68	-65.79	MH143
MH144	45 23.81	-121 24.60	3475.0	980377.45	980665.21	0.01	2.10	1.15	38.97	-78.61	-60.99	MH144
MH145	45 22.79	-121 26.78	3683.0	980358.92	980663.67	0.03	3.04	1.20	41.53	-81.44	-63.02	MH145
MH146	45 23.15	-121 28.66	4561.0	980302.79	980664.22	0.04	4.51	1.35	67.38	-85.03	-62.19	MH146
MH147	45 21.04	-121 26.41	4309.0	980319.89	980661.03	0.01	4.02	1.31	63.17	-81.00	-59.47	MH147
MH148	45 19.08	-121 27.92	5651.0	980218.77	980658.89	6.85	16.73	1.47	91.91	-85.57	-58.98	MH148
MH149	45 20.31	-121 27.52	4753.0	980287.60	980659.94	0.28	5.92	1.38	74.51	-83.06	-59.45	MH149
MH150	45 21.54	-121 29.07	5217.0	980258.67	980661.80	0.02	6.22	1.43	87.33	-85.02	-59.88	MH150
MH151	45 20.56	-121 31.38	6525.0	980157.61	980660.31	9.41	23.33	1.51	110.66	-90.07	-60.00	MH151
MH152	45 22.92	-121 32.11	5143.0	980257.45	980663.87	0.01	6.98	1.43	77.08	-92.77	-67.33	MH152
MH153	45 25.43	-121 36.73	3982.0	980334.81	980667.64	0.10	4.88	1.26	41.56	-90.63	-70.83	MH153
MH154	45 25.47	-121 38.83	4588.0	980291.06	980667.70	0.05	7.40	1.36	54.70	-95.74	-73.20	MH154
MH155	45 24.93	-121 38.19	4811.0	980278.00	980666.89	0.02	7.31	1.39	63.41	-94.76	-71.86	MH155
MH156	45 24.00	-121 38.80	5718.0	980213.74	980665.49	0.01	10.92	1.48	85.78	-99.80	-72.00	MH156
MH157	45 31.66	-121 37.80	1660.0	980488.61	980677.03	0.09	2.98	0.65	-32.32	-86.69	-78.54	MH157
MH158	45 27.98	-121 39.77	3837.0	980341.12	980671.48	0.02	8.18	1.23	30.39	-93.52	-74.96	MH158

ID	LAT	LONG	ELEV	OG	THG	HTC	TTC	CC	FAA	CBA1	CBA2	ID
MH159	45 28.93	-121 39.39	3204.0	980385.83	980672.92	0.04	3.35	1.09	14.17	-92.85	-78.82	MH159
MH160	45 29.43	-121 38.18	2678.0	980420.87	980673.66	0.00	2.96	0.96	-1.74	-90.80	-77.46	MH160
MH161	45 30.09	-121 39.98	3212.0	980389.21	980674.65	0.00	3.19	1.09	16.57	-90.89	-74.79	MH161
MH162	45 29.56	-121 40.72	3726.0	980354.94	980673.86	0.00	4.80	1.21	31.40	-92.09	-73.59	MH162
MH163	45 27.93	-121 42.00	4450.0	980303.22	980671.40	0.01	6.61	1.34	50.19	-96.31	-74.36	MH163
MH164	45 29.51	-121 42.25	3636.0	980362.44	980673.79	0.05	3.64	1.19	30.51	-91.85	-72.84	MH164
MH165	45 29.52	-121 43.74	4378.0	980306.85	980672.30	0.03	9.14	1.32	46.15	-95.35	-74.15	MH165
MH166	45 30.87	-121 42.77	3778.0	980350.76	980675.83	0.26	9.96	1.22	30.14	-89.97	-71.98	MH166
MH167	45 27.66	-121 44.37	3975.0	980331.21	980671.00	0.21	6.05	1.26	33.94	-96.84	-77.25	MH167
MH168	45 26.44	-121 46.24	2615.0	980417.60	980669.16	0.01	6.60	0.94	-5.68	-89.21	-76.78	MH168
MH169	45 29.39	-121 36.31	2234.0	980449.04	980673.61	0.02	2.86	0.83	-14.58	-88.67	-77.56	MH169
MH170	45 24.15	-121 46.49	4591.0	980283.13	980665.73	11.38	17.14	1.36	49.83	-91.77	-78.68	MH170
MH171	45 24.91	-121 47.58	4534.0	980288.49	980666.87	10.78	16.48	1.35	47.89	-91.62	-78.72	MH171
MH172	45 28.91	-121 48.81	3148.0	980395.81	980672.89	0.01	3.03	1.08	18.91	-86.51	-78.71	MH172
MH173	45 29.17	-121 47.56	3810.0	980338.67	980671.77	14.10	17.01	1.22	25.11	-89.05	-71.94	MH173
MH174	45 30.85	-121 46.67	2651.0	980425.62	980675.79	0.01	3.91	0.95	-8.91	-88.37	-75.26	MH174
MH175	45 29.76	-121 47.68	4468.0	980296.43	980674.15	12.16	19.57	1.34	42.34	-91.82	-71.72	MH175
MH176	45 28.68	-121 36.89	5860.0	980256.98	980668.50	0.02	6.88	1.42	72.18	-95.73	-70.58	MH176
MH177	45 21.51	-121 36.21	4801.0	980276.40	980661.76	0.17	6.56	1.39	66.88	-92.57	-68.81	MH177
MH178	45 22.86	-121 35.67	4169.0	980320.62	980663.79	0.09	6.66	1.29	48.79	-88.03	-67.53	MH178
MH179	45 23.96	-121 35.49	3744.0	980354.68	980665.43	0.40	5.98	1.21	41.26	-81.65	-63.25	MH179
MH180	45 19.38	-121 38.80	4472.0	980292.79	980658.54	0.00	4.56	1.34	54.68	-94.62	-72.25	MH180
MH181	45 19.10	-121 33.59	5916.0	980195.45	980658.12	10.28	19.60	1.49	93.47	-90.19	-62.68	MH181
MH182	45 19.87	-121 31.47	3899.0	980341.40	980658.07	0.03	7.27	1.24	49.91	-77.04	-58.02	MH182
MH183	45 19.88	-121 30.30	3586.0	980358.75	980658.09	3.52	7.91	1.18	37.83	-77.75	-60.43	MH183
MH184	45 18.80	-121 29.96	3424.0	980368.00	980657.67	3.56	8.19	1.14	32.27	-77.47	-61.83	MH184
MH185	45 17.49	-121 28.80	3049.0	980386.84	980655.71	0.87	8.55	1.06	17.82	-78.69	-64.22	MH185
MH186	45 17.08	-121 27.95	2848.0	980397.40	980655.08	0.18	8.57	1.00	10.11	-79.46	-66.04	MH186
MH187	45 16.12	-121 26.36	2549.0	980409.29	980653.64	0.29	7.60	0.92	-4.67	-84.93	-72.91	MH187
MH188	45 16.37	-121 29.87	4378.0	980299.25	980654.02	8.37	4.24	1.32	56.08	-98.05	-68.16	MH188
MH189	45 15.44	-121 29.34	4261.0	980299.97	980652.62	0.02	3.93	1.31	47.96	-94.75	-73.37	MH189
MH190	45 19.97	-121 39.86	5358.0	980229.32	980659.44	0.01	8.81	1.45	73.59	-101.79	-75.52	MH190
MH191	45 21.03	-121 39.44	5550.0	980215.57	980661.03	0.28	12.91	1.47	76.29	-101.56	-74.91	MH191
MH192	45 21.14	-121 37.99	5656.0	980213.07	980661.19	0.05	8.57	1.47	83.59	-102.22	-74.39	MH192
MH193	45 21.56	-121 38.74	6633.0	980140.46	980661.82	9.97	22.82	1.52	102.15	-102.78	-72.88	MH193
MH194	45 22.43	-121 39.58	7360.0	980096.09	980663.13	0.39	22.73	1.51	124.78	-105.82	-70.60	MH194
MH195	45 23.41	-121 39.48	6658.0	980146.84	980664.60	0.12	16.72	1.52	107.34	-104.26	-72.56	MH195
MH196	45 31.43	-121 34.00	1649.0	980493.41	980676.60	0.00	3.41	0.65	-28.21	-81.68	-73.67	MH196
MH197	45 29.86	-121 33.68	1831.0	980478.63	980674.31	0.02	5.71	0.71	-23.51	-88.96	-72.35	MH197
MH198	45 27.89	-121 34.12	2157.0	980452.56	980671.34	0.83	6.23	0.81	-15.95	-84.10	-73.89	MH198
MH199	45 26.77	-121 34.67	2401.0	980434.28	980669.66	0.03	8.16	0.88	-9.61	-84.23	-73.85	MH199
MH200	45 23.70	-121 34.14	3075.0	980391.24	980665.04	0.06	9.03	1.06	15.33	-81.50	-67.06	MH200
MH201	45 22.45	-121 33.96	3305.0	980364.42	980663.16	0.02	7.46	1.12	12.01	-94.37	-78.44	MH201

ID	LAT	LONG	ELEV	OG	THG	HTC	TTC	CC	FAA	CBA1	CBA2	ID
MH202	45 20.37	-121 34.19	3550.0	980357.88	980660.04	0.01	7.85	1.17	32.37	-82.30	-65.12	MH202
MH203	45 31.19	-121 36.52	1704.0	980485.98	980676.32	0.01	2.43	0.67	-30.10	-86.46	-78.01	MH203
MH204	45 30.78	-121 40.99	2803.0	980416.45	980675.69	0.28	5.24	0.99	4.32	-87.04	-73.35	MH204
MH205	45 30.52	-121 50.08	4057.0	980334.62	980675.30	16.04	28.01	1.27	40.75	-78.08	-60.96	MH205
MH206	45 24.28	-121 39.90	5994.0	980192.55	980665.80	0.31	15.28	1.58	90.22	-100.43	-71.87	MH206
MH207	45 24.34	-121 41.45	5915.0	980198.93	980666.00	0.00	13.85	1.49	88.98	-100.40	-72.03	MH207
MH208	45 24.84	-121 41.87	5828.0	980203.62	980666.76	0.00	15.23	1.49	84.73	-100.30	-72.50	MH208
MH209	45 24.76	-121 43.81	5653.0	980217.43	980666.64	0.13	12.82	1.47	82.21	-99.25	-72.06	MH209
MH210	45 24.16	-121 43.89	5579.0	980221.75	980665.73	0.10	14.12	1.47	80.49	-97.14	-70.53	MH210
MH211	45 21.37	-121 51.86	3866.0	980389.96	980661.53	0.12	6.40	1.06	16.71	-82.52	-67.65	MH211
MH212	45 22.49	-121 51.49	2450.0	980427.46	980663.23	0.58	6.61	0.90	-5.40	-83.24	-71.58	MH212
MH213	45 23.53	-121 49.91	2895.0	980401.58	980664.79	0.05	4.85	1.02	9.00	-85.91	-71.69	MH213
MH214	45 24.81	-121 53.99	2571.0	980421.18	980665.51	0.20	4.81	0.93	-2.58	-87.19	-74.51	MH214
MH215	45 24.88	-121 52.53	2943.0	980399.69	980666.78	0.08	3.80	1.03	9.71	-87.90	-73.27	MH215
MH216	45 25.75	-121 51.35	3633.0	980357.57	980668.12	0.01	2.73	1.19	31.03	-91.34	-73.81	MH216
MH217	45 26.99	-121 53.86	2791.0	980414.86	980669.99	0.06	2.38	0.99	7.38	-86.50	-72.45	MH217
MH218	45 26.03	-121 52.80	3043.0	980396.86	980668.54	0.03	4.32	1.05	13.64	-86.88	-71.83	MH218
MH219	45 27.04	-121 52.38	2938.0	980404.65	980670.06	0.19	3.42	1.03	10.84	-86.98	-72.32	MH219
MH220	45 28.43	-121 54.16	2739.0	980421.78	980672.15	0.01	2.58	0.98	7.09	-84.72	-70.97	MH220
MH221	45 28.71	-121 52.73	2622.0	980427.81	980672.58	0.09	4.78	0.94	0.97	-84.62	-71.88	MH221
MH222	45 29.52	-121 54.06	2489.0	980437.07	980673.88	0.01	3.39	0.91	-2.78	-85.10	-72.76	MH222
MH223	45 27.65	-121 50.64	3166.0	980392.23	980670.98	0.09	2.94	1.08	18.93	-87.19	-71.30	MH223
MH224	45 26.17	-121 49.87	4112.0	980324.46	980668.76	0.09	5.48	1.28	42.38	-93.82	-73.43	MH224
MH225	45 27.23	-121 48.32	4565.0	980284.17	980670.35	15.68	22.36	1.35	43.88	-91.69	-71.51	MH225
MH226	45 27.94	-121 49.43	4338.0	980308.38	980671.43	9.66	14.79	1.32	44.80	-89.68	-69.54	MH226
MH227	45 28.38	-121 50.86	4566.0	980291.15	980672.08	10.74	16.84	1.35	48.34	-91.98	-70.89	MH227
MH228	45 25.12	-121 46.11	2999.0	980388.93	980667.18	0.80	8.79	1.04	3.74	-90.88	-76.64	MH229
MH230	45 29.91	-121 58.65	2935.0	980405.07	980674.38	0.00	5.88	1.03	6.65	-88.60	-74.33	MH230
MH231	45 20.82	-121 46.78	4185.0	980311.17	980659.58	0.00	5.14	1.29	45.13	-93.76	-72.95	MH231
MH232	45 22.48	-121 41.69	11235.0	979763.58	980663.09	42.52	125.87	0.87	156.25	-181.94	-63.26	MH232
GS 1	45 18.18	-121 49.23	2798.0	980394.28	980656.74	0.89	7.37	0.99	-0.28	-88.98	-75.68	GS 1
GS 2	45 18.28	-121 43.16	4380.0	980292.94	980656.89	0.03	4.57	1.32	47.85	-98.38	-76.48	GS 2
GS 3	45 15.73	-121 38.39	4515.0	980283.25	980653.85	0.10	5.69	1.35	54.68	-94.97	-72.55	GS 3
GS 4	45 17.15	-121 40.26	4881.0	980328.43	980655.19	0.01	3.83	1.27	48.93	-88.58	-67.91	GS 4
GS 5	45 18.14	-121 36.13	4195.0	980306.98	980656.68	0.19	4.45	1.29	44.71	-95.21	-74.25	GS 5
GS 6	45 26.38	-121 37.40	3685.0	980357.47	980669.07	0.01	4.57	1.20	34.86	-87.45	-69.12	GS 6
GS 7	45 24.75	-121 36.23	3920.0	980339.03	980666.62	0.05	5.08	1.24	40.96	-88.98	-69.44	GS 7
GS 8	45 23.70	-121 29.90	4577.0	980301.26	980665.04	0.00	3.98	1.35	66.53	-86.95	-63.96	GS 8
GS 9	45 25.66	-121 32.86	3923.0	980339.45	980667.99	0.03	3.83	1.25	48.29	-90.92	-71.26	GS 9
GS10	45 26.46	-121 32.51	3730.0	980357.77	980669.19	0.01	4.07	1.21	39.27	-85.08	-66.45	GS10
GS11	45 21.38	-121 33.99	3445.0	980366.99	980661.55	0.00	6.93	1.15	29.35	-82.37	-65.63	GS11
GS12	45 17.50	-121 34.83	5220.0	980242.74	980655.71	0.39	6.52	1.44	77.76	-95.19	-69.28	GS12
GS13	45 18.41	-121 34.28	5585.0	980219.18	980657.88	0.38	18.61	1.47	87.13	-94.21	-67.04	GS13

ID	LAT	LONG	ELEV	OG	THG	HTC	TTC	CC	FAA	CBA1	CBA2	ID
GS14	45 20.00	-121 32.86	5220.0	980256.40	980659.48	0.01	7.07	1.44	87.66	-84.74	-58.91	GS14
GS15	45 22.85	-121 31.75	5495.0	980238.42	980662.56	0.01	8.48	1.46	92.44	-88.04	-61.00	GS15
GS16	45 21.48	-121 30.45	5685.0	980225.79	980661.70	0.00	8.37	1.48	90.52	-89.48	-60.47	GS16
GS17	45 23.82	-121 51.76	2870.0	980453.61	980664.02	0.00	5.15	0.78	-15.76	-82.00	-72.07	GS17
GS18	45 23.13	-121 50.33	2330.0	980437.13	980664.18	0.00	5.09	0.86	-7.96	-83.20	-71.93	GS18
GS19	45 23.03	-121 49.20	2940.0	980397.81	980664.03	0.25	4.69	1.03	10.21	-86.48	-71.93	GS19
GS20	45 21.43	-121 47.63	3230.0	980374.11	980661.63	4.76	8.86	1.10	16.18	-86.22	-70.88	GS20
GS21	45 23.79	-121 50.91	2540.0	980427.30	980665.18	0.02	3.92	0.92	0.95	-82.68	-70.15	GS21
GS22	45 24.44	-121 49.45	2900.0	980400.79	980666.16	0.12	4.69	1.02	7.31	-87.93	-73.66	GS22
GS23	45 24.06	-121 49.65	3410.0	980372.07	980665.58	0.57	5.33	1.14	27.90	-84.21	-67.41	GS23
GS24	45 24.19	-121 47.57	3865.0	980334.34	980665.78	0.33	6.54	1.23	31.95	-94.57	-75.62	GS24
GS25	45 23.28	-121 47.55	3015.0	980388.62	980664.41	0.39	6.34	1.05	7.78	-89.84	-75.23	GS25
GS26	45 23.75	-121 47.91	2820.0	980403.54	980665.12	0.08	5.88	1.00	3.58	-87.88	-74.11	GS26
GS27	45 23.43	-121 48.46	2750.0	980410.61	980664.63	0.00	5.31	0.98	4.55	-84.91	-71.51	GS27
GS28	45 19.11	-121 42.83	5220.0	980238.18	980658.14	0.38	7.94	1.44	78.78	-100.75	-75.85	GS28
GS29	45 18.79	-121 43.17	4920.0	980258.02	980657.65	0.01	6.59	1.40	62.91	-99.78	-75.34	GS29
GS30	45 16.82	-121 43.94	3620.0	980342.43	980654.69	0.08	2.54	1.19	28.10	-94.01	-75.72	GS30
GS31	45 17.91	-121 42.97	4192.0	980306.08	980656.33	0.03	3.94	1.29	43.87	-96.46	-75.43	GS31
GS32	45 17.63	-121 43.21	4040.0	980315.20	980655.91	0.05	3.56	1.27	39.13	-96.37	-76.87	GS32
N 1	45 19.85	-121 42.54	5910.0	980192.75	980659.25	0.01	11.35	1.49	89.08	-102.63	-73.91	N 1
N 2	45 19.90	-121 42.56	5949.0	980190.03	980659.32	0.04	11.66	1.49	89.95	-102.79	-73.91	N 2
N 3	45 19.94	-121 42.59	6004.0	980186.02	980659.38	0.04	12.17	1.50	91.04	-103.06	-73.98	N 3
N 4	45 19.99	-121 42.62	6041.0	980183.54	980659.46	0.05	12.50	1.50	91.97	-103.07	-73.85	N 4
N 5	45 20.03	-121 42.62	6101.0	980179.21	980659.52	0.16	12.89	1.50	93.22	-103.48	-74.01	N 5
N 6	45 20.07	-121 42.66	6148.0	980175.88	980659.58	0.08	13.07	1.50	94.24	-103.88	-74.20	N 6
N 7	45 20.11	-121 42.67	6190.0	980173.00	980659.65	0.11	13.24	1.50	95.24	-104.15	-74.28	N 7
N 8	45 20.15	-121 42.67	6229.0	980170.41	980659.71	0.07	13.38	1.51	96.25	-104.33	-74.28	N 8
N 9	45 20.20	-121 42.68	6274.0	980167.30	980659.78	0.11	13.72	1.51	97.30	-104.47	-74.24	N 9
N10	45 20.24	-121 42.68	6315.0	980164.54	980659.84	0.04	13.99	1.51	98.33	-104.57	-74.17	N10
N11	45 20.29	-121 42.70	6357.0	980161.59	980659.90	0.07	14.48	1.51	99.26	-104.58	-74.04	N11
N12	45 20.32	-121 42.70	6412.0	980157.52	980659.95	0.10	15.21	1.51	100.31	-104.68	-73.97	N12
N13	45 20.35	-121 42.71	6460.0	980153.95	980660.01	0.10	15.89	1.51	101.20	-104.75	-73.90	N13
N14	45 20.38	-121 42.72	6504.0	980150.69	980660.05	0.07	16.54	1.51	102.03	-104.77	-73.79	N14
N15	45 20.42	-121 42.74	6553.0	980147.00	980660.11	0.07	17.28	1.51	102.89	-104.85	-73.73	N15
N16	45 20.45	-121 42.77	6605.0	980142.95	980660.15	0.12	18.09	1.52	103.68	-105.02	-73.76	N16
N17	45 20.48	-121 42.78	6646.0	980139.88	980660.19	0.06	18.42	1.52	104.34	-105.43	-74.00	N17
N18	45 20.52	-121 42.76	6691.0	980136.58	980660.26	0.06	18.17	1.52	105.28	-106.28	-74.58	N18
N19	45 20.56	-121 42.76	6741.0	980132.90	980660.31	0.10	18.38	1.52	106.24	-106.81	-74.89	N19
N20	45 20.58	-121 42.76	6784.0	980129.68	980660.35	0.10	18.59	1.52	107.03	-107.28	-75.18	N20
N21	45 20.63	-121 42.75	6858.0	980124.62	980660.43	0.10	18.98	1.52	108.84	-107.68	-75.17	N21
S 1	45 19.86	-121 42.67	5932.0	980190.92	980659.27	0.04	11.65	1.49	89.30	-102.87	-74.08	S 1
S 2	45 19.82	-121 42.68	5886.0	980194.21	980659.21	0.04	11.19	1.49	88.32	-102.73	-74.10	S 2
S 3	45 19.79	-121 42.68	5854.0	980196.48	980659.16	0.05	10.90	1.49	87.56	-102.69	-74.19	S 3

ID	LAT	LONG	ELEV	OG	THG	HTC	TTC	CC	FAA	CBA1	CBA2	ID
S 4	45 19.75	-121 42.69	5804.0	980199.95	980659.09	0.06	10.51	1.48	86.47	-102.46	-74.15	S 4
S 5	45 19.70	-121 42.70	5759.0	980202.99	980659.03	0.06	10.26	1.48	85.35	-102.30	-74.18	S 5
S 6	45 19.66	-121 42.71	5696.0	980207.48	980658.96	0.07	10.04	1.48	83.99	-101.72	-73.98	S 6
S 7	45 19.62	-121 42.71	5640.0	980211.36	980658.90	0.07	9.95	1.47	82.67	-101.22	-73.67	S 7
S 8	45 19.57	-121 42.71	5582.0	980215.50	980658.83	0.05	9.93	1.47	81.43	-100.49	-73.24	S 8
S 9	45 19.52	-121 42.72	5541.0	980218.19	980658.75	0.07	9.86	1.46	80.34	-100.25	-73.19	S 9
S10	45 19.47	-121 42.73	5452.0	980223.92	980658.68	0.17	9.39	1.46	77.78	-100.24	-73.57	S10
S11	45 19.42	-121 42.73	5411.0	980226.70	980658.61	0.23	9.02	1.45	76.78	-100.20	-73.69	S11
S12	45 19.38	-121 42.74	5387.0	980228.33	980658.54	0.19	8.72	1.45	76.22	-100.24	-73.80	S12
S13	45 19.33	-121 42.76	5346.0	980231.06	980658.46	0.21	8.37	1.45	75.18	-100.24	-73.96	S13
S14	45 19.27	-121 42.76	5349.0	980230.50	980658.37	0.01	8.16	1.45	74.99	-100.74	-74.41	S14
E 1	45 19.99	-121 42.57	6022.0	980185.01	980659.47	0.05	12.19	1.50	91.64	-103.05	-73.89	E 1
E 2	45 19.98	-121 42.51	6019.0	980185.07	980659.45	0.05	12.12	1.50	91.44	-103.22	-74.06	E 2
E 3	45 20.01	-121 42.42	5998.0	980187.31	980659.49	0.15	12.15	1.50	90.91	-102.73	-73.72	E 3
E 4	45 20.03	-121 42.33	5977.0	980188.06	980659.52	0.50	12.76	1.49	90.41	-102.18	-73.33	E 4
E 5	45 20.01	-121 42.26	5951.0	980189.68	980659.50	0.01	12.30	1.49	89.61	-102.55	-73.76	E 5
E 6	45 20.02	-121 42.18	5939.0	980190.38	980659.50	0.03	12.23	1.49	89.18	-102.64	-73.91	E 6
W 1	45 19.98	-121 42.65	6058.0	980182.17	980659.44	0.05	12.86	1.50	92.21	-103.04	-73.79	W 1
W 2	45 19.99	-121 42.70	6071.0	980181.14	980659.46	0.05	13.04	1.50	92.38	-103.14	-73.85	W 2
W 3	45 20.00	-121 42.76	6083.0	980180.15	980659.47	0.85	13.21	1.50	92.51	-103.25	-73.92	W 3
W 4	45 20.01	-121 42.80	6072.0	980181.05	980659.50	0.05	12.87	1.50	92.35	-103.37	-74.05	W 4
W 5	45 20.03	-121 42.84	6067.0	980181.43	980659.52	0.11	12.83	1.50	92.23	-103.36	-74.06	W 5
W 6	45 20.04	-121 42.89	6044.0	980182.81	980659.53	0.12	12.62	1.50	90.65	-104.37	-75.15	W 6
W 7	45 20.04	-121 42.89	6045.0	980182.73	980659.54	0.05	12.56	1.50	91.45	-103.66	-74.43	W 7
W 8	45 20.05	-121 43.02	6057.0	980181.17	980659.55	0.05	12.55	1.50	91.01	-104.52	-75.23	W 8
W 9	45 20.06	-121 43.10	6033.0	980182.41	980659.57	0.22	12.61	1.50	89.98	-104.68	-75.51	W 9
W10	45 20.06	-121 43.16	6032.0	980182.13	980659.57	0.05	12.52	1.50	89.60	-105.11	-75.94	W10
CS33	45 19.71	-121 42.60	5776.0	980202.29	980659.04	0.12	10.37	1.48	86.23	-101.88	-73.70	CS33

HEAT FLOW MODELING OF THE MOUNT HOOD VOLCANO, OREGON

By

DAVID D. BLACKWELL
and
JOHN L. STEELE

Department of Geological Sciences

Southern Methodist University

Dallas, Texas 75275

June 1979

Final report of work carried out under Grant SMU #86-09 from the Oregon Department of Geology and Mineral Industries; July 1977 through March 1979.

TABLE OF CONTENTS

LIST OF FIGURES

LIST OF FIGURES (Con't.) Page

LIST OF TABLES

INTRODUCTION

Most of the currently active volcanoes are associated with volcanic arcs which form over subducting slabs of lithosphere in plate collision areas. Large stratocone volcanoes of generally andesitic composition are typically associated with these active volcanic arcs, although extrusions of basaltic composition are probably more volumetrically important. Along the western Pacific there is an almost continuous string of volcanic arcs associated with subducting slabs of lithosphere. Along the western margin of the North American Continent the subduction is more fragmented than in the western Pacific; however, there are several distinct regions where volcanic arcs are developed. These regions are the Aleutian arc of Alaska, the Cascade Range of the northwestern United States, the trans-Mexico volcanic belt in Mexico, and the Central American volcanic arc. Active subduction is definitely occurring at the first and last of these areas, as evidenced by large numbers of intermediate and deep focus earthquakes generated within the cold sinking block of lithosphere. Along southwestern Mexico there are numerous earthquakes of intermediate focal depth which generally line up to indicate a slab with a very shallow dip.

On the other hand, in the Pacific Northwest, there are no intermediate or deep focus earthquakes, so direct seismic evidence for the existence of a subducting slab does not exist. However, the deepest earthquakes in the conterminous United States (60 km) are associated with the Puget Sound area of

northwestern Washington, and so apparently the tectonic situation must be different in some way from the remainder of the western United States. Moreover, based on the evidence of abundant volcanism in the Cascade Range, and the present-day existence of many large stratocone volcanoes which would be rapidly removed by erosion, it is apparent that subduction has been active in the Pacific Northwest within the past few thousand years. Subduction may be continuing, but at a low level or with the block too hot to generate earthquakes.

Although extrusive rocks of basaltic composition often are volumetrically dominant in the volcanic arcs associated with subduction zones, the associated intrusive rocks are dominantly of granitic composition. Thus, it is felt that geothermal systems are more likely to be associated with volcanic rocks of andesitic to rhyolitic composition where the magmas are more viscous and more likely to solidify as intrusive rocks rather than proceed to the surface and be extruded (see Smith and Shaw, 1975). By cooling below the surface, more thermal energy is transferred into the shallow crust and hydrothermal convection systems are more likely to be formed. In fact, epizonal plutons probably cool dominantly, if not completely, by hydrothermal convection rather than conduction.

Around the world, many geothermal systems are associated with andesite volcanoes. In particular, several of the geothermal systems in Japan, such as Matzukawa and Otaki, are associated with stratocone volcanoes. In Central America, the geothermal fields at Ahuachapán, El Sálvador; Mombotambo, Nicaragua; and in Costa Rica are also associated with stratocone

volcanoes and are currently producing or will soon produce electrical power. Therefore, the Cascade Range of the Pacific Northwest represents an obvious focus for geothermal exploration. However, in spite of the abundant evidence of voluminous volcanism of variable composition in the Cascade Range, thermal manifestations are much more subdued than those typically associated with the island arcs. The only thermal manifestations which appear major from their surface evidence are associated with Mt. Lassen, in northern California. The remainder of the andesite volcanoes in the Cascade Range display only weak evidence of hydrothermal activity, although most of the volcanoes have vent fumaroles and have been historically active.

The overall thrust of this project was to investigate the geothermal potential of the Mt. Hood volcano as a guide to estimating the geothermal potential of other stratocone volcanoes in the Cascades. The assumption was made, therefore, that Mt. Hood represents a typical stratocone volcano and that the information obtained in the study of Mt. Hood could be transferred to other stratocone volcanoes in the western United States. A location map showing the Cascade stratovolcanoes is given in Figure 1. In view of the generality of the approach, part of the research carried out in the project was a more generally-oriented study of thermal effects of magma chamber systems associated with stratocone volcanoes and of regional heat flow in the Cascades.

The report is essentially divided into three sections. In the first section, some examples of simple cooling models of different shapes of magma chambers that might be associated

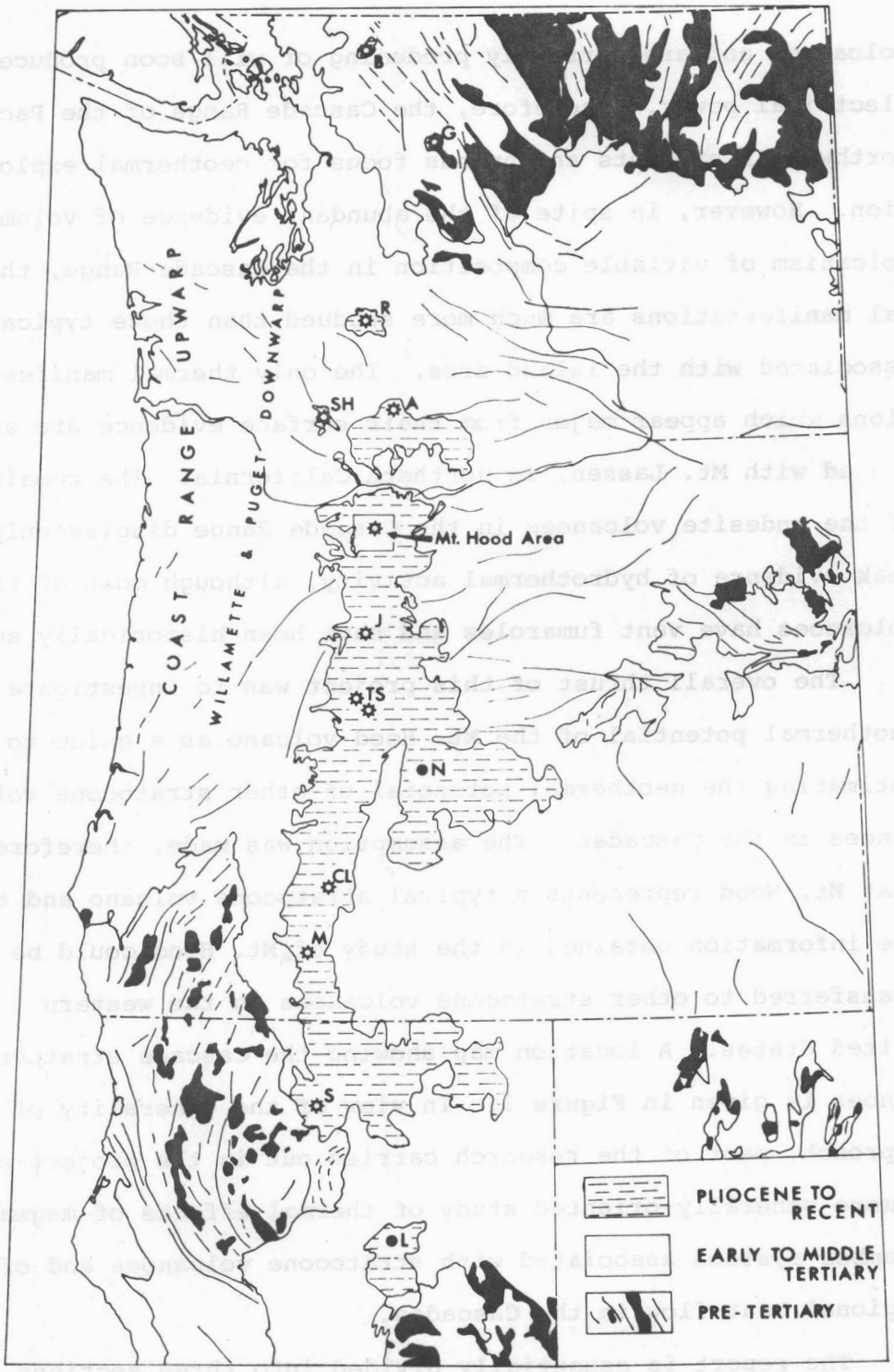

Figure 1. Location map of Cascade stratocone volcanoes (from Wise, 1969).

with stratocone volcanoes are discussed. These simple models are calculated in order to investigate the effects of different geometry on the total heat transfer of the system, rate of cooling, and volcanic recurrence times necessary to keep the crust hot.

In the second section, a description of a detailed study of the Western Cascade-High Cascade boundary in the Western Cascade province is discussed along with the results of heat flow studies along the eastern boundary of the Northern Cascade Range of Oregon. These studies are presented here for completeness and for comparison with the data obtained in the Mt. Hood region.

The final section is a discussion of the heat flow in the vicinity of Mt. Hood, including near-regional exploration holes, and deep exploration holes at Timberline Lodge and at Old Maid Flat at the foot of the Mt. Hood volcano.

THERMAL MODELS OF MAGMA CHAMBERS WITH SPECIFIC APPLICATIONS TO STRATOCONE VOLCANOES

Introduction

A number of different models for the cooling of magma chambers have been discussed in the literature. Most of the models have included discussion of the cooling of a magma emplaced instantaneously at constant temperature, with subsequent cooling from this constant initial temperature (Jaeger, 1963, 1964; Blackwell and Baag, 1974; Lachenbruch and others, 1976). In these models, the magma is assumed to cool conductively once it is in place, and no modifications are included to allow for possible convection in the magma during cooling, permeation of water through the cooling country rock or solidified intrusive rock, or any complexities that might be involved with emplacement of a major magma chamber. In the simplest form, the model predicts that the country rock temperature in contact with the magma chambers never reaches a temperature greater than 0.5 T_m,, where T_m is the melt temperature. This model is referred to as the instantaneous model.

Another simple conduction model for magma chamber evolution assumes emplacement of the magma at some time and its subsequent maintenance as a magma chamber over a long period of time. In this case, the rock in contact with the magma will eventually be heated up to the magma temperature. This model, the continuous mode, would be more appropriate for a long-lived magma chamber into which batches of magma were repeatedly emplaced or, for moderate times at least, a very large convecting

magma chamber. Of course, at some time such a chamber must eventually begin to cool off, but there is geological evidence that many magma chambers are resupplied by magma and thus can maintain a liquid zone over a long period of time relative to the cooling period of the instantaneous model.

If the magma chamber is maintained for an extreme period of time, the thermal effects eventually reach a steady-state. Ultimately, of course, the magma must start to cool off. Yuhara (1974) has presented some steady-state models of a linear volcano with a plane (vertical) source magma chamber. He illustrates the temperature for such a model for different depths to the plane source.

In general, the geological evidence indicates that most, if not all, magma chambers emplaced in the epizonal region of a crust (1-5 km) actually cool dominantly by convection of heated ground water through the cooling rock in a hydrothermal system. Very seldom is it likely that a large magma chamber would cool conductively. However, analysis of the rate of heat transfer in typical geothermal systems suggests that typical efficiency of convective cooling is not particularly great; the heat transferred by a convection system being on the order of two to ten times the rate of heat loss by conductive cooling alone. So the average heat loss for convective cooling as contrasted with conductive cooling of an active magma chamber might be estimated to be on the order of five.

Basic Model Shapes

Figure 2 shows a topographic cross-section along an

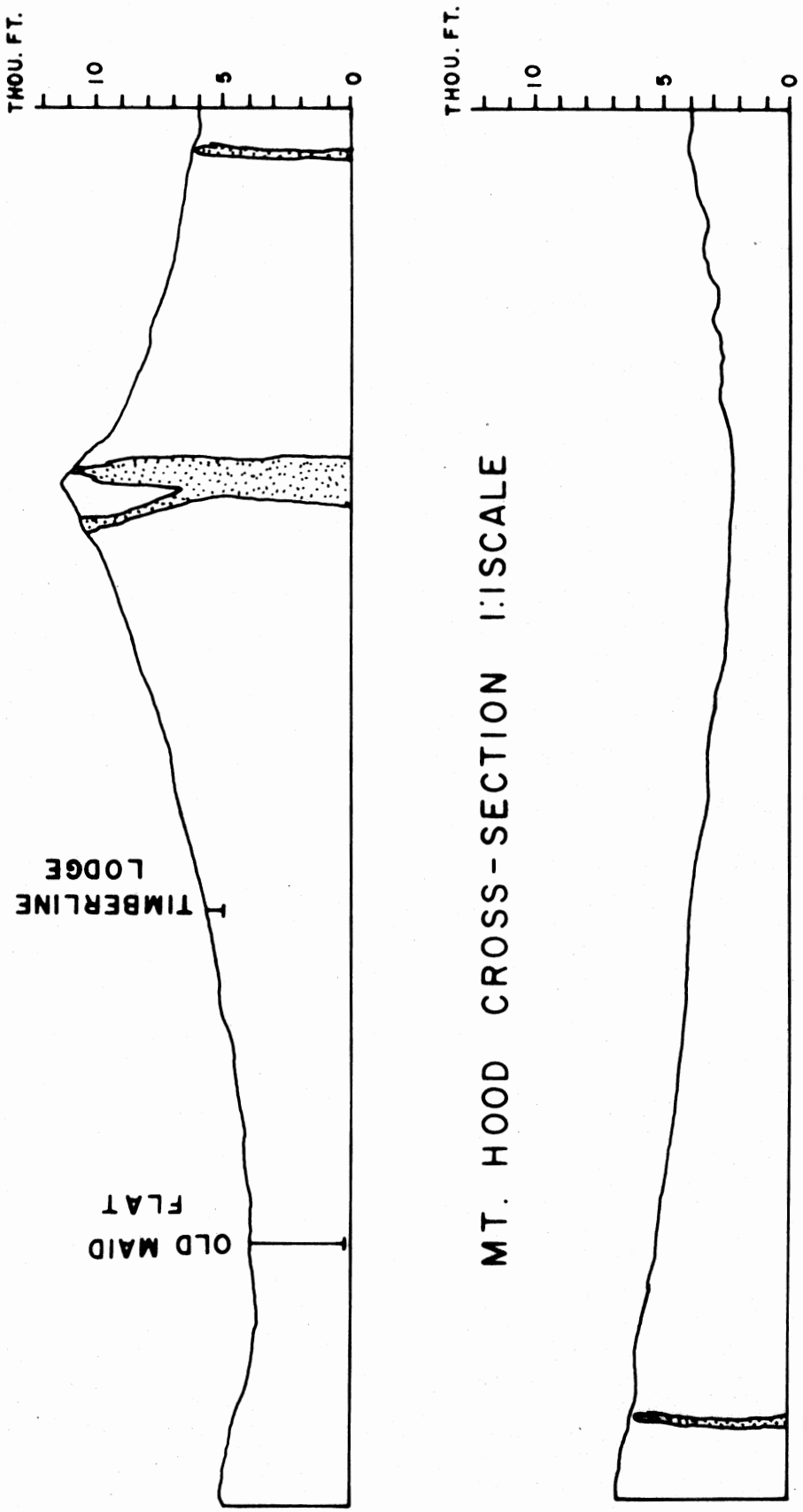

Figure 2. Topographic cross-section of Mt. Hood: east-west profile at a scale of 1:1. Locations and drilled depths of two major heat flow holes are shown.

approximately east-west line through Mt. Hood. This cross-section has equal horizontal and vertical scales. Also shown on the volcano are the locations and scaled depths of two relatively deep exploratory holes which have been drilled for geothermal studies.

Mt. Hood is a typical stratocone volcano. It has a relief of about 1.5 km and a radius of 5 km, giving an approximate surface area of 80 km^2 and a volume of 40 km^3. The geology of the volcano has been discussed by Wise (1968). Most of the volcano was formed in late Pleistocene, and a major eruption which formed most of the south flank of the volcano occurred about 1,600 years ago. The most recent major activity has been dated at about 220 years ago (Crandell and Rubin, 1977). The volcano was in minor eruption between 1848 and 1865, according to newspaper accounts. There is an active fumarolic system near the top of the volcano, but only a "single" thermal spring with several orifices is associated with the volcano (Swim Spring). The spring is along the southern edge of Mt. Hood.

In the discussion of the conductive cooling of magma chambers, two basic shapes will be considered (Figure 3). The first is a parallelepiped with infinite extent in the Y direction, a width equal to 2A, and a thickness equal to L, emplaced at a constant initial temperature (T_o), and at a depth D below the surface. This particular model might apply to a linear magma chamber, such as might exist if several stratocone volcanoes coalesced, or to a dike or sheet-like magma chamber. This sort of model might apply if there is a large regional magma chamber associated with the entire Cascade Range,

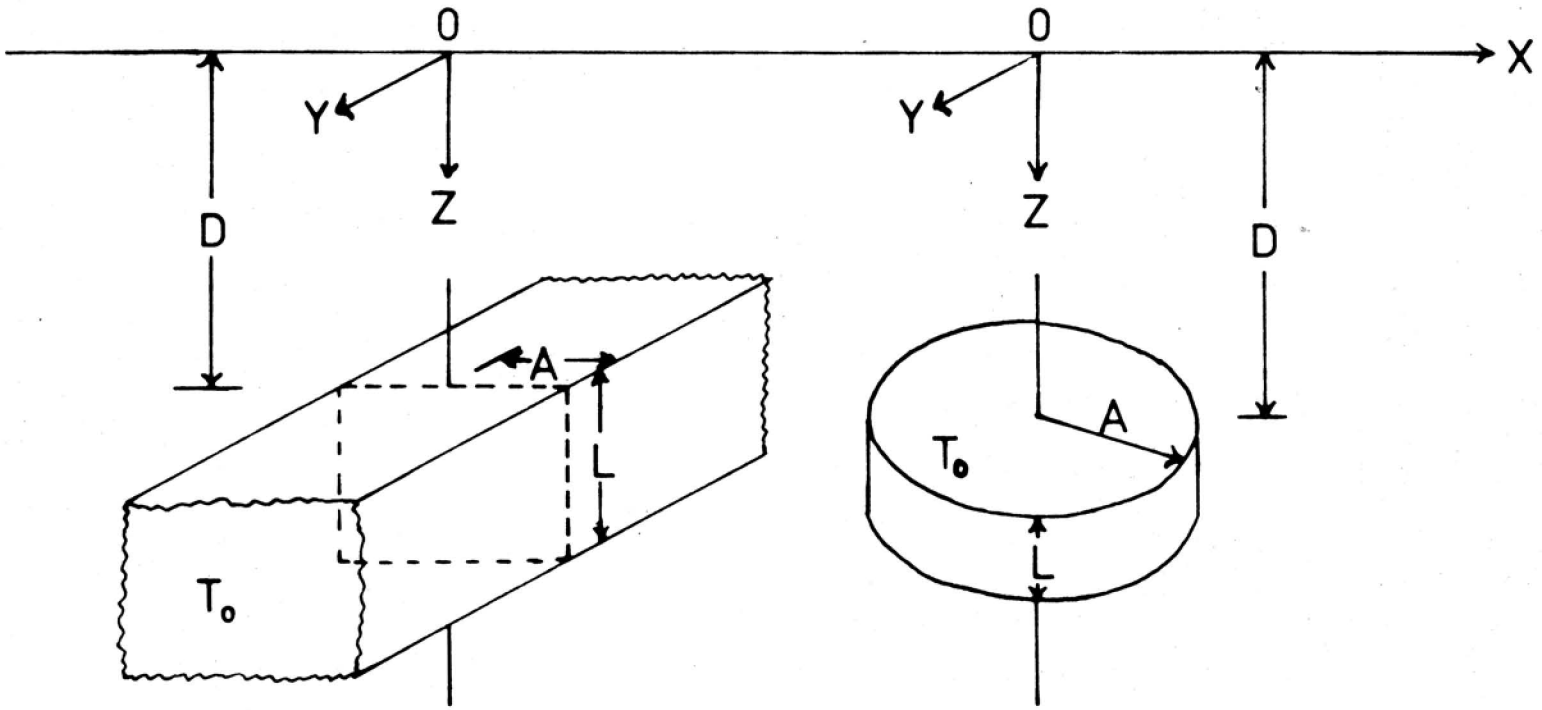

Figure 3. Basic model shapes for two-dimensional magma chamber models. A = half-width or radius; L = thickness; D = depth from surface to top of body; T_o = initial emplacement temperature.

rather than individual magma chambers associated with each stratocone volcano.

The other basic shape investigated is a cylinder that is considered to be buried at a depth D, to have a radius A, and a thickness L. This model would be more typical of a single magma chamber associated with a volcano, a volcanic pipe, or a very large circular magma chamber which might underlie several adjacent volcanoes. For example, it has been suggested by LaFehr (1965) that a single magma chamber may underlie the Medicine Lake Highland and Mt. Shasta area in California.

Comparing the two geometries, A is the half-width of the slab, or the radius of the cylinder; L is the thickness of the body; D is the depth of the top of the body from the surface; T_o is the initial temperature (assumed constant) of the body. In all the solutions, the medium is assumed to be homogeneous and to have constant thermal conductivity not dependent on temperature. In the solution, the magma is assumed to have the same thermal conductivity as the country rock. Intrinsically, although both are two-dimensional, a slab will have a larger heat content than a cylinder for equal values of A and D, and therefore will tend to cool more slowly.

In addition to the two types of geometry, two different models of magma chamber behaviors were calculated. The first of these is the instantaneous model discussed above, where emplacement of the magma at a given temperature takes place at a certain time and conductive cooling occurs subsequent to this emplacement. For the second set of models, the continuous

models, the magma is assumed to be emplaced at a constant temperature, and the boundary of the magma chamber is assumed to remain at this temperature for subsequent time so that the whole half-space is heated by the magma chamber.

In certain of the cases, a plane boundary above the magma chamber has been assumed so that a half-space solution applies. In several of the solutions for the cylinder, the effect of topography has been included so that the effect of the topographic edifice of the volcano on top of the magma chamber can be examined. In these models, the results have been illustrated for certain characteristic locations along the surface such as the apex of the volcano (A), the center of the slope (S), the toe (T), and the plane surface (F), as illustrated in Figure 4.

Plane Surface Instantaneous Magma Chamber Models

The plane surface instantaneous models are the simplest of the solutions and in the rectangular case have been discussed by many authors (Carslaw and Jaeger, 1959; Simmons, 1967; Blackwell and Baag, 1974; Lachenbruch and others, 1976). Some results for a spherical source and for a cylindrical source have been discussed in the literature (Carslaw and Jaeger, 1959; Rititaki, 1959; Blackwell and Baag, 1974). The object of this set of models is to show the relationship between heat flow, depth of burial, and cooling time. All solutions in this section can be calculated analytically from the results given by Carslaw and Jaeger (1959).

Throughout all these models, for consistency, certain shape parameters have been assumed to be constant. These have been

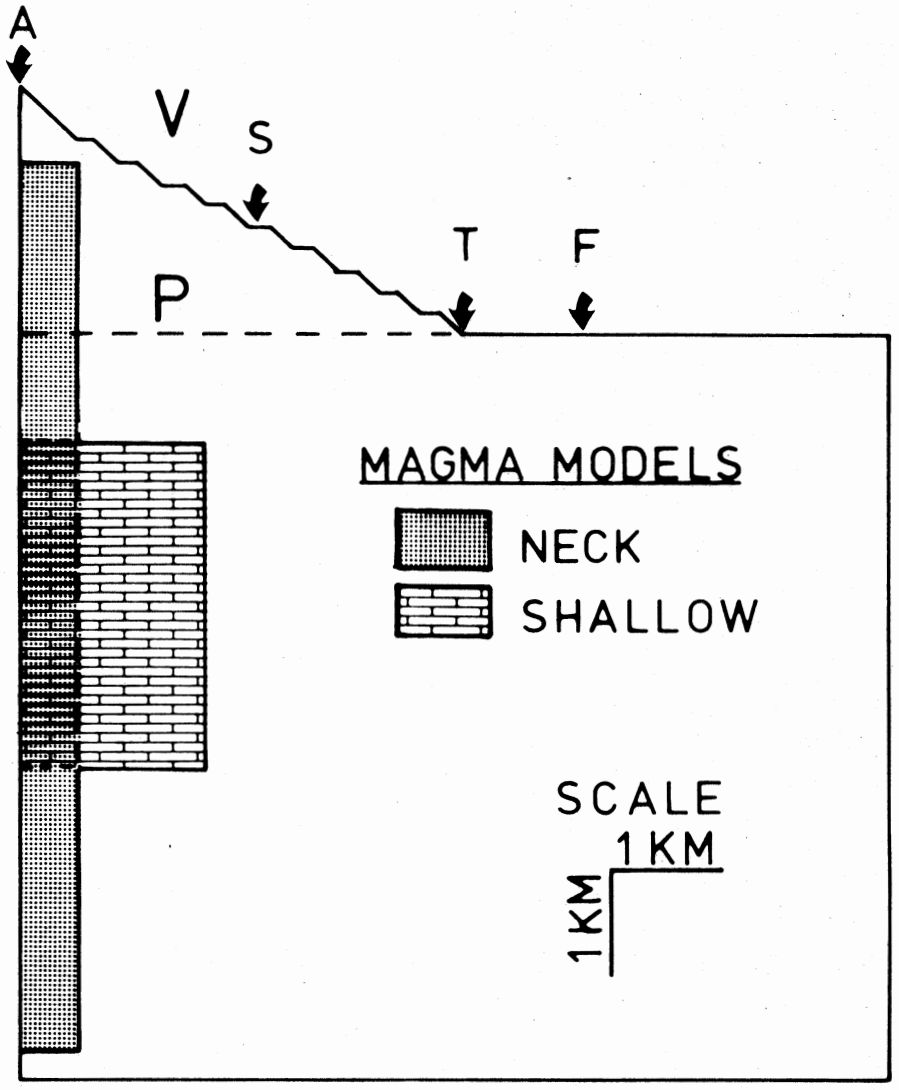

Figure 4. Magma chamber model sizes in relation to surface half-space. P = plane surface half-space boundary; V = volcano half-space boundary. Locations of detailed studies are indicated by A (apex), S (slope), T (toe), and F (flat) of the volcano.

given the dimensions of kilometers, but they can be scaled by the conduction length parameter (Lachenbruch and others, 1976). The assumed values of the parameters are shown in Table 1. Some sample results for the instantaneous models are shown in Figure 5. In all of these models the heat flow at the time of maximum surface heat flow over the apex of the magma chamber is illustrated. Results for both the rectangular and the cylindrical models are shown. The distance is measured from the center line or center point of the body.

The assumed emplacement temperature for these models is 800°C. This temperature is approximately typical of rhyolitic magmas. The actual temperature associated with an andesitic magma might be somewhat higher (1000°C), particularly if the effect of latent heat were included. It is a simple matter to scale the heat flow to any assumed T_o, however, as it is merely a matter of multiplying the heat flow shown on the ordinate by the ratio of the assumed T_o to 800°C.

Some points of interest from these solutions are that in the case of the neck model, where the magma chamber approaches within 100 m of the surface, there is a significant difference between the heat flow associated with the cylindrical neck model and the rectangular neck model. This difference is primarily because of the much larger volume associated with the rectangular chamber. It is also apparent that these anomalies are quite limited in lateral extent. The width of both bodies is assumed to be 500 m and their depth of burial is assumed to be 100 m. The time of maximum heat flow associated with the bodies is approximately 2,000 years in both cases.

TABLE 1

VALUES OF PARAMETERS FOR

THERMAL MODELS OF MAGMA CHAMBERS

		Magma Chamber Type		
		Neck	Shallow	Deep
Radius	(A)	0.25 km	1.5 km	25.0 km
Thickness	(L)	10.0 km	3.0 km	10.0 km
Depth	(D)	0.10 km	1.0 km	10.0 km

Thermal conductivity = 5 mcal/cm-sec-°C

Thermal diffusivity = 0.01 cm^2/sec

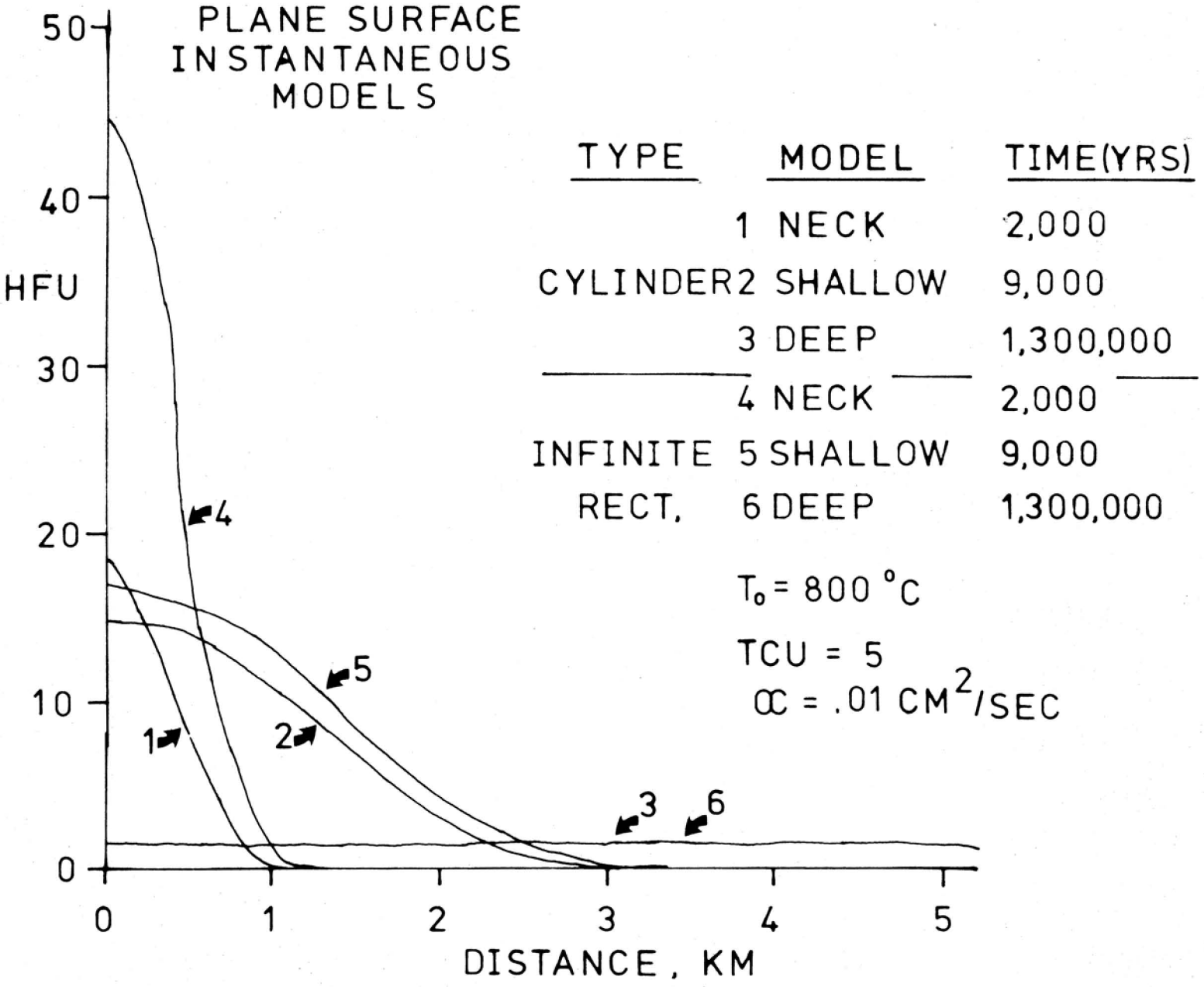

Figure 5. Surface heat flow-versus-distance curves for plane surface instantaneous models. Maximum surface heat flow over the apex of the volcano corresponds to time (yrs.) shown at right of figure; curves are labeled by number of respective models.

As the magma chamber becomes deeper and larger, the difference in heat flow, at the time of maximum heat flow, between the cylinder and the rectangular model chambers becomes less, until in the case of the largest magma chamber modeled (where the depth of burial is 10 km and the half-width, or radius, is 25 km) there is no significant difference between the two anomalies. Also illustrated is the dramatic effect of the depth of emplacement on the maximum heat flow value. Obviously, the cooling times are quite different; the cooling time for the large deep magma chamber is increased by a factor of over 100 compared to the shallow magma chamber, and over 500 compared to the neck model. In general, the cooling times are rather short geologically and, for deep chambers, the increase in heat flow is rather modest. For the rectangular plane surface model, a more complete set of heat flow-versus time curves are given by Lachenbruch and others (1976).

More Realistic Models

In order to obtain solutions for magma chamber models in addition to the simple analytical solutions available, a finite difference program was written for transient-radial heat conduction problems. Using this finite difference model, solutions were obtained that included a model surface shape based on the topographic profile of Mt. Hood (Figure 2 and Figure 4, boundary V). The heat flow effects were calculated at the surface for both instantaneous and continuous models for "neck" and "shallow" magma chambers under the apex of the volcano, of the characteristic dimensions shown in Table 1. A solution

was calculated for both cylindrical and rectangular coordinate geometry volcanoes and magma chambers, although the rectangular results are not discussed here. These types of solutions are illustrated schematically in Figure 6 for the "shallow" magma chamber model. The boundary labeled V in Figure 4 was used with the magma chambers placed below V according to the values of parameters given in Table 1.

Because the deepest magma chamber (Table 1) generates a more regional anomaly, rather than a local anomaly, discussion is focused in this and subsequent sections of this chapter on the two smaller magma chamber models calculated. The "shallow" model might correspond to a single magma chamber associated with an individual andesite volcano. The second solution ("neck" model) might be more characteristic of conditions associated with emplacement of a narrow neck or central magma chamber along the conduit of a volcano.

Shallow Magma Chamber

The dimensions of the magma chamber assumed in this discussion are given in Table 1. All models are assumed to be cylindrical, except for model 2 in Figure 6 (the slab model). The two contrasting types of heat conduction solutions, instantaneous and continuous, are shown for the shallow magma chamber model with both the volcano-surface and the plane-surface topography. The results for heat flow-versus-distance at the time of maximum surface heat flow for the models are shown in Figure 6. In Figure 6, the "plane" and "volcano" surface models refer to solutions using a cylindrical magma chamber.

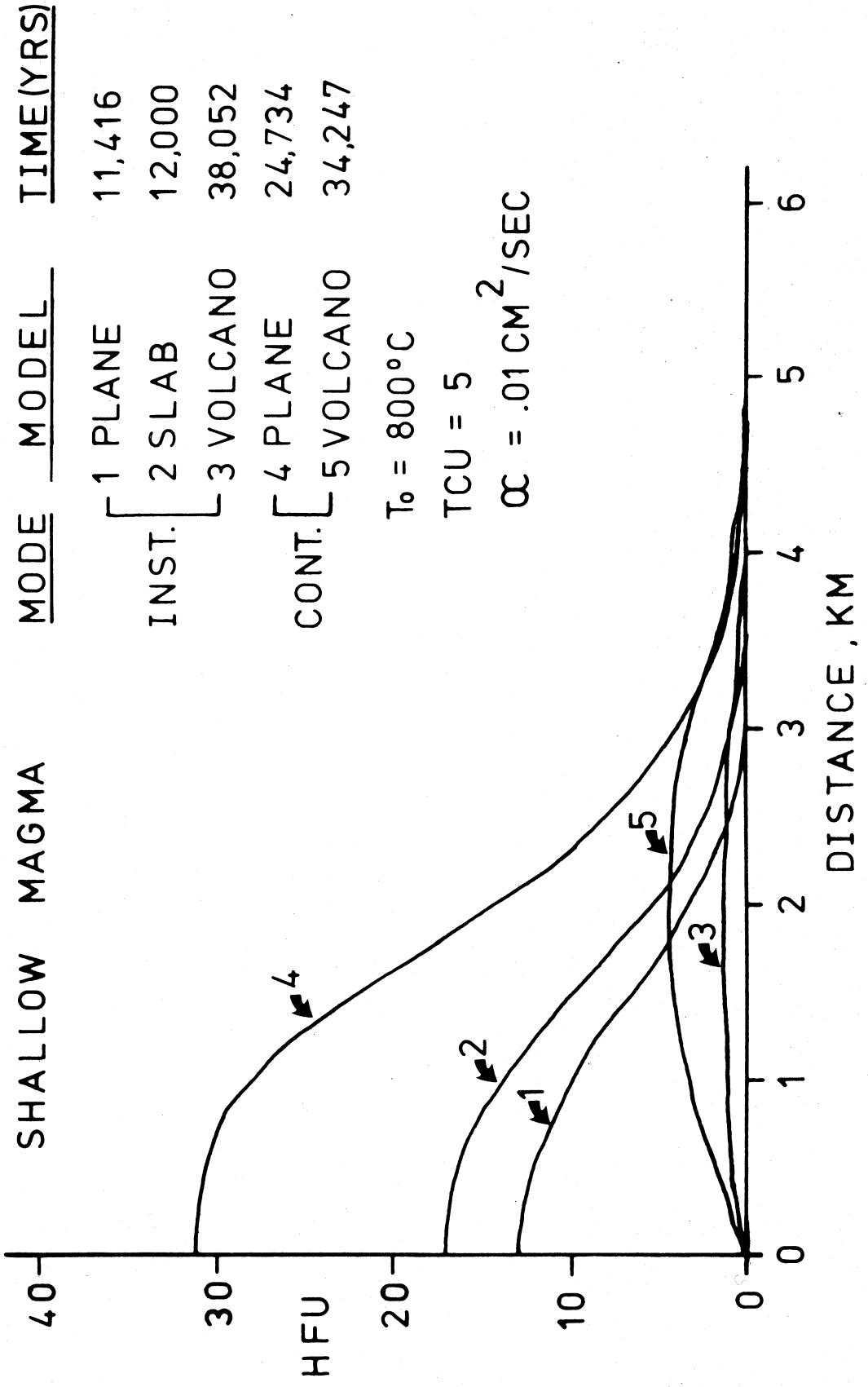

Figure 6. Surface heat flow-versus-distance curves for shallow magma chamber model. Maximum surface heat flow over the apex of the volcano corresponds to time (yrs) shown at right of figure; curves are labeled by number of respective models.

On the other hand, the slab model refers to a solution with a plane surface and an infinite rectangular magma chamber. The times indicated in the figure are the times of maximum surface heat flow associated with the instantaneous magma chamber and the maximum run time for the continuous magma chamber model. The horizontal distance shown in Figure 6 is measured from the apex of the volcano and/or the center of the magma chamber.

Curve 1 (Figure 6) is the maximum heat flow curve for the instantaneous plane magma chamber discussed previously, and curve 4 represents the heat flow for the continuous plane magma chamber at an age of 25,000 years. The continuous magma chamber has essentially reached its equilibrium heat flow in the center part of the anomaly, although the solution has still not reached equilibrium at distances of 2-4 km away from the center line. The maximum heat flow for the continuous (as opposed to the instantaneous) model differs by a factor of slightly over two. Similarly, the continuous plane solution has a much higher heat flow at any distance away from the magma chamber because of the continuous heat input of the replenished or convecting magma chamber. Thus, at any given period of time, the total heat output of the continuous magma chamber will exceed by a minimum of two times the maximum heat output of the instantaneous solution. Over the area of the magma chamber, this heat output might average a maximum of approximately 10 HFU for the instantaneous model, and 20-30 HFU for the continuous model illustrated.

The slab solution is essentially equivalent in dimensions to the instantaneous plane solution, except that the magma

chamber is assumed to be infinite in the Y axis direction instead of radially symmetrical. As noted previously, the heat flow is greater for the rectangular model due to the greater volume of magma involved. However, the characteristic cooling time and temperatures are not appreciably different for models 1 and 2 (Figure 6).

Very different results are obtained for the heat flow associated with conductive cooling of a magma chamber beneath a volcanic edifice. In this particular solution (curves 3 and 5, Figure 6) the times of maximum heat flow are much delayed because of the greater average distance between the magma chamber and the surface. Furthermore, the mean heat flow is decreased because of the much larger surface area over which the heat is dissipated in the volcano model, as opposed to the plane surface magma chamber. For these models, the maximum heat flow is associated with the edge of the volcanic edifice. Even for the continuous magma chamber, heat flow values are relatively modest compared to those associated with the cylindrical magma chamber beneath the plane surface. Part of this effect is due to the topographic effects of the volcano, and part is due to the greater effective depth of burial. Of course, if the magma chamber were larger or shallower than that assumed, then higher heat flow values would be associated with the volcanic edifice than with the areas at the toe of the volcano. There are many different solutions that might be developed, and the object is discussion of only a few typical examples.

Heat flow-versus-time curves are shown in Figure 7 for

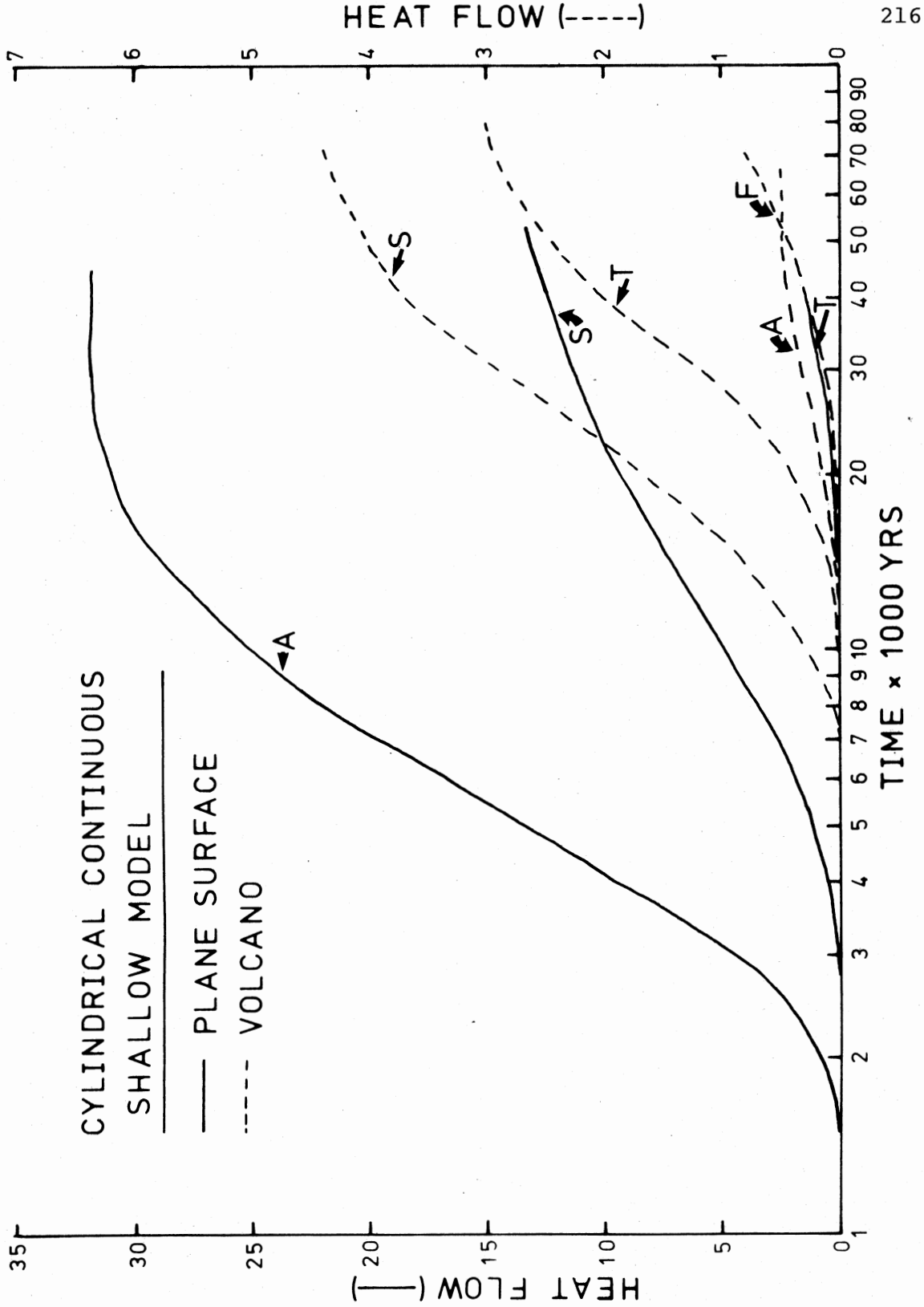

Figure 7. Heat flow-versus-time curves for the shallow cylindrical continuous model. The curves are shown for various positions along the surface of the volcano, keyed to the letters in Figure 4. The scale on the left side of the figure corresponds to the plane surface half-space, and the scale on the right side of the figure corresponds to the volcano surface half-space.

the continuous shallow cylindrical magma chamber model. Heat flow-versus-time curves are shown for various positions along the surface, keyed to the letters in Figure 4. In the case of the instantaneous model, the heat flow builds up rapidly and decays over a longer period of time. The times of maximum heat flow for the particular models described are given in Figure 6. In the case of the cylindrical continuous shallow magma chamber model (Figure 7), the heat flow builds rapidly over the first 10,000-50,000 years of the existence of the chamber to a maximum value (and constant heat flow) after the initial increase. The calculated heat flow continues to rise at larger distances from the volcano for 50,000-100,000 years, but the values are never particularly large.

These models indicate that if the heat transfer is primarily by conduction, then a period of some tens of thousands of years is required to heat up the volcano from a relatively local magma chamber below the volcano. The maximum heat flow values will be observed along the lower slopes of the volcano.

Figure 8 shows isotherms associated with the continuous and the instantaneous shallow cylindrical magma chambers after a period of approximately 38,000 years. The assumed thermal properties are shown in the figure. A comparison is made between the temperatures for the instantaneous cooling solution and the continuous solution. No regional background gradient has been added to these temperature data, so the actual temperature would be slightly higher in proportion to the depth and the background geothermal gradient. After this period of time, temperatures in the volcanic edifice have essentially

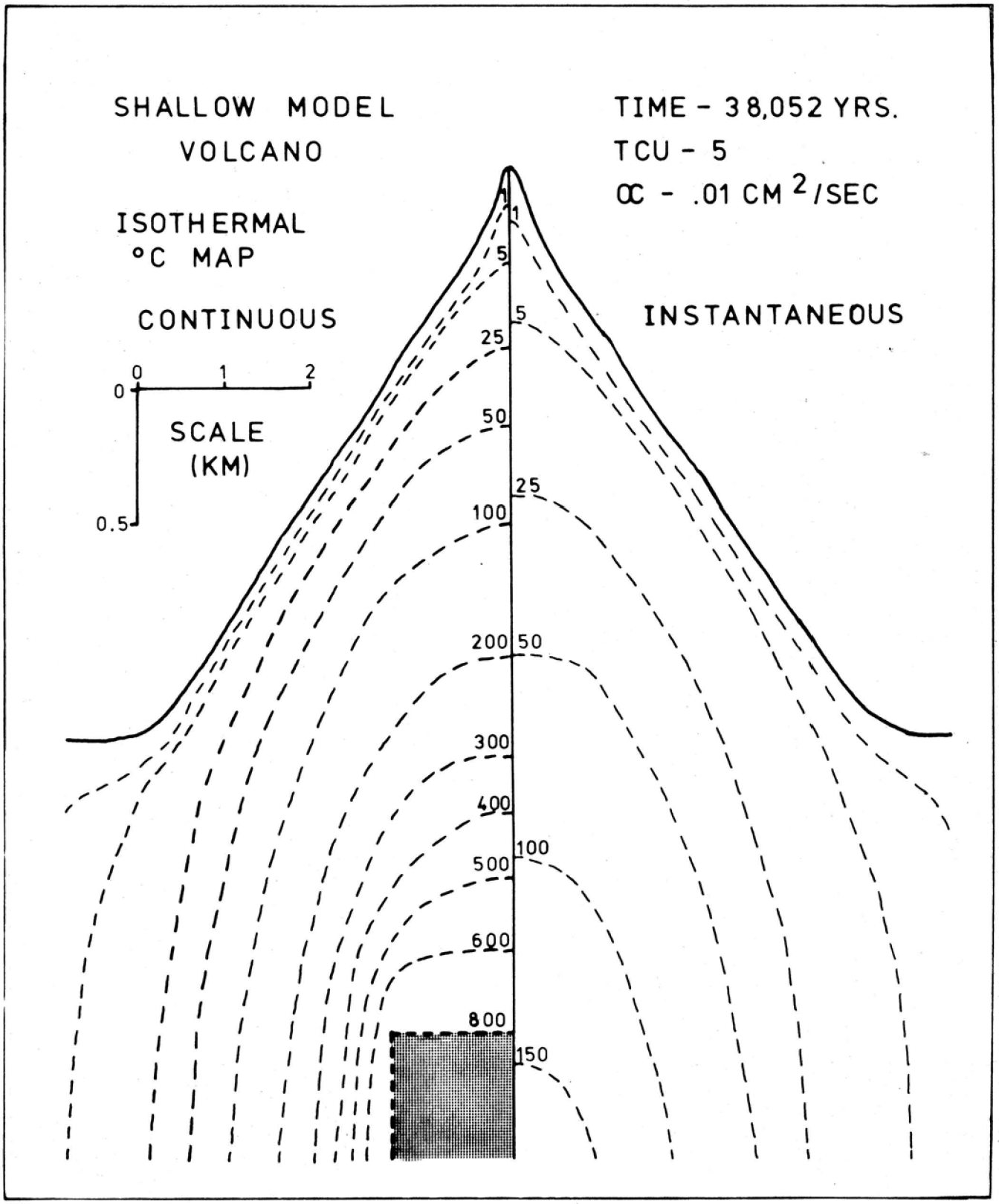

Figure 8. Isothermal cross-section map of the volcanic edifice for the shallow magma chamber model. The continuous model isotherms are on the left side of the volcano apex, and the instantaneous model isotherms are on the right side of the volcano apex. A portion of the shallow magma chamber is indicated by the shaded area at the bottom of the figure.

reached a steady-state for the continuous model; and for the instantaneous model, temperatures are well on their way to complete cooling, as indicated by the low temperatures.

Continuous Neck Magma Chamber Model

The final configuration discussed is the solution for a small neck type of magma chamber associated with a plane surface or with a volcano. The heat flow as a function of time at characteristic positions along the surface is shown in Figure 9. The solid lines are the heat flow values associated with the neck beneath a plane surface, while the dotted lines are the heat flow values associated with emplacement of the neck within a volcanic edifice (note difference in scales).

The spreading effect of the volcano surface is again apparent in the heat flow, as indicated by the factor of five difference in heat flow values associated with the magma chamber beneath the plane surface and the magma chamber beneath the volcano. Of course, the time to reach steady-state is relatively short for the magma chamber within the volcano, because of proximity to the surface. On the other hand, it takes some time for the effect to build up along the slope of the volcano. The heat flow never reaches significant values at the edge of the volcano. The instantaneous cooling of the plane surface and volcano magma chamber is also shown. In both cases, the heat flow anomaly has decayed significantly in a period of 2,000-3,000 years after emplacement. Significant heat flow is not seen along the slopes and flanks of the volcano.

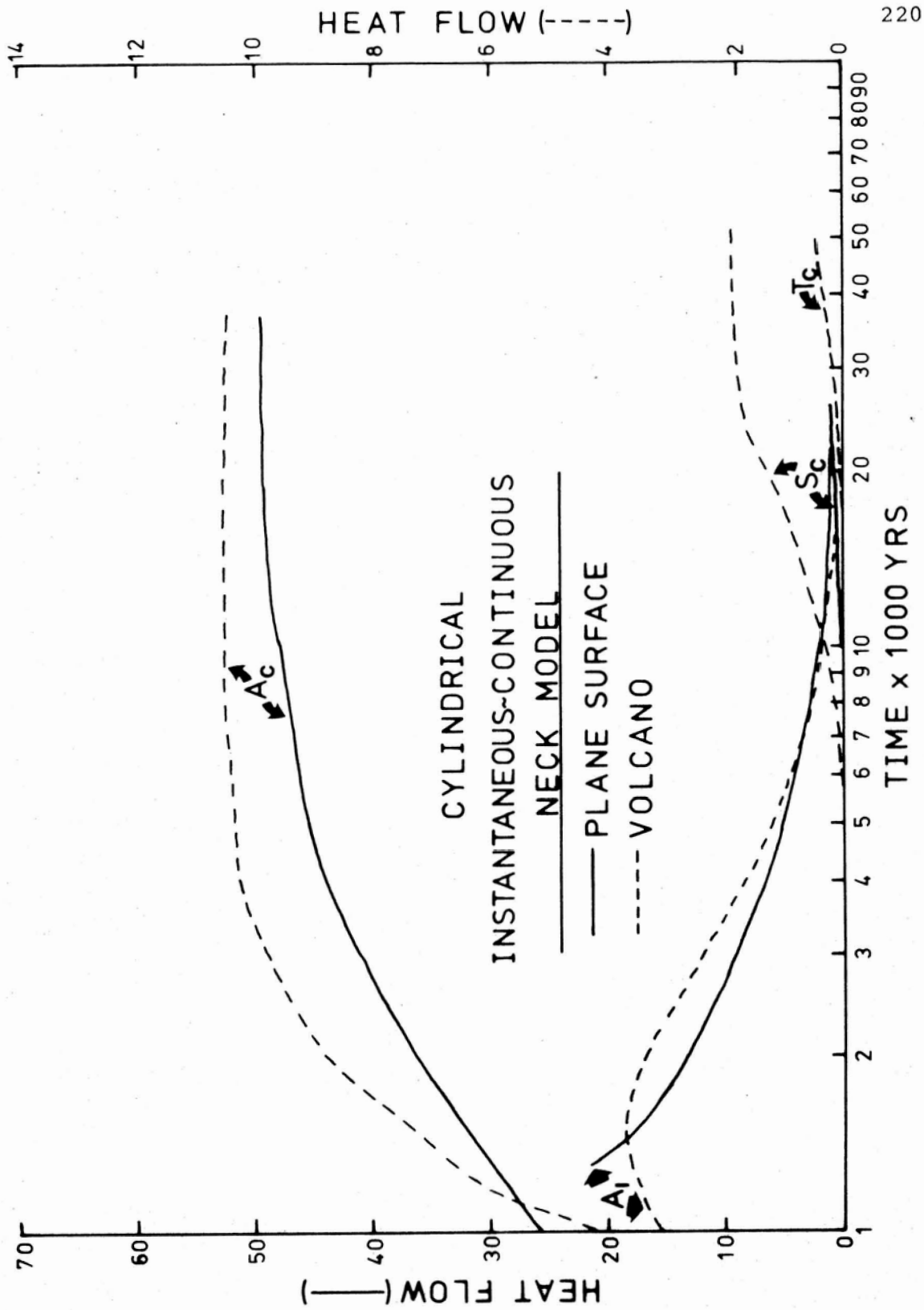

Figure 9. Heat flow-versus-time curves for the cylindrical instantaneous and continuous neck models. The curves are shown for various positions along the surface of the volcano, keyed to the letters in Figure 4. The scale on the left side of the figure corresponds to the plane surface half-space, and the scale on the right side of the figure corresponds to the volcano surface half-space. The subscript letters on the letters labeling the curves indicate the instantaneous (I) or the continuous (C) solutions.

The continuous neck model is reasonable only if the rate of occurrence of volcanism is rapid enough to cycle magma along the neck and thus to maintain a high temperature. Based on these solutions, it would appear that the recurrence of extrusive events would have to be less than 1,000-2,000 years if the axis of the volcano is to be kept at near-magma temperatures.

Discussion

The magma chamber models herein presented are highly idealized and the purpose of the following discussion is to briefly summarize their applications to the problem of geothermal resources associated with a stratocone volcano. In order to have a commercially attractive geothermal prospect, two things are needed: (1) high temperature, and (2) fuild flow sufficient to allow generation of economic amounts of power. The minimum heat loss that might be associated with an economic geothermal system is somewhere between 5×10^6 and 10×10^6 cal/sec. For a volcano such as Mt. Hood, with a radius of approximately 5 km and a total basal area of approximately 50 km^2, a mean heat flow, or thermal extraction rate, of 10-20 HFU would be required to maintain such a geothermal system. Furthermore, as discussed above, the rates of cooling of magma chambers associated with hydrothermal convection are probably greater by a factor of two to ten times than those associated with conductive cooling. Thus it is obvious that a single batch of magma, which might be approximated by the instantaneous conductive cooling model, would not be sufficient to

generate a very long-lived hydrothermal system, and the cooling of a magma chamber associated with a stratocone volcano (and of the same order of dimensions) would take place in less than a few thousand years.

It might appear that the application of the plane models to the stratocone volcano is somewhat questionable. However, one approach to modeling the cooling of a magma chamber associated with a stratocone volcano might be to assume that, for thermal purposes, the actual edifice of the volcano does not exist. Typically, the volcano edifice is composed of an alternating series of ashes and blocky flows, with a large horizontal permeability. Furthermore, these volcanoes are typically large topographic features and thus are subject to relatively high rainfall. Large amounts of meteoric water which are transferred into the subsurface along porous units tend to flow out at the edge of the volcano. Water flow may be so rapid as to prevent any appreciable heating of the volcanic edifice, or to confine heating to areas which have been hydrothermally altered where permeability has been significantly decreased. In a simple model, where the fluid flow is very high, the bottom of the aquifer could be treated as an upper boundary condition of constant temperature in the conductive solution, instead of treating the volcano surface itself as a constant temperature boundary. Therefore, the heat flow for the plane boundary model might approximate the amount of heat input from a magma chamber beneath the volcano into the circulating groundwater system.

It would appear, then, that if significant geothermal

systems are associated with andesite volcanoes, then either larger instantaneous magma chambers than those modeled are required, or volcanism must recur over a considerable period of time, so that the continuous solutions give a better estimate of potential heat transfer into the hydrothermal system.

While a neck type of magma chamber is capable of transmitting a large amount of heat into the volcanic edifice, it is relatively short-lived and a recurrence time of a few hundred years would be required for enough heat input from a neck type magma chamber to drive a hydrothermal system of any significance within the edifice of the volcano.

A somewhat more deeply buried magma chamber typical of the shallow magma chamber model could, if replenished over periods of a few thousands of years, easily impart the amount of heat required to drive significant geothermal systems. The presence of the volcano surface, as well as the probable flux of groundwater associated with the topographic features of the volcano, serve to indicate that whatever the shape of a magma chamber beneath a stratocone volcano, the maximum heat loss will probably be located along the lower slope of the volcano. Unless a magma chamber actually penetrates into the volcano itself, it is unlikely that significantly high temperatures will be associated with the upper part of the edifice. The general locations of thermal manifestations associated with stratocone volcanoes are usually near the outer edges of the volcanic carapace. The localization of the manifestations may be controlled by several different mechanisms, such as ring structures, etc. However, it appears that both the hydrologic

and the conductive heat loss models are consistent with such a localization, except in cases where the volcano has been active enough to thoroughly heat up its cone.

REGIONAL HEAT FLOW IN THE NORTHERN CASCADE RANGE OF OREGON

Regional Heat Flow Setting

The heat flow associated with the stratocone volcanoes in the Cascade Range can only be understood with respect to the regional background setting of heat flow in and around the Cascade Range itself. For several years DOGAMI and SMU have been involved in a systematic program of exploring the geothermal character of the Northern Cascade Range in Oregon. The studies have included location and logging of free holes in the Willamette Valley-Western Cascade Range areas during 1976; a drilling program involving 15 holes in the Western Cascade and High Cascade Range provinces during 1976; a free hole study of heat flow along the eastern margin of the High Cascade Range and the western portion of the Deschutes-Umatilla Plateau province in 1977; and regional investigation of heat flow around Mt. Hood in 1978. In addition, during 1977-79, a heat flow evaluation of deep holes drilled in the vicinity of, and on, Mt. Hood has been part of the program. In this section regional heat flow in the Northern Oregon Cascade Range, exclusive of the Mt. Hood region, will be discussed. Most of these data were obtained during 1976-77, but have not been summarized in any readily available report. Qualitative results have been discussed by Blackwell and others (1978).

A generalized heat flow map of Oregon based primarily on the data by Blackwell and others (1978), and updated using the data from Table 2, is shown in Figure 10. All of the heat flow

TABLE 2. Thermal and location data in the Northern Cascade Range of Oregon.

Location	N Latitude	W Longitude	Collar Elevation	Depth Interval	Avg. Thermal Conductivity [standard error]	N†	Corrected Gradient	Corrected Heat Flow	Quality
3N/12E-32cd	45°41.8'	121°20.7'	53.20 m	20.0 - 67.5	3.8		46.0	1.7	B
2N/12E- 6bb	45°41.4'	121°22.6'	85.10	10.0 - 80.0	3.8		28.0	1.1	B
2N/12E-16cba	45°39.5'	121°19.8'	380.00	100.0 - 185.0	3.8		34.0	1.3	A
2N/11E-20ab	45°38.8'	121°28.1'	629.30	60.0 - 120.0	2.8		37.0	1.0	B
2N/ 9E-29ad	45°37.8'	121°42.8'	1146.00		4.15 [0.92]	3		**	
2N/12E-30ad	45°37.7'	121°21.4'	457.30	20.0 - 120.0	3.8		39.0	1.5	A
2N/ 1W-32bb	45°37.2'	122°50.6'	282.70	0.0 - 200.0	3.8		25.0-32.0	1.1	B
2N/ 7E-31bd	45°36.8'	121°59.8'	536.70	50.0 - 150.0	3.79 [0.14]	5	42.2	1.6	A
2N/13E-31cd	45°36.7'	121°14.7'	279.70	90.0 - 175.0	3.8		52.0	2.0	B
1N/ 9E- 1ac	45°36.2'	121°38.1'	267.50	0.0 - 175.0	3.8		64.0	2.4	C
1N/ 2E-24da	45°33.3'	122°30.0'	4.60	60.0 - 95.0	4.8		27.0	1.3	B
1N/ 1W-25bc	45°32.6'	122°45.6'	326.80	70.0 - 150.0	3.8		23.0	0.9	B
1N/ 2E-29da	45°32.4'	122°34.9'	62.30	160.0 - 230.0	3.0	6	32.1	1.0	A
1N/ 3E-33ad	45°31.7'	122°26.0'	60.50	130.0 - 330.0	3.0	1	37.3	1.1	A
1N/ 6E-31cd	45°31.2'	122° 7.0'	743.70					**	
1S/10E- 9bc	45°29.8'	121°33.8'	560.00	10.0 - 25.0	3.70 [0.27]	5	256.0	9.5	C
1S/13E-20da	45°28.1'	121°11.8'	354.00	50.0 - 135.0	3.50		41.9	1.4	B
1S/10E-29ca	45°27.1'	121°34.8'	725.40		4.38 [0.20]	5			
2S/15E- 3bb	45°25.9'	120°55.5'	793.40	10.0 - 55.0	3.8		39.0	1.5	B

Location	N Latitude	W Longitude	Collar Elevation	Depth Interval	Avg. Thermal Conductivity [standard error]	N	Corrected Gradient	Corrected Heat Flow	Quality
2S/11E- 6aad	45°25.7'	121°27.7'	1161.00 m	95.0 - 150.0	3.80 [0.15]	5	30.4	1.15	A
2S/ 4E-18dda	45°23.5'	122°21.4'	196.60	50.0 - 225.0	2.8		34.0	0.95	A
2S/ 8E-15cd	45°23.5'	121°48.5'	777.40	1000.0 -1200.0	4.19 [0.14]	21	55.0	2.3	A
2S/ 8E-17cc	45°23.3'	121°51.6'	658.40	100.0 - 200.0	4.04 [0.32]	5	51.2	2.07	A
2S/ 4E-16cd	45°23.4'	122°19.3'	220.40	20.0 - 75.0	3.0		39.0-42.0	1.2	B
2S/ 2E-20bd	45°22.8'	122°35.4'	18.30	45.0 - 75.0	3.8		21.0	0.8	B
2S/ 6E-24ca	45°22.8'	122° 1.1'	359.70	70.0 - 150.0	4.33 [0.21]		42.7	1.85	A
2S/ 7E-34bb	45°21.5'	121°56.1'	442.10	35.0 - 85.0	4.30 [0.80]		47.0	2.0	A
2S/13E-36cd	45°20.9'	121° 8.0'	753.90	10.0 - 45.0	3.8		35.0	1.3	C
3S/ 6E- 3a	45°20.6'	121°55.4'	148.60					**	
3S/11E- 1aa	45°20.6'	121°21.6'	919.90	50.0 - 125.0	3.60 [0.30]	3	43.8	1.58	A
3S/ 9E- 6dd	45°19.9'	121°42.5'	1798.80		4.42 [0.16]	4		**	
3S/ 9E- 7ab	45°19.7'	121°42.6'	1761.70					**	
3S/14E- 7dc	45°19.0'	121° 5.9'	832.40	10.0 - 65.0	3.8		26.0	1.0	B
3S/ 8E-16cd	45°18.4'	121°49.9'	762.20	50.0 - 120.0	5.22 [0.15]	9	24.0	1.25	A
3S/ 8E-24bbd	45°18.1'	121°46.5'	1106.60	10.0 - 60.0	5.20		60.0	3.1	C
3S/8½E-25aa	45°17.2'	121°43.7'	1167.70		4.53 [0.26]	6		**	

Location	N Latitude	W Longitude	Collar Elevation	Depth Interval	Avg. Thermal Conductivity [standard error]	N	Corrected Gradient	Corrected Heat Flow	Quality
3S/ 8E-29ddc	45°16.6'	121°54.5'	722.40 m	80.0 - 140.0	6.32 [0.44]	5	28.2	1.78	C
4S/13E- 1ca	45°14.9'	121° 7.4'	340.50	10.0 - 75.0	2.8		77.0	2.2	B
4S/12E-10dd	45°13.8'	121"16.7'	530.50	20.0 - 90.0	3.8		36.0	1.4	B
4S/ 9E-28dd	45°11.3'	121°40.1'	1036.00					**	
4S/13E-32dc	45°10.5'	121°12.2'	547.20	20.0 - 145.0	3.0		60.0	1.8	B
4S/14E-33cb	45°10.5'	121° 4.1'	313.10	50.0 - 70.0	3.8		68.0	2.6	B
5S/16E-20cb	45° 7.1'	120°50.9'	755.40	10.0 - 80.0	3.8		34.0	1.3	B
5S/12E-31aa	45° 6.0'	121°20.5'	677.90	20.0 - 107.5	3.8		38.0	1.4	C
6S/15E- 5ba	45° 5.0'	120°57.9'	802.60	35.0 - 70.0	3.8		44.0	1.7	B
6S/ 7E- 4dc	45° 4.3'	121°57.6'	686.00					**	
6S/ 1E-13da	45° 2.9'	122°37.2'	326.10	95.0 - 140.0	3.9	1	39.0	1.4	A
6S/14E-13dd	45° 2.6'	120°59.8'	940.90	80.0 - 120.0	3.8		45.0	1.7	B
6S/ 7E-21cd	45° 1.8'	121°57.7'	603.70	10.0 - 40.0	3.52 [0.17]	4	168.1	5.91	C
6S/ 7E-30bb	45° 1.3'	122° 0.5'	512.10	50.0 - 130.0	3.95 [0.19]	9	203.5	8.04	C
6S/ 6E-34cd	44°60.0'	122°3.8'	487.80	10.0 - 50.0	3.91 [0.09]	9	65.7	2.57	A
7S/ 1E-11aca	44°58.8'	122°38.8'	214.00	0.0 -2379.0	3.50		26.0	0.9	B
7S/ 5E-22aa	44°57.1'	122°10.4'	655.50	20.0 - 90.0	3.48 [0.12]	7	66.1	2.3	A
8S/ 1E- 8db	44°53.3'	122°42.5'	303.30	95.0 - 215.0	4.1	1	28.0	1.1	A
8S/ 1E-17da	44°52.2'	122°42.3'	315.50	105.0 - 110.0	3.8		25.0	1.0	B
8S/ 2W-24bc	44°51.7'	122°53.0'	127.10	22.5 - 60.0	3.8		25.0	0.95	B

Location	N Latitude	W Longitude	Collar Elevation	Depth Interval	Avg. Thermal Conductivity [standard error]	N	Corrected Gradient	Corrected Heat Flow	Quality
8S/ 1W-32bb	44°50.3'	122°50.4'	115.80	30.0 - 80.0	3.8	1	34.0	1.3	A
8S/ 5E-31cc	44°49.9'	122°14.8'	705.30	35.0 - 345.0	4.30 [0.80]		28.0	1.2	A
9S/17E- 6cad	44°48.7'	120°44.0'	987.80	45.0 - 120.0	4.5		37.0	1.7	A
9S/ 3E-11ba	44°48.5'	122°24.5'	317.00	47.5 - 85.0	3.2	1	25.4	0.7	A
9S/ 3E-11cb	44°48.1'	122°24.8'	333.80	25.0 - 60.0	3.2	2	24.3	0.8	A
9S/ 6E-23bb	44°47.0'	122° 2.4'	550.00	30.0 - 105.0	3.84 [0.27]	7	54.1	2.08	A
9S/ 7E-21ad	44°46.7'	121°57.1'	725.40	70.0 - 150.0	3.67 [0.23]	12	81.5	2.38	A
9S/ 2E-21da	44°46.2'	122°33.6'	213.40	22.5 - 47.5	3.0	1	41.0	1.2	B
11S/ 1E- 7da	44°37.5'	122°43.3'	158.50	40.0 - 57.5	3.2	1	25.0	0.8	B
11S/ 1W-14dd	44°36.5'	122°45.9'	182.90	30.0 - 125.0	3.2	1	41.0	1.3	A
11S/15E-22cd	44°35.6'	120°55.1'	963.40	605.0 - 820.0	6.5	1	31.0	2.0	A
11S/ 1W-32bbb	44°34.6'	122°50.6'	108.20	0.0 -1345.0	3.8		19.0	0.7	B
12S/ 1W- 4dc	44°33.1'	122°48.7'	135.00	30.0 - 65.0	3.20 [0.30]	3	36.4	1.2	A
13S/ 2W- 3aa	44°28.3'	122°54.4'	317.00	40.0 - 95.0	3.2	1	31.0	1.0	A
13S/ 1W- 8db	44°27.1'	122°49.9'	329.20	15.0 - 195.0	3.8	1	21.0	0.8	A
13S/ 1W-10ca	44°27.1'	122°47.7'	149.40	27.5 - 62.5	3.2	1	23.0	0.75	B
13S/ 2W-18cb	44°26.2'	122°59.1'	378.00	95.0 - 190.0	3.8		26.0	1.0	B
13S/ 1E-20ba	44°25.9'	122°43.0'	402.90	90.0 - 130.0	3.2	1	40.0	1.3	B
13S/ 1E-35ab	44°24.1'	122°38.9'	310.90	90.0 - 150.0	3.2	1	40.1	1.3	A
14S/ 3W-24dc	44°20.0'	122°59.6'	207.30	10.0 - 47.5	3.2	1	25.0	0.8	B
15S/ 6E-11dc	44°16.1'	122° 3.2'	716.50					**	

	Location	N Latitude	W Longitude	Collar Elevation	Depth Interval	Avg. Thermal Conductivity [standard error]	N	Corrected Gradient	Corrected Heat Flow	Quality
	15S/ 7E-28aa	44°14.8'	121°58.4'	1143.30 m					**	
	15S/15E-30ad	44°14.8'	120°58.0'	1002.80	40.0 - 65.0	>3		96.4	>2.9	B
	15S/14E-36ac	44°13.2'	120°59.6'	1023.00	20.0 - 75.0	>3		123.5	>3.7	C
	16S/ 6E- 2ca	44°12.1'	122° 3.0'	70.10	100.0 - 150.0	4.15 [0.06]	11	81.7	3.39	A
	16S/14E-16daa	44°11.2'	121° 2.8'	1024.00	15.0 - 75.0	>3		181.8	>5.5	C
	16S/ 4E-14dbb	44°10.1'	122°17.5'	457.20	12.5 - 45.0	4.30 [0.80]	2	38.0	1.6	B
	16S/ 6E-27bb	44° 9.1'	122° 4.7'	573.00	30.0 - 150.0	3.75 [0.12]	12	73.8	2.77	A
	17S/ 1W-26da	44° 3.7'	122°47.1'	327.70	20.0 - 145.0	3.8		27.3	1.0	A
	17S/ 2W-36ca	44° 2.8'	122°52.7'	213.40	40.0 - 105.0	3.2	1	25.0	0.8	A
*	18S/12E- 5bbd	44° 2.8'	121°19.1'	1102.00					**	
	18S/ 2W- 4ad	44° 2.2'	122°55.8'	175.30	45.0 - 125.0	3.2	1	33.0	1.1	A
*	18S/11E-25bd	43°59.4'	121°21.4'	1195.00					**	
	18S/ 1W-32cc	43°57.3'	122°50.4'	192.10	70.0 - 215.0	3.8		37.0	1.4	A
	19S/ 2W- 2ac	43°56.9'	122°53.7'	231.70	25.0 - 120.0	3.2	1	32.0	1.0	A
	19S/ 2W-10ad	43°55.9'	122°54.6'	218.00	10.0 - 42.5	3.2		30.6	1.0	A
*	19S/16E-16dc	43°54.9'	120°49.1'	1376.00	25.0 - 300.0	3.6		51.1	1.8	B
*	19S/11E-25ba	43°54.4'	121°21.5'	1373.00					**	
*	20S/14E-25aa	43°48.8'	120°59.4'	1428.00	45.0 - 125.0	<4.4	4	34.4	1.5	B
	20S/ 3E-26da	43°48.0'	122°25.0'	719.50	70.0 - 140.0	3.8		38.0	1.4	B
	20S/ 3E-26cd	43°47.9'	122°25.2'	707.30	10.0 - 125.0	3.8		29.0	1.1	B
*	21S/17E- 1ad	43°47.0'	120°36.9'	1440.00	40.0 - 90.0	2.4	4	82.5	2.0	B

	Location	N Latitude	W Longitude	Collar Elevation	Depth Interval	Avg. Thermal Conductivity [standard error]	N	Corrected Gradient	Corrected Heat Flow	Quality
	21S/ 3E-10ad	43°45.6'	122°25.9'	548.80 m	22.5 - 100.0	7.6	1	35.0	1.3	B
*	21S/15E-16ab	43°45.2'	120°56.2'	1476.00	70.0 - 150.0	4.2	6	55.0	2.3	C
*	21S/11E-25bb	43°43.9'	121°21.7'	1515.00	27.5 - 35.0	3.6	2	65.3	2.4	C
	21S/ 4E-28ad	43°43.2'	122°20.0'	533.50	10.0 - 150.0	4.54	13	58.0	3.0	A
*	22S/19E- 5cc	43°41.4'	120°28.7'	1450.00	10.0 - 37.5	2.4	1	83.0	2.0	B
	22S/ 3E-10cd	43°40.3'	122°27.0'	490.70	20.0 - 90.0	3.76		39.4	1.48	B
	22S/ 5E-26bc	43°38.2'	122°11.3'	975.40	30.0 - 150.0	4.72 [0.14]	13	53.0	2.7	A
*	22S/19E-32ad	43°37.6'	120°27.4'	1520.00	42.5 - 47.5	1.60	1	118.0	1.9	B
*	23S/19E- 5b	43°37.0'	120°28.4'	1550.00	70.0 - 150.0	3.90	1	50.9	2.0	A

† N is number of samples used to determine the average thermal conductivity. Where N is blank, value used is average estimate of type rock. Where standard error is blank when a value is given for N, this indicates value used is estimate from composite samples from drill hole.

* Hull et al., 1977.

** Considered unsuitable for heat flow calculations.

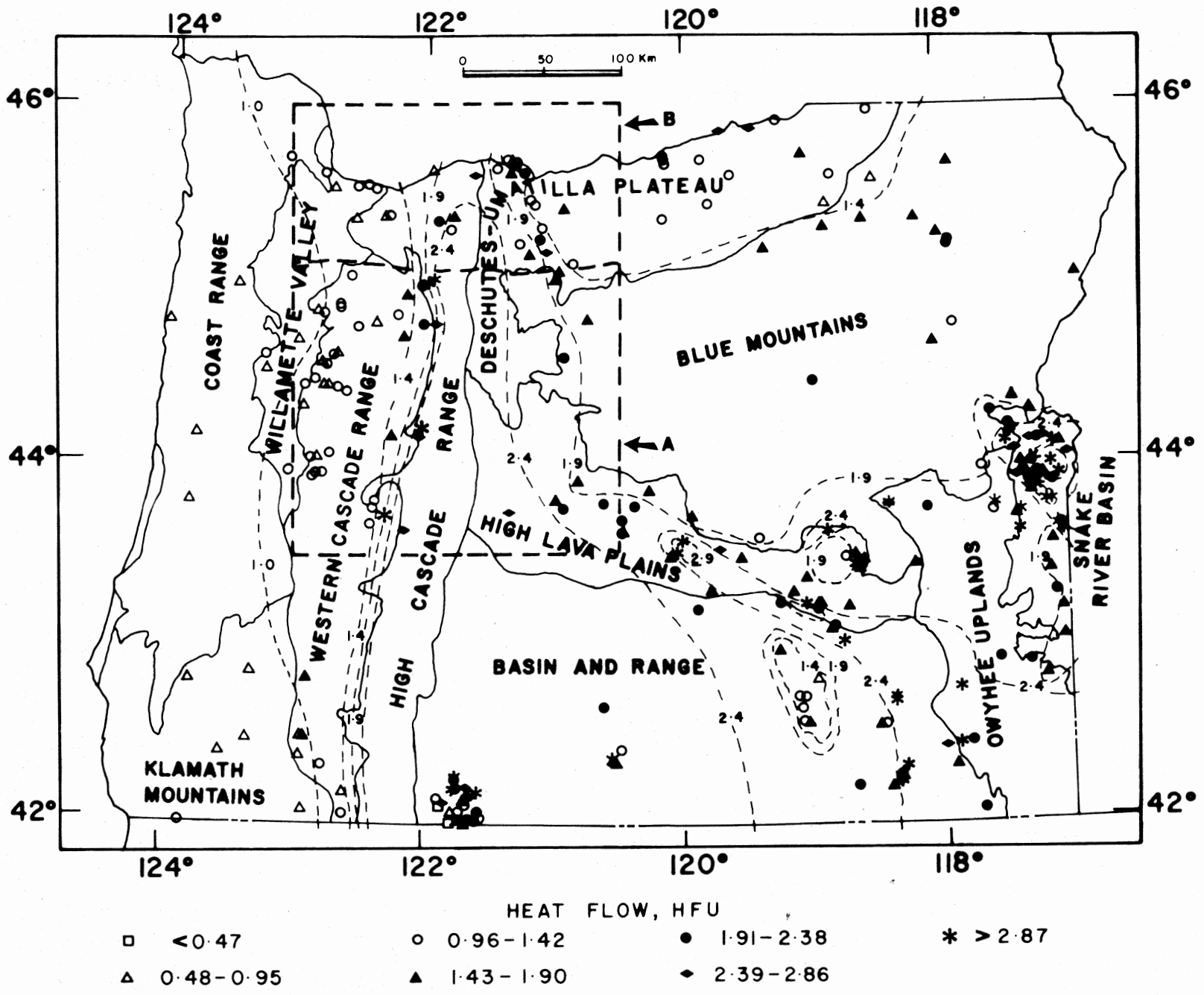

Figure 10. Generalized heat flow map of Oregon.

data discussed in this report are listed in Table 2. Included in this Table are all of the pertinent thermal and location data including latitude and longitude, township and range, elevation, interval of gradient calculation, average thermal conductivity, geothermal gradient and heat flow. All appropriate reductions have been performed to the data set, including terrain corrections. The data values are ranked by quality as discussed by Blackwell and others (1978), and Sass and others (1971).

It is apparent from Figure 10 that the northern part of the High Cascade Range in Oregon represents an area of higher heat flow than the Willamette Valley-Western Cascade Range provinces to the west and the Deschutes-Umatilla-Blue Mountains provinces to the east. The boundary between the High Cascade Range heat flow provinces is well-defined on the basis of the available data. The boundary between the High Cascade Range and the Deschutes-Umatilla-Blue Mountain provinces does not appear to be as well defined, and additional data are needed in order to completely delineate the location of the heat flow boundary and the magnitude of the heat flow contrast.

Northern Oregon Cascade Range Heat Flow

The heat flow data in the vicinity of the northern Cascade Range of Oregon are shown in greater detail in Figure 11. Available heat flow data from southern Washington (Schuster and others, 1978; Blackwell, unpublished) are also shown. Only the data south of Mt. Hood are discussed in the section (Box A, Figure 10).

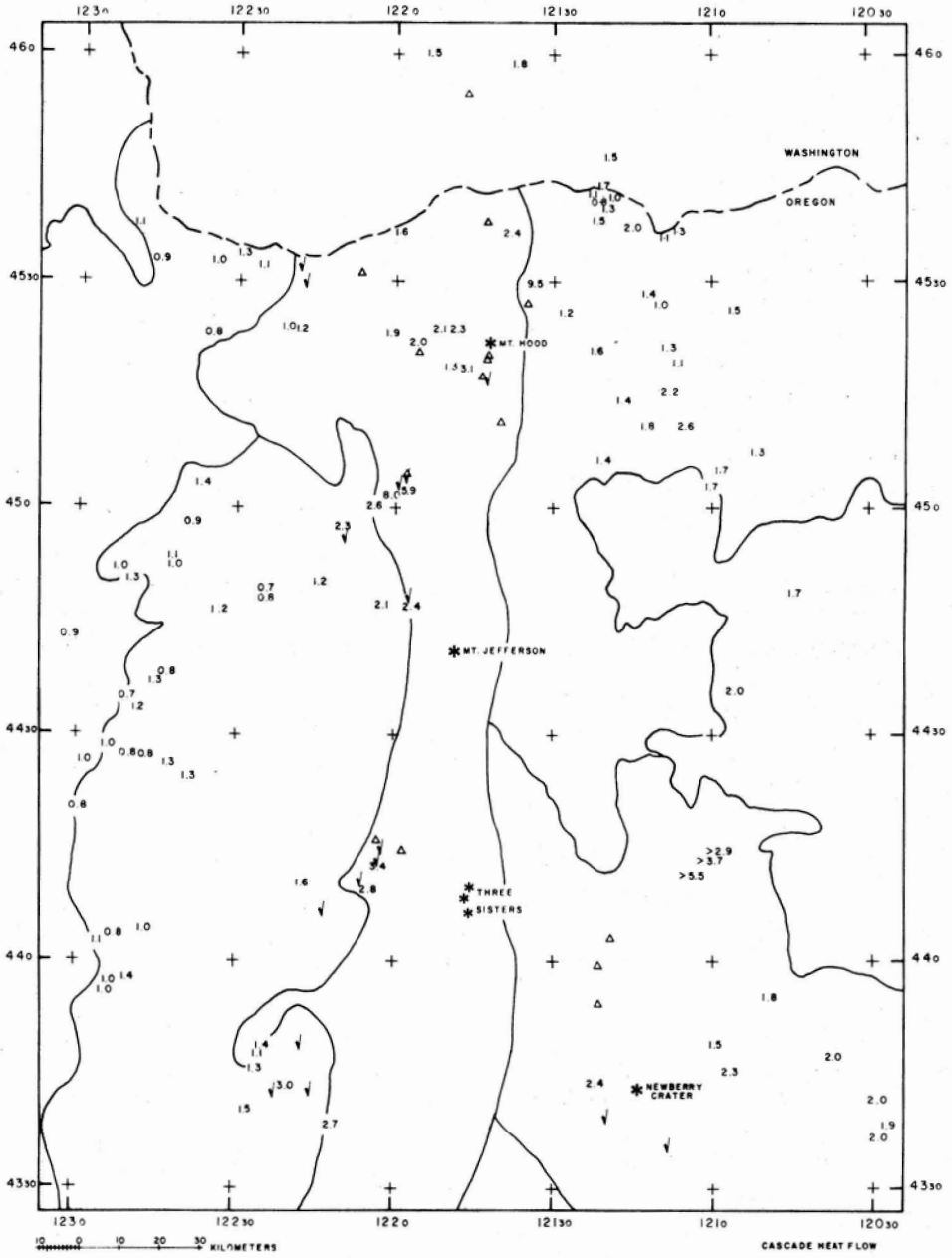

Figure 11. Heat flow map of the Northern Cascade Range area of Oregon (detail of area enclosed by heavy dashed lines in Figure 10). Heat flow values (in HFU) are plotted over their locations, with the decimal point of each value being the actual hole location. Holes drilled for heat flow studies, but considered unsuitable for heat flow calculations, are indicated by open triangles. Wells logged which are associated with regional aquifer disturbances are also shown by open triangles. Physiographic province boundaries are shown by solid lines. Locations of major volcanoes are indicated by the asterisks, and locations of major hot springs are indicated by √s.

The heat flow data in the Western Cascade Range west of the high heat flow boundary are very homogeneous. A histogram of the heat flow data from Figure 11 in the Western Cascade Range and Willamette Valley provinces is shown in Figure 12. Also shown in this figure is a histogram of the heat flow associated with the Western Cascade Range-High Cascade Range boundary south of 45°10'N as well as a histogram of heat flow values along the eastern boundary of the High Cascade Range.

The heat flow data in the Western Cascade Range-Willamette Valley average 1.1 HFU. Heat flow values along the Western Cascade Range-High Cascade Range boundary average 2.5 HFU, while heat flow values along the eastern boundary of the High Cascade Range average approximately 2.0 HFU, and the average has a large standard error. The average gradients associated with these heat flow values are 30°C/km, 60°C/km and 50°C/km respectively.

Typical temperature-depth curves observed in domestic water-supply wells in the Western Cascade Range-Willamette Valley provinces are shown in Figure 13. The holes are generally along major drainages where development is taking place. In general, the heat flow regime is completely conductive within the bedrock units of these two provinces with only occasional evidence of local water circulation and no evidence of regional water flow. The basic-to-intermediate composition volcanic and volcanoclastic rocks typical of these provinces seem to be pervasively altered to clay and zeolite minerals, resulting in relatively impermeable rocks. The staircase temperature-depth patterns, typical of water flow within drill

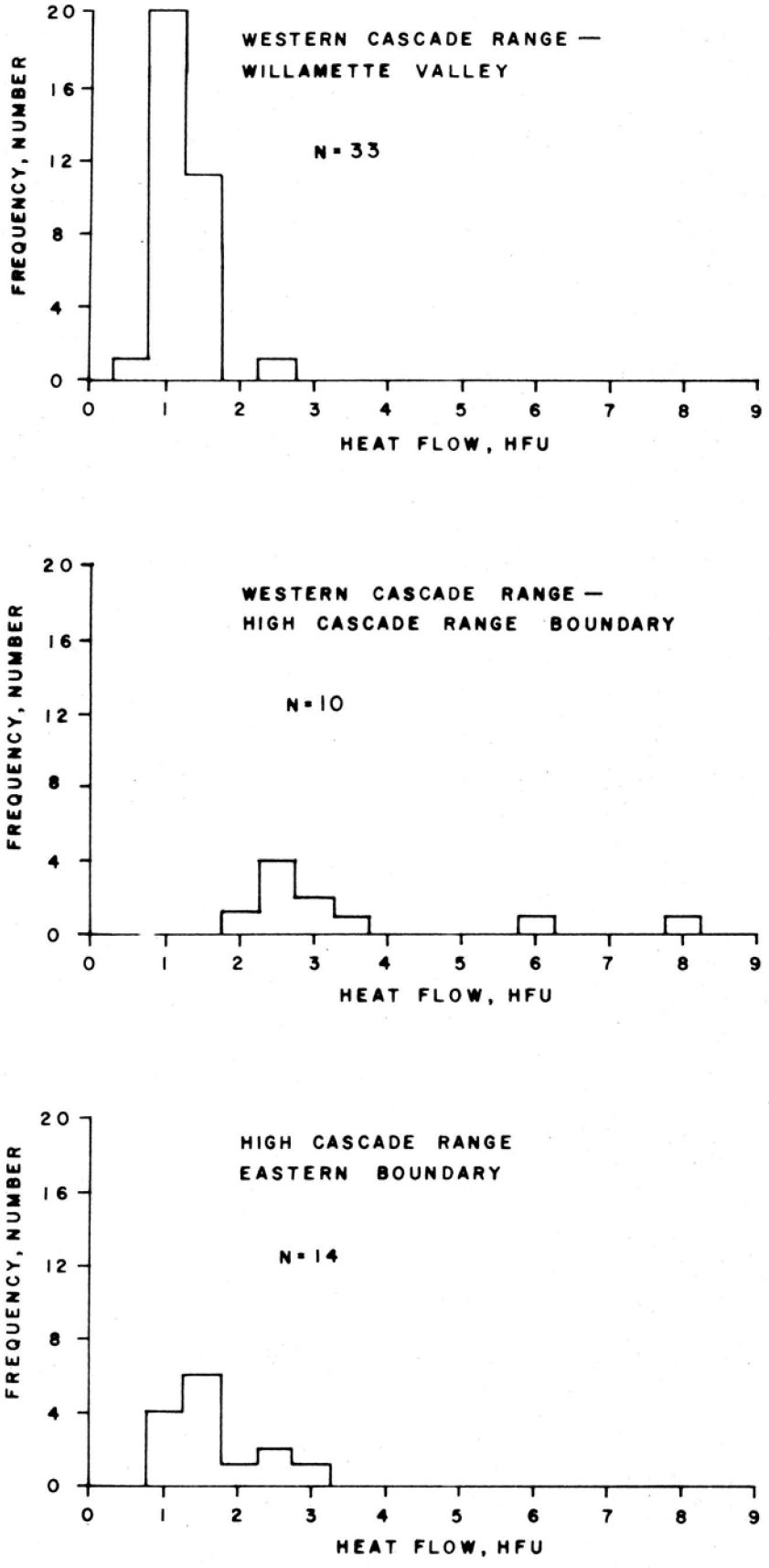

Figure 12. Heat flow histograms for the Northern Cascade Range province boundaries. Values for the histograms are shown in Figure 11.

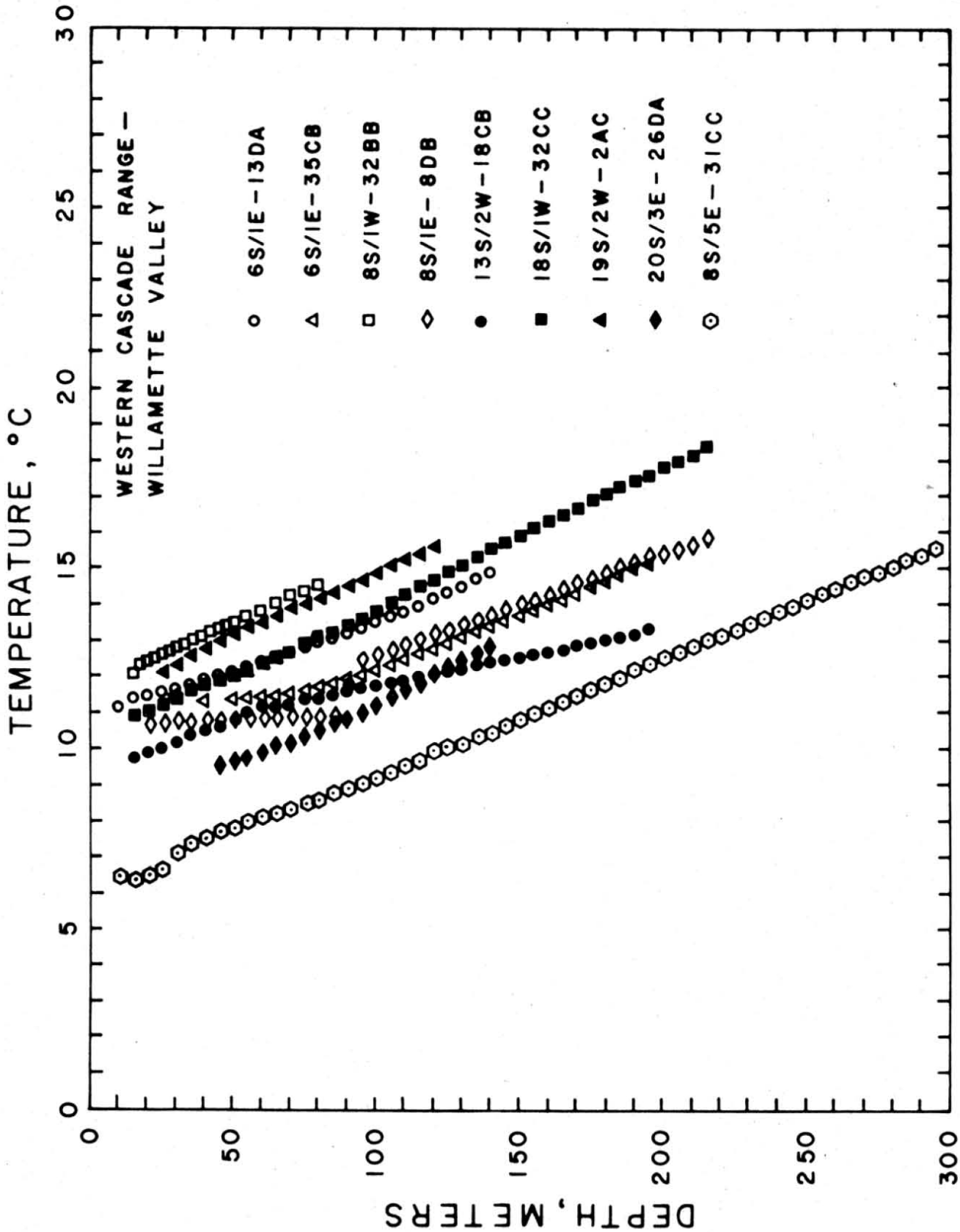

Figure 13. Typical temperature-depth curves for the Western Cascade Range-Willamette Valley province boundary. Locations of holes are given by township/range-section.

holes, which are typically noted in relatively high relief areas and in more brittle acidic rocks are seldom observed in the altered volcanic rocks of the Western Cascade Range-Willamette Valley regions.

Typical temperature-depth curves in the Western Cascade Range-High Cascade Range boundary region are shown in Figure 14. Most of the holes shown in this figure were drilled specifically for heat flow studies and were sited in the general vicinity of existing hot springs which are concentrated along the physiographic boundary between the Western Cascade Range-High Cascade Range provinces.

Detailed cross-sections of the heat flow results are shown in Figure 15 A-B. The cross-sections include corrected geothermal gradients and heat flow. From north to south, clusters of data are along the Clackamas River in the vicinity of Austin Hot Springs, along the Santiam River in the vicinity of Breitenbush Hot Springs, along the McKenzie River in the vicinity of Belknap and Foley Hot Springs, and along the Middle Fork of the Willamette River in the vicinity of McCredie Hot Springs. Each of the cross-sections also includes heat flow values derived from water wells in the western and central parts of the sections. The zero line for distance scale is the mean location of the physiographic boundary between the High Cascade Range and the Western Cascade Range (Figure 11).

Although many of the values plot within the High Cascade Range province (Figure 15 A-B), most of the holes were actually drilled in Western Cascade rocks. The province boundary is quite irregular with the High Cascade rocks generally lying at

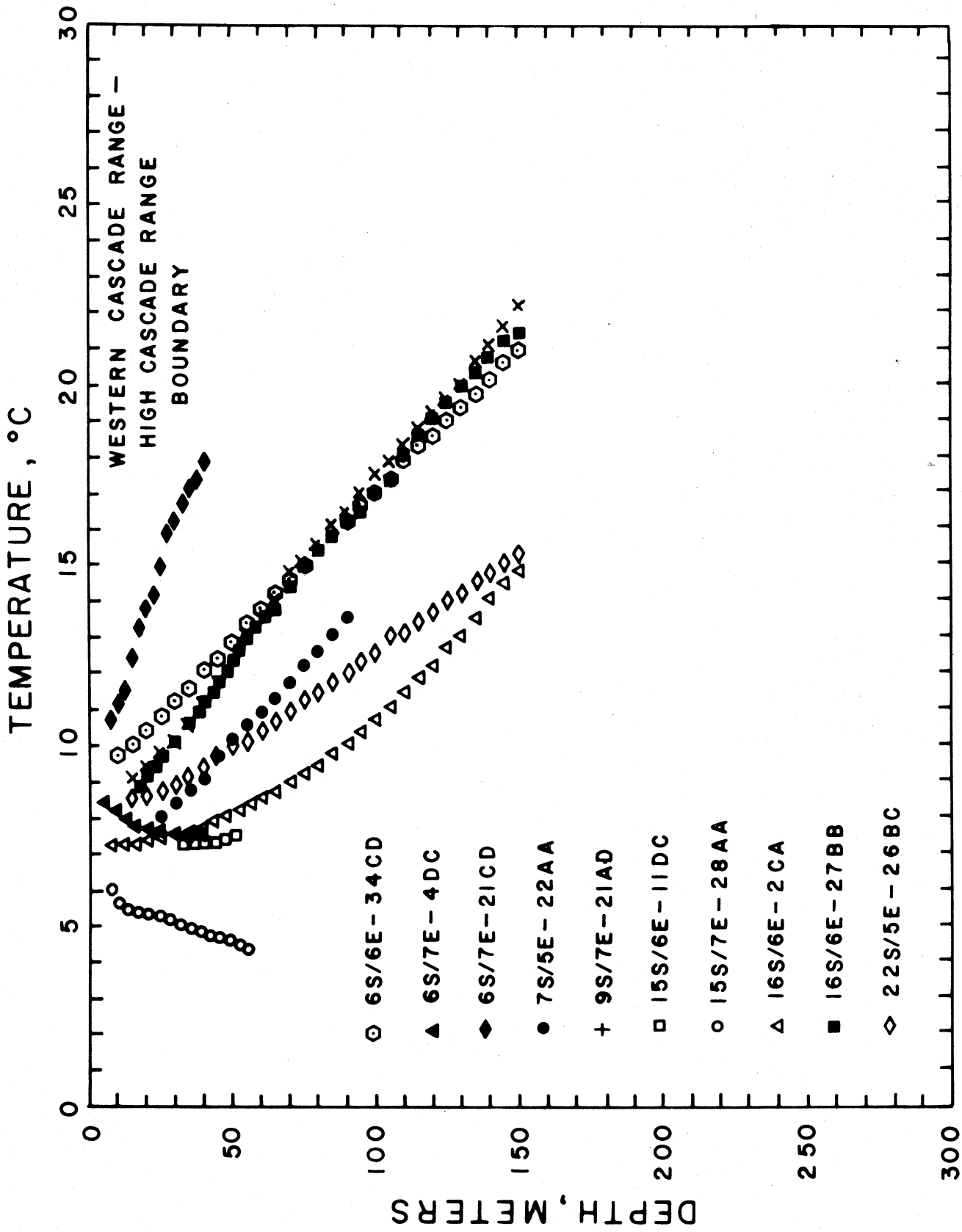

Figure 14. Typical temperature-depth curves for the Western Cascade Range-High Cascade Range province boundary. Locations of holes are given by township/range-section.

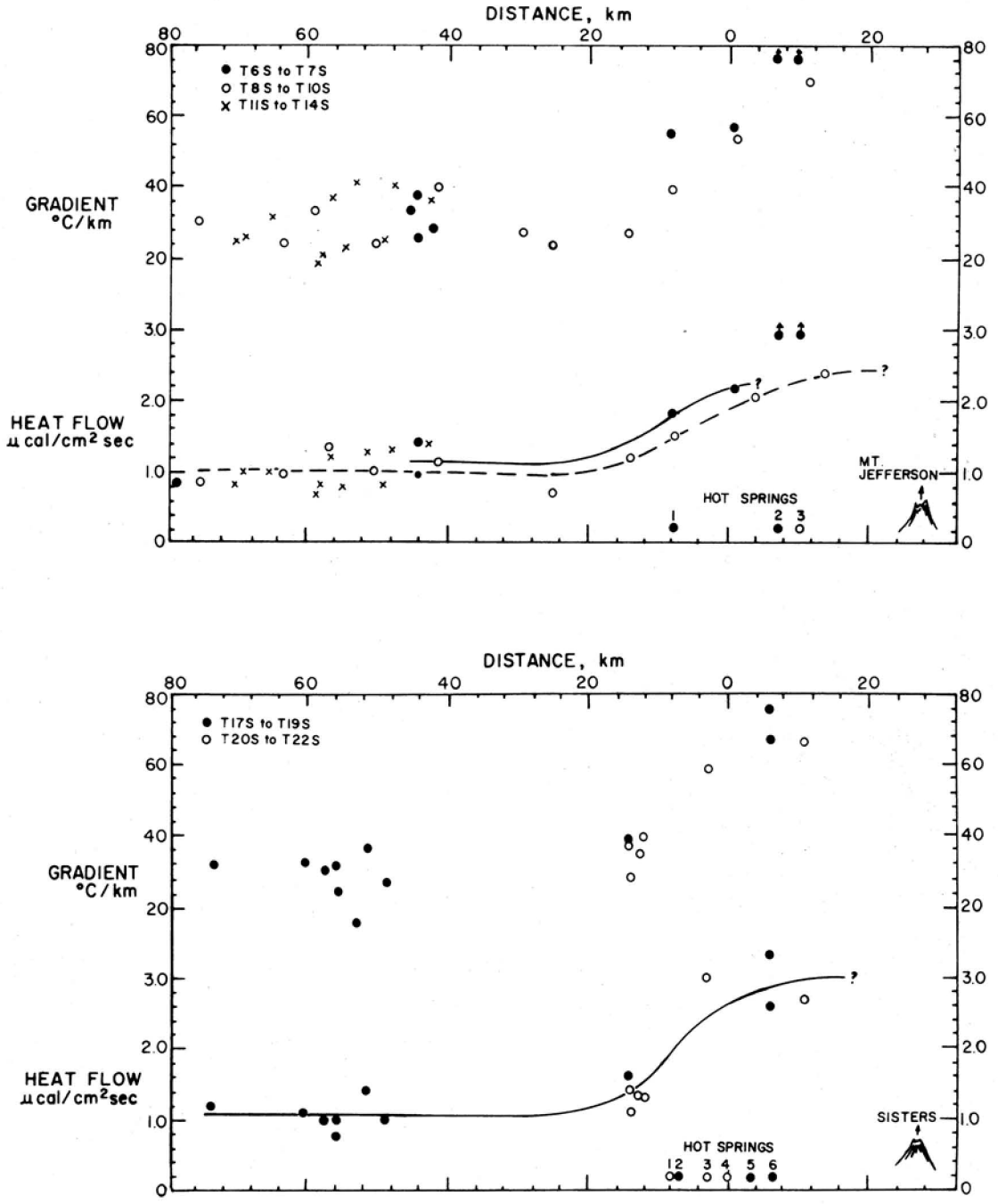

Figure 15 A-B. Heat flow cross-sections of the Willamette Valley-Western Cascade Range-High Cascade Range province boundaries. Heat flow and gradient values are grouped by townships as indicated. The hot springs near Mt. Jefferson (15-A) are (1) Bagby; (2) Austin; and (3) Breitenbush. The hot springs near Three Sisters (15-B) are (1) Cougar Reservoir; (2) Kitson; (3) Foley; (4) McCredie; (5) Wall Creek; and (6) Belknap.

higher elevations than the Western Cascade rocks, so that the latter tend to outcrop along the valleys while the former generally outcrop along the ridges. Three holes in the High Cascade rocks shown in Figure 14 were drilled in inter-canyon flow sequences that descend to lower elevations. All three holes have gradients typical of the downflow or lateral flow regime of an aquifer, although the gradients appear to be regional in the bottom of the drill holes. With these three exceptions, most of the holes have completely conductive gradients.

The data shown on the cross-sections in Figure 15 A-B is discussed in sequence from north to south. The northernmost data set includes the area of Townships 6S and 7S. At the High Cascade Range-Western Cascade Range boundary, the cross-section includes Austin Hot Springs and Bagby Hot Springs along the Clackamas River. A total of eight reliable heat flow values were obtained but the data are relatively widely spaced, one group being in the Willamette Valley and the second group being at the Western Cascade Range-High Cascade Range province boundary. Approximately 10 km west of the physiographic boundary, a heat flow value of 1.8 HFU was noted. The heat flow rises to approximately 2.2 HFU near the physiographic boundary. Two holes within 2 km to the east of Austin Hot Springs display heat flow values in excess of 5 HFU and indicate a relatively large geothermal system along the Clackamas River. This cross-section is the only one along which such high heat flow values, typical of hydrothermal circulation, were located during the drilling phase of the project, even though most of the holes drilled for heat flow values were within 5-10 km of hot springs.

The second set of data was obtained along a cross-section including the areas in Townships 8S and 10S. Eleven reliable heat flow measurements were obtained along this section. This cross-section is primarily along the Santiam River and crosses Breitenbush Hot Springs. The data show an almost constant heat flow of 0.9-1.1 HFU within the Western Cascade Range province. The heat flow rises gradually about 10 km west of the physiographic boundary and attains a value of 2.4 HFU approximately 15 km into the High Cascade Range province and at a distance of about 25 km from the easternmost low heat flow value.

No heat flow data were obtained along the heat flow boundary between Townships 11S and 14S; however, 11 heat flow measurements were obtained in the Western Cascade Range province. These heat flow values average 1 HFU, typical of those observed elsewhere in the province.

A third cross-section lies along the McKenzie River and includes data from Townships 16S to 19S. Holes were drilled just to the west of Belknap Hot Springs and Foley Hot Springs. Ten reliable heat flow measurements were obtained along this cross-section. Approximately 10 km east of the physiographic boundary, a heat flow value of 1.6 HFU was noted. Approximately 5 km east of the physiographic boundary, values of 2.0 HFU and 3.0 HFU were measured near Belknap Hot Springs and Foley Hot Springs, respectively. The distance between the high heat flow and the normal heat flow values is approximately 15 km.

The southernmost cross-section spans the area between Townships 20S and 22S. The holes were drilled in the vicinity of McCredie Hot Springs along the Middle Fork of the Willamette

River. Several free holes were also obtained in this area. These data show that the mean heat flow is 1.2 HFU approximately 8 km west of the physiographic boundary, whereas a value of 3.0 HFU is obtained only 5 km east of the boundary in a drill hole near McCredie Hot Springs. This value drops to 2.7 HFU about 10 km further to the east.

These data document clearly a systematic west-to-east increase in heat flow from 1 HFU to greater than 2.5 HFU over a lateral distance of 10 to 30 km and approximately coinciding with the mean physiographic boundary between the High Cascade Range and the Western Cascade Range provinces.

Interpretation of Heat Flow Transition Zone

All the profiles along the boundary between the Western Cascade Range and High Cascade Range provinces show the same characteristics: an almost constant heat flow with a mean value of 1 HFU in the High Cascade Range, and a mean heat flow of 2.6 HFU in holes drilled in Western Cascade rocks; an exceedingly abrupt transition zone between the two regions of heat flow, not exceeding 30 km in any location. The most remarkable aspect is the uniformity of the transition zone from north to south; although small variations may exist, the data suggest very similar conditions along the whole area under discussion.

In order to interpret the results, heat flow profiles representing several possible transition zones were constructed. These are shown in Figure 16 A-B. The different profiles represent different half-widths for the heat flow transition

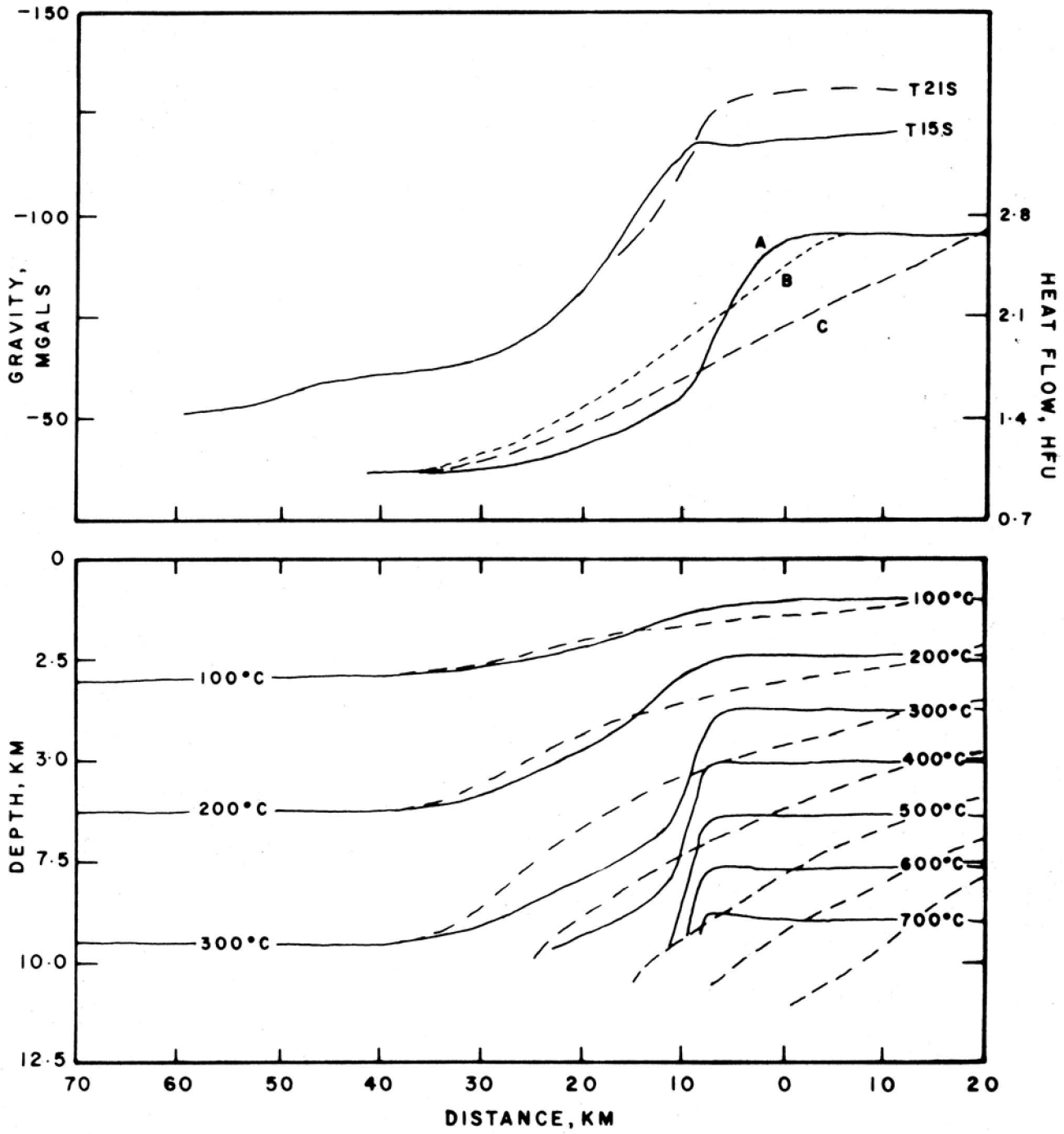

Figure 16 A-B. Heat flow-gravity transition zone models. In 16A, gravity curves are indicated by latitude, and heat flow curves are indicated by A, B, C. The heat flow curves are based on data from Figure 15: curve C, from the 6S-7S profile (15A); curve A, from the 20S-22S profile (15B). In 16B, steady-state isotherms corresponding to curve A are indicated by the solid lines, and those corresponding to curve C are indicated by the dashed lines.

based on the data in the 6S-7S profile (the largest half-width, curve C), the 20S-22S profile (the shortest half-width, curve A), and an intermediate half-width representing an average of the whole data set (see Blackwell and others, 1978).

Based on these heat flow transition zone profiles, temperature-depth cross-sections were calculated for two extreme cases of transition zones represented by curves A and C. The temperature values are based on a modification of the continuation of thermal data method discussed by Brott (1976). The more gradual transition zone has most of the heat flow difference occurring over a distance of 30 km, while the other shows a much sharper transition zone (over a distance of approximately 15 km). The isotherms were constructed for a steady-state and a transient model. In both models, homogeneous thermal conductivity was assumed. Because the geologic evidence indicates that greater than 6 m.y. BP the Western Cascade Range was the locus of intrusive activity, and because the heat flow now observed is low, there is strong evidence for a major temporal change in heat flow. The temperature sections were calculated assuming steady-state conditions, and assuming a uniform heat flow for the whole region of 2.5 HFU up to 6 m.y. ago with subsequent imposition of a constant strength heat sink beneath the Western Cascade Range which has resulted in the low heat flow values now observed. Over the scale of the area involved here, however, the steady-state and 6 m.y. temperatures do not differ significantly and so only the steady-state results are illustrated.

Both models imply very high temperature at relatively

shallow depth beneath the High Cascade Range and extending approximately 10 km into the Western Cascade Range. Any one of the isotherms shown could satisfy the heat flow anomaly so the source does not necessarily have to reach or exceed 700°C; however, the source does have to be relatively shallow and relatively intense. Because of the uniformity of the heat flow data from north to south, it seems unlikely that the boundary can be simply related to hydrology and therefore must be related to some regional crustal effect.

As discussed elsewhere, attempts to investigate the extension of the heat flow pattern further to the east toward the axis of the High Cascade Range have been unsuccessful. Volcanism has been most continuous during the Quaternary along the axis of the High Cascade Range and the cover of young volcanic rocks, with concomitant horizontal water circulation, effectively prevented successful heat flow determinations in this area at depth of 150 m or less.

Also shown in Figure 16A are two Bouguer gravity cross-sections, one at 44°15'N latitude and one at 43°45'N latitude. These profiles have been constructed from data discussed by Couch and Baker (1977). The profile for 44°15'N was extended west of the area based on the regional change in Bouguer areal gravity associated with (but opposite in sign to) the heat flow data. This gravity change is of major magnitude (over 50 milligals) and of relatively short half-width (10-15 km). The short half-width implies a crustal source for the density contrast which results in the gravity change. The coincidence of this gravity anomaly with the heat flow anomaly is additional

evidence that the heat flow data are related to regional crustal effects and not to upper crustal groundwater circulation.

Because of the close correspondence of the two sets of data, an interpretation of the gravity data was attempted based on the continuation model of crustal temperatures presented in Figure 16. In an attempt to model the gravity anomaly, a density contrast corresponding to the expansion of the rocks, based on the calculated temperatures, was assumed. These density contrast models did not generate a large enough gravity anomaly. Of course, in a complicated mountainous terrain with young volcanic rocks, density variations may be related to different factors. For example, in the High Cascade Range, shallow volcanic rocks may have a much lower density than the $2.67\ g/cm^3$ assumed in the reduction, whereas the density of the low-porosity rocks of the Western Cascade Range may be closer to the Bouguer reduction density.

The overall result of the interpretation is that a regional magma chamber or area of thermally anomalous crust exists under the High Cascade Range of Oregon. The width of the thermal anomaly is somewhat larger than the apparent width of the zone of volcanism and it extends at least 10 km west of the physiographic boundary of the province. Regional heat flow and gravity anomalies are associated with this disrupted crustal zone.

Most of the hot springs in the Cascade Range are located near the boundary of this region of high heat flow. This location may be related to a number of different effects such as the hydrologic conditions; location of faults, or fractures, along the boundary which focus the circulation of water;

outcrop of some horizontal unit that transmits water from higher elevations to the east; the location of permeable fractured acidic rocks at depth; and/or the possible location of a slightly more effective heat source.

Heat Flow Along the Eastern Boundary of the High Cascade Range

The heat flow data relating to the eastern boundary of the High Cascade Range geothermal anomaly are considerably less detailed and less consistent than those associated with the western boundary. The heat flow values in this area are shown in Figures 10 and 11. Typical temperature-depth curves are shown in Figure 17.

Around Bend, most of the holes are isothermal or show very irregular gradients to the maximum depth reached in each hole. To the north, generally conductive temperature-depth curves are obtained for holes in the older rocks immediately to the east of the High Cascade lavas. One hole (11S/15E-22cd) which was logged to a depth of over 800 m gives a heat flow of 2.0 HFU. A number of values are available further to the north. They are somewhat variable, ranging from average values for the Columbia Plateau (1.5 $\pm$ 0.3 HFU) to values greater than 2.0 HFU. On the basis of the data available at this time, no clear pattern has emerged and in fact, there may be considerable variations in the regional anomalies along the northeastern margin of the High Cascade Range.

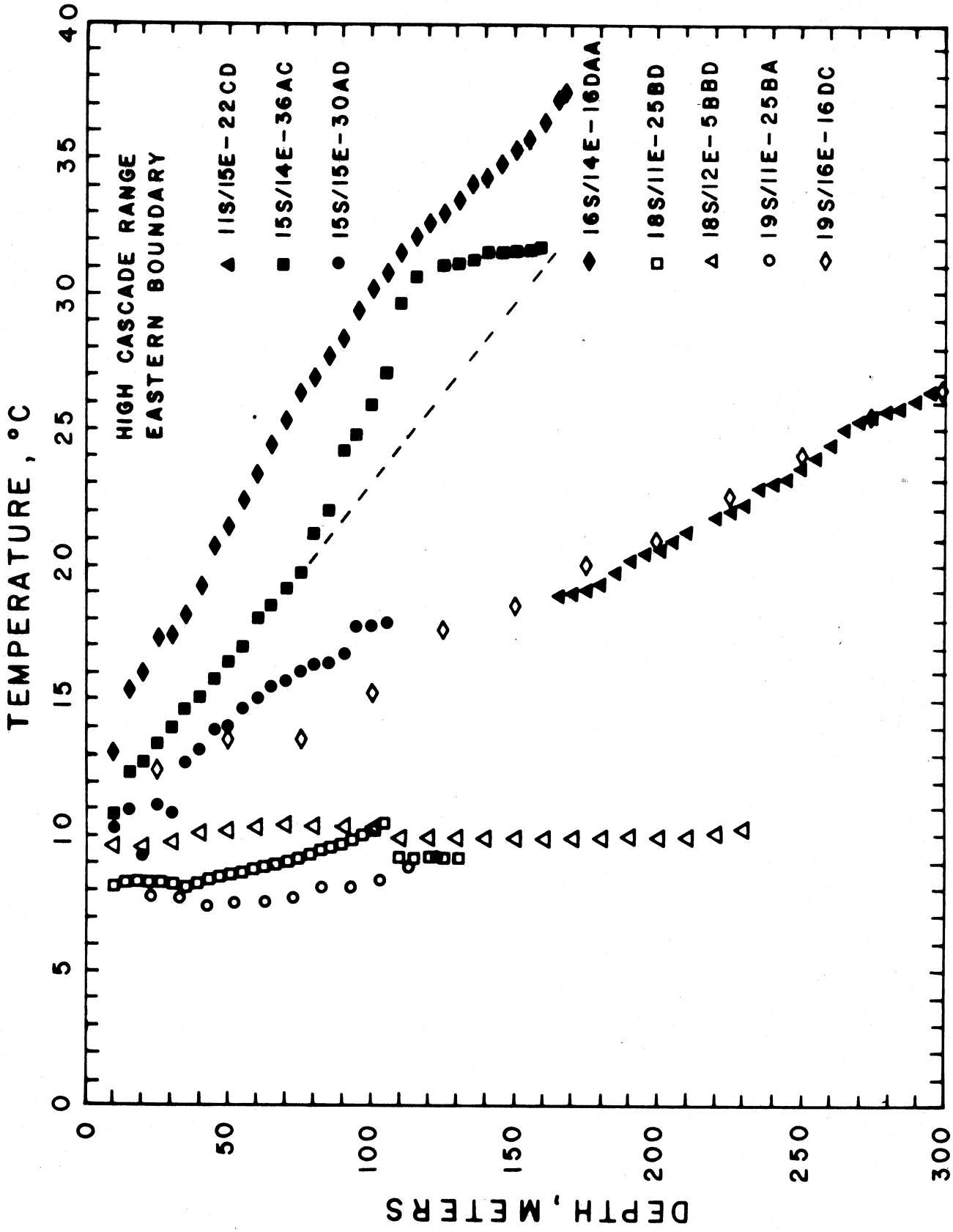

Figure 17. Typical temperature-depth curves for the eastern High Cascade Range province boundary. Locations of the holes are given by township/range-section.

GEOTHERMAL STUDIES ASSOCIATED WITH MT. HOOD

The main emphasis of this project was the analysis or theoretical study of magma chambers possibly associated with andesite volcanoes and a heat flow study of the Mt. Hood region. As part of the heat flow study of the Mt. Hood region, several holes were located during 1976 and 1977 in the Willamette Valley, along the eastern border of the High Cascade Range, and west of the Hood River Valley. In 1976, three holes were drilled specifically by DOGAMI for heat flow, one near Timberline Lodge, one near the southern margin of Mt. Hood, and one in the fine-grained plutonic rocks approximately 10 km southwest of Mt. Hood.

In 1977-78, two deep holes were drilled, one on the slope of Mt. Hood near Timberline Lodge, and one at Old Maid Flat along the Sandy River. In addition, eleven 150 m holes were drilled by DOGAMI for heat flow studies in the near-region of Mt. Hood in the fall of 1978. Temperature-depth curves for most of these holes are shown in Figure 18. The locations of all these drill holes and heat flow values (where appropriate) are shown in Figure 11.

Mt. Hood Regional Heat Flow Studies

The same dichotomy in heat flow regime is observed in the vicinity of Mt. Hood that is seen in holes drilled to the south. Drill holes that encounter rocks characteristic of the Western Cascade Range province, generally display conductive geothermal gradients. However, when the rocks drilled are of Pliocene or Pleistocene age, characteristic of the High Cascade

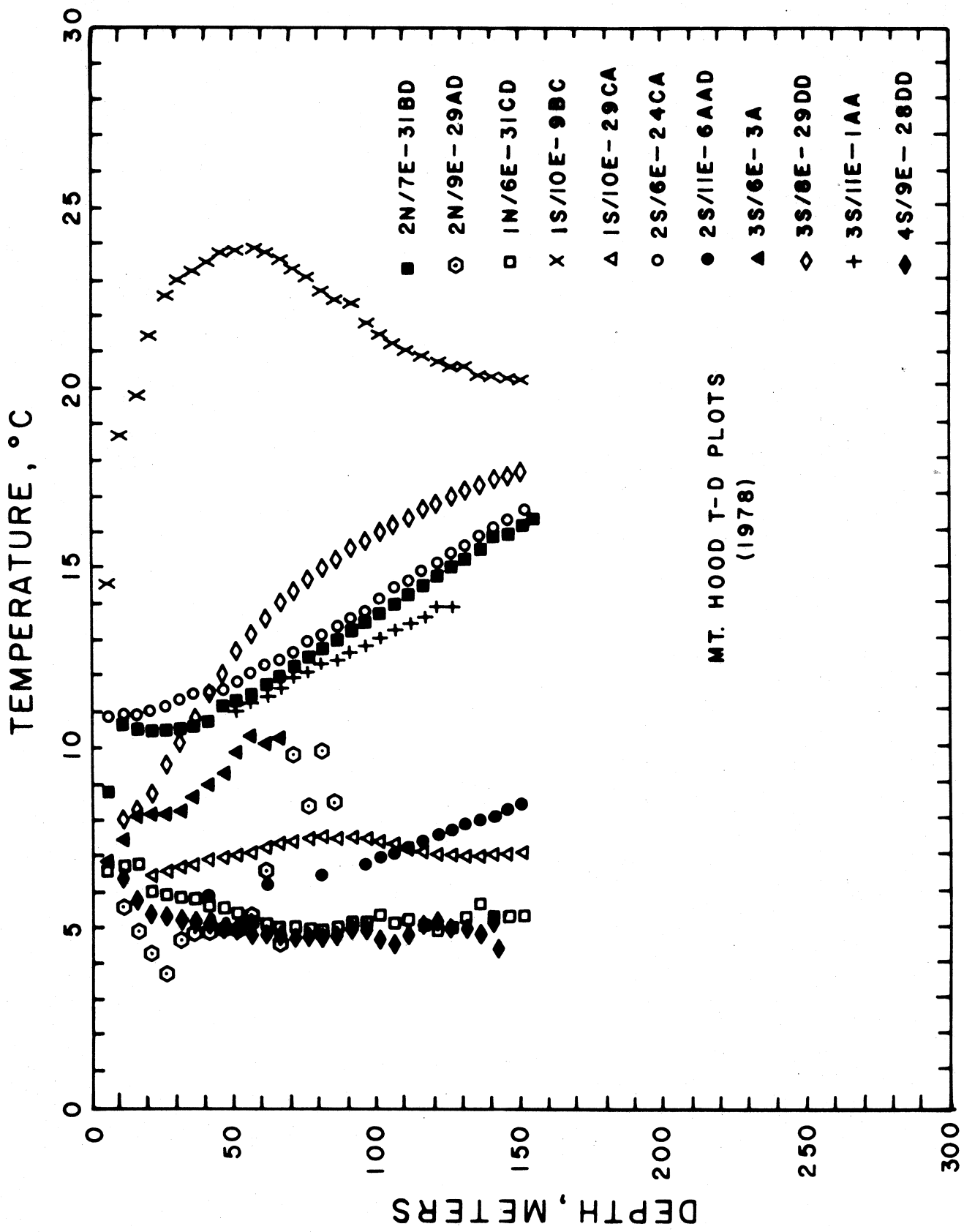

Figure 18. Temperature-depth curves for holes drilled by DOGAMI in 1978 in the Mt. Hood area. Locations of the holes are given by township/range-section.

Range, the holes do not yield useful geothermal gradient data. Most of the 150 m holes in these latter rocks gave isothermal temperature-depth curves.

The heat flow data are shown in Figure 19 projected onto a cross-section of the Cascade Range in the vicinity of Mt. Hood. The major transition zone observed to the south appears to exist in a somewhat subdued form at the latitude of Mt. Hood. Regional values of heat flow away from the volcanic edifice appear to be on the order of 1.5-1.8 HFU, as compared to values in excess of 2.5 HFU in locations to the south.

Only in the Old Maid Flat exploratory hole (2S/8E-15cd), at the toe of the volcano, is a value comparable to those to the south observed. Similarly, a gravity anomaly related to the heat flow transition also appears to be somewhat subdued compared to that further south (see Figure 16). The gravity data currently available are much less detailed than those used in the south. More detailed studies soon to be available (Couch, personal communication, 1979) will possibly allow better analysis of the relationship between gravity data and heat flow data at the latitude of Mt. Hood.

The continuation temperature model using these data shows lower temperatures (except in the immediate vicinity of Mt. Hood) than those shown in Figure 16. This model (not shown herein) is largely hypothetical due to the paucity of data in the immediate vicinity of the volcano and the large scatter of values, especially on the east side of the volcano.

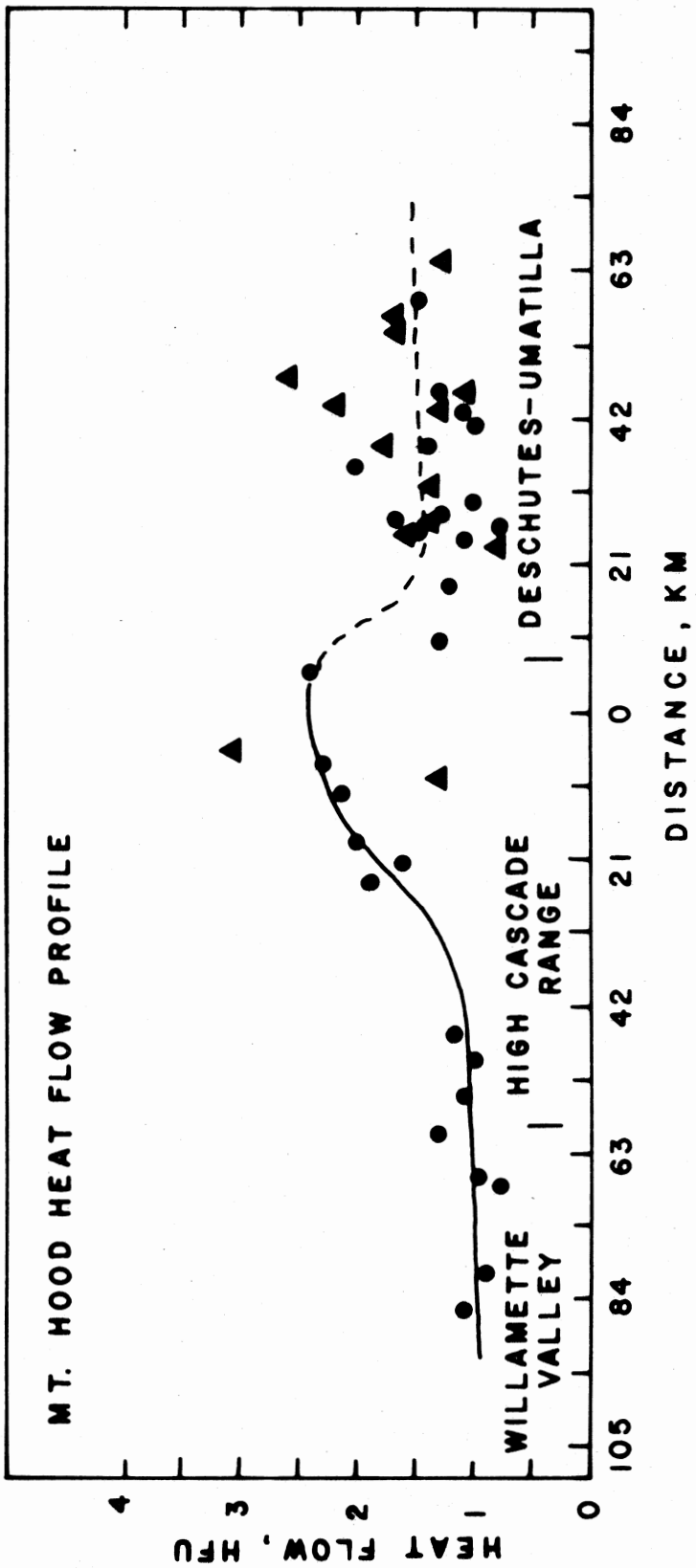

Figure 19. Heat flow profile of Mt. Hood. Baseline reference is through the profile of Mt. Hood. Heat flow values occurring south of Mt. Hood down to Latitude 45°N are represented by solid triangles, and heat flow values occurring north of Mt. Hood up to the Oregon-Washington border are represented by solid circles. All heat flow values are from Figure 11.

Old Maid Flat Holes #1/2 and #3

A major part of the project involved geothermal analysis by SMU and DOGAMI of a 1220.4 m deep geothermal test well drilled in the immediate vicinity of the Mt. Hood volcano. The hole is located at 2S/8E-15cd, along Old Maid Flat in the Sandy River valley, approximately 5 km from the apex of Mt. Hood, but almost 2 km lower in elevation.

The hole was initially drilled in the winter of 1977 to a total depth of 480 m, and designated Old Maid Flat #1. The drilling was done in two phases. A set of near-equilibrium temperature measurements was made during a pause in the drilling, for the purpose of setting casing, when the total depth was 230 m. This log (11/15/77) is shown in Figure 20. The gradient shows a disturbance in the uppermost 75 m of the hole. Below that, the gradient is linear, with a mean value of 67°C/km.

Upon completion of the hole (480 m), the temperature log (12/20/77) shows essentially equilibrium temperatures after completion of the second phase of the drilling. The log shows a somewhat higher temperature at the depths measured in the first log, with a uniform gradient of 67°C/km between 100-300 m. Below 300 m, the gradient decreases and then increases again with a value of approximately 65°C/km observed between 430-475 m. The absolute temperature values between 70-200 m in the 11/15/77 log and between 435-475 m in the 12/20/77 log are compared in Figure 20. At the time of the 12/20/77 log, there was a flow of about 10 ℓ/min from the collar of the drill hole. The nature of the temperature-depth curves indicates that a

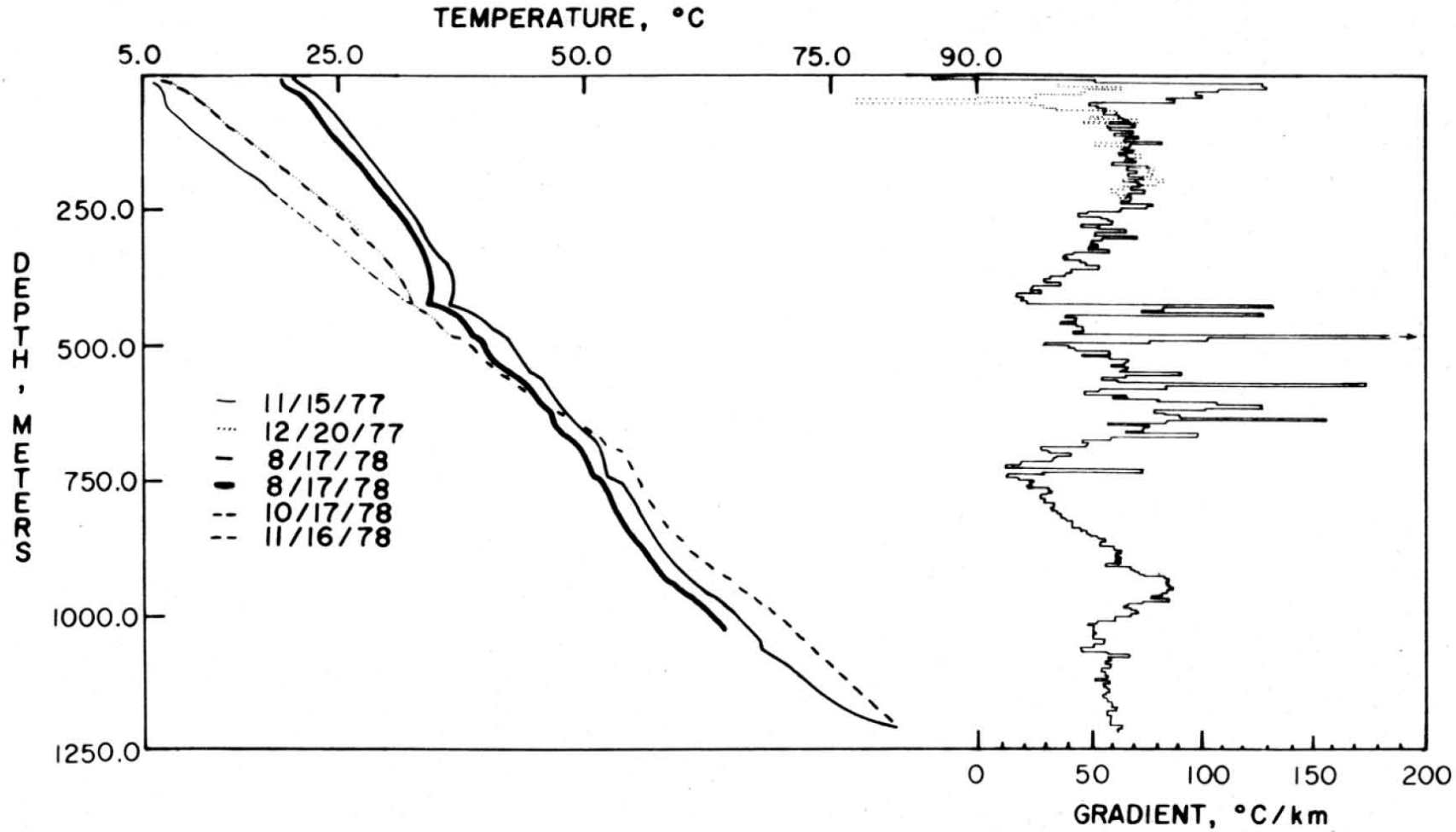

Figure 20. Temperature-depth curves for the Old Maid Flat Hole #1/2. Different dates of logging are represented by the symbols indicated. The bar graph at the right side of the figure is from the 11/16/78 data.

fracture zone with artesian fluid pressure was encountered at a depth of 430 m. At the time of the second logging, water was moving slowly up the borehole from that depth and out at the collar. The temperature of the water column is offset by about 4°C by this upflow in the borehole; thus, undisturbed temperatures in the borehole would agree approximately with the 11/15/77 log.

During the summer of 1978, the hole was deepened to a total depth of 1220.4 m and designated Old Maid Flat #2. Immediately after completion of the drilling, two temperature logs were made on 8/17/78. The lighter line on Figure 20 represents measurements by a commercial well-logging firm, while the heavier line represents measurements made with SMU's truck-mounted logging system, with a total depth capability of 1035 m. The shapes of the temperature-depth curves are essentially the same, but are offset by approximately 2°C. This could be due either to a calibration difference between the two sets of gear, or to differences in the actual temperature of the hole at the times of logging; however, the offset is probably due to a combination of causes.

The rapid return to equilibrium of temperatures in the artesian zone (around 435 m) is illustrated in the logs made immediately after the drilling. After completion, a 2" diameter observation pipe was set into the hole, but no attempt was made to grout the tubing as the hole is to be used to obtain fluid samples. Therefore, natural inter-formation flow in the annulus is not prevented by the completion technique.

After stabilization, the hole was logged on 10/17/78 by

SMU, to a total depth of 1035 m, and on 11/16/78 by USGS, to a total depth of 1214 m (John Sass, personal communication, 1978). Only the 11/16/78 USGS log is shown in detail, as the 10/17/78 SMU log is not significantly different. The temperature-depth curves observed at equilibrium are quite irregular. Even after the theoretical time needed for recovery of the temperatures, gradients in the middle part of the hole (between 300-1000 m) remained highly irregular, with significant changes which cannot be attributed to lithology. These changes are represented by the bar graph on the right side of Figure 20.

The only reasonable explanation for these gradients is a very large amount of borehole fluid communication. In fact, the only part of the hole which appears unaffected by intra-borehole fluid communication is that below 1,100 m. In this bottom portion of the hole, two distinct gradients are observed: a gradient of 52°C/km between 1010-1070 m, and a gradient of 61°C/km between 1170 m-total depth. The gradients in the central part of the hole appear to be due to fluid flow between fracture zones or flow contacts. There appears to be no instance of water flow from a single fracture zone all the way up or down the borehole, but merely localized effects. Each of the spikes of high gradient (Figure 20) corresponds to a fracture zone or flow contact. It appears that upflow is generally seen in the upper part of the hole, whereas downflow is typical of the bottom part of the hole.

If the hole had been grouted, this fluid flow would have been eliminated and a much simpler conductive gradient would be seen. Details of geothermal gradient cannot be deciphered

from the complexities of intra-borehole fluid flow. However, it is clear that the mean gradient over the entire borehole is relatively well-established, even if the detailed variations are not.

Thermal conductivity measurements were made on cuttings from between 580-1219 m. The measurements were made at intervals of approximately 30 m. Porosity values for the various depths were estimated from a neutron log. Most porosity values averaged between 1-10 percent, and these values were taken into account when calculating in situ conductivity. The mean thermal conductivity for all samples is 4.12 $\pm$ 0.14 mcal/cm-sec-°C. There are no systematic depth variations based on the bulk conductivity; however, if porosity is taken into account it would appear that slightly lower values of thermal conductivity (approximately 3.8 mcal/cm-sec-°C) occur between approximately 850-1000 m, with higher values (approximately 4.5 mcal/cm-sec-°C) above and below that zone.

The break in gradient at 1070 m, indicated in the temperature-depth curves, does not correspond with a change in thermal conductivity; however, on the commercial temperature log of 8/17/78 a "kink" in the curve was observed at that point, indicating the location of a possible fracture zone. Possibly there is some flow in the hole around this point, with the disturbed conditions only observed below 1070 m.

The mean gradient for the entire hole is 65°C/km, while that for the most undisturbed portion (below 1070 m) is 60°C/km. The gradients for the two apparently undisturbed sections of the upper part of the borehole (25-200 m and 430-475 m) are

60°C/km and 65°C/km, respectively. Taking all these data into consideration, the mean terrain-corrected heat flow for the Old Maid Flat hole is 2.4 HFU. The significance of this value with respect to the surrounding values has been discussed in the preceding section on regional heat flow in the vicinity of Mt. Hood.

Another hole, drilled to completion on 12/13/78 by Northwest Geothermal Corp., to a total depth of 400 m, was designated Old Maid Flat #3. This hole (2S/8E-17cc) is located about 3 km southwest of Old Maid Flat #1/2. The general lithology encountered in the hole is: recent mudflow debris, 0-35 m; pyroclastics with volcanic debris, 35-305 m; and an alternating sequence of Columbia River basalt and andesitic volcanic rock down to 400 m.

The first temperature-depth measurement by DOGAMI (Figure 21) was made on 12/5/78, when the hole was at a total depth of 152 m. The linear portion of the curve, from 75 m to total depth, appears undisturbed and yields a thermal gradient of 50°C/km. The disturbed upper portion of the temperature curve is probably due to fluid motion and drilling effects in the mudflow and upper pyroclastic sequence of rocks.

The hole was temperature-logged again by DOGAMI on 12/21/78 after being drilled to completion (Figure 21). The gap in the curve from 215-325 m is due to lost paperwork. However, from hand-plotted field results, the curve in this interval indicates a fluid disturbance originating around 275 m and affecting the entire missing interval. Excluding the data gap, the upper portion of the 12/21/78 log agrees in general with

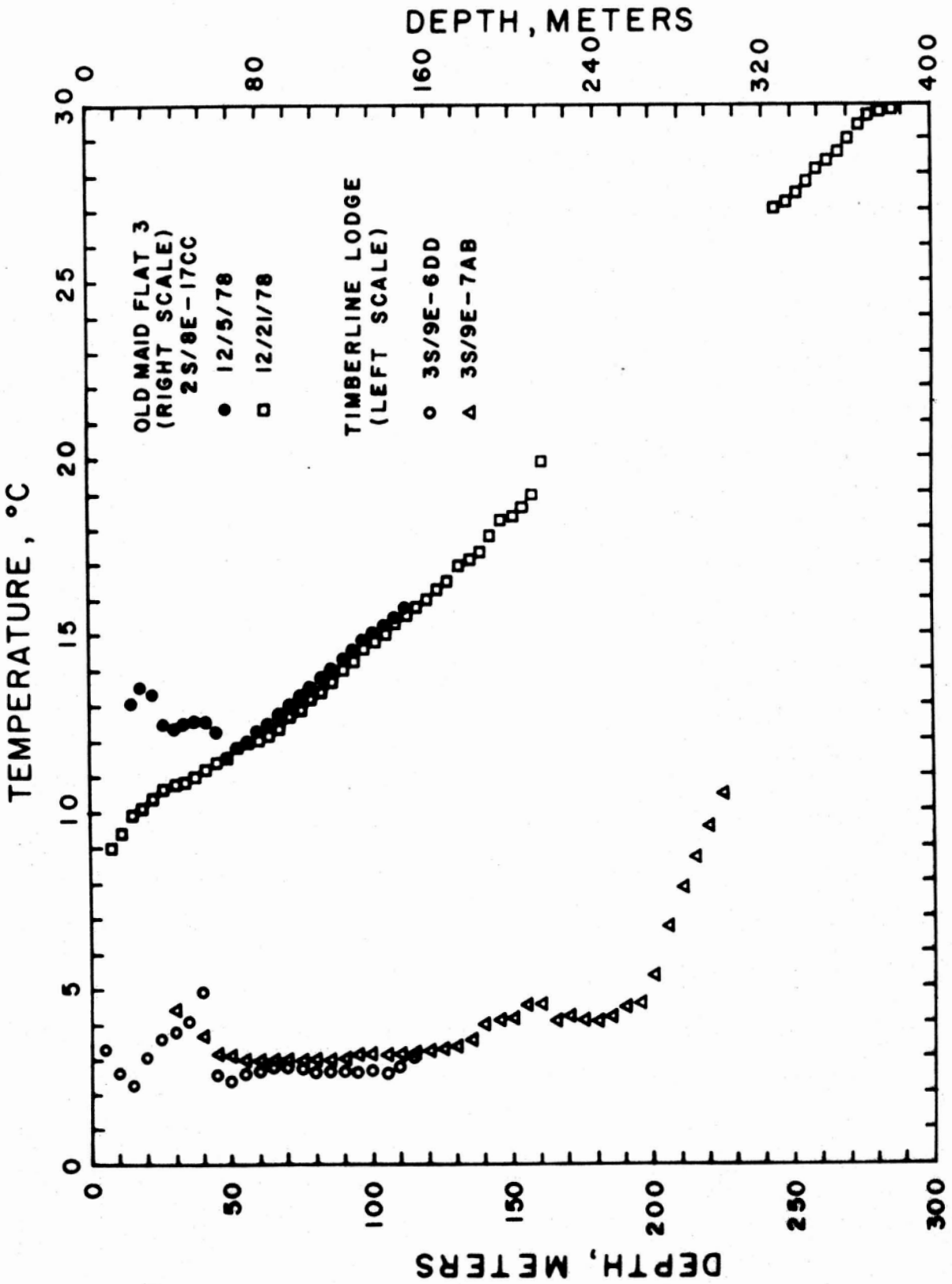

Figure 21. Temperature-depth curves for the Old Maid Flat hole #3 and the Timberline Lodge holes #1 and #2. The scale on the right side of the figure is for the Old Maid Flat hole #3 curve, and the scale on the left side of the figure is for the Timberline Lodge holes #1 and #2 data.

the 12/5/78 log; the lower portion of the 12/21/78 log gives a thermal gradient of 63°C/km.

Based on five measurements of the pyroclastic sequence of rocks, a thermal conductivity value of 4.04 $\pm$ 0.31 mcal/cm-sec-°C was obtained. A terrain-corrected thermal gradient of 51.2°C/km, with the above thermal conductivity, yields a corrected heat flow value of 2.1 HFU.

Timberline Lodge Drill Holes #1 and #2

On 9/8/76, a hole was completed to a total depth of 152 m on the carapace of Mt. Hood, about 0.2 km east of the Timberline Lodge Ski Resort. Timberline Lodge #1 (3S/9E-6dd) encountered mostly andesitic-type rocks, ranging from scoriaceous to basaltic andesite with fracture zones at 43 m, 91 m, and possibly at 122 m. The fracture at 43 m had an aquifer flow of about 19 ℓ/m.

The hole was temperature-logged on 9/8/76, 9/13/76, and 9/14/76. The 9/14/76 temperature curve (Figure 21) shows the effect of the aquifer at 43 m. The rest of the curve is essentially isothermal and not suitable for heat flow studies.

Two years later, another hole was drilled about 0.5 km south of the Lodge. Timberline #2 (3S/9E-7ab) encountered the same type of rocks as Timberline #1, to a total depth of 421 m. The resulting 12/13/78 temperature log (Figure 21) only reached 225 m, due to caving and drilling problems in the hole. Again, this hole shows fluid flow problems similar to Timberline Lodge #1, and over a similar depth interval. The linear gradient in the last 30 m of the hole appears to occur below

the aquifer zone, but has not yet approached the expected undisturbed gradient. The hole is currently considered unsuitable for heat flow studies.

REFERENCES

Blackwell, D. D., and Baag, C., 1973, Heat flow in a "blind" geothermal area near Marysville, Montana, Geophysics, 38, 941-956.

Blackwell, D. D., Hull, D. A., Bowen, R. G., and Steele, J. L., 1978, Heat flow in Oregon, Special Paper 4, Dept. of Geology and Mineral Industries, State of Oregon.

Brott, C. A., 1976, Heat flow and tectonics of the Snake River Plain, Idaho, Ph.D. thesis, Southern Methodist University, Dallas, Texas.

Carslaw, H. S., and Jaeger, J. C., 1959, Conduction of Heat in Solids, 2nd ed., University Press, Oxford, England.

Couch, R., and Baker, B., 1977, Geophysical investigations of the Cascade Range in Central Oregon, Final Report, U. S. Geological Survey, grant #14-08-0001-G-231.

Crandell, D. R., and Rubin, M., 1977, Late-glacial and post-glacial eruptions at Mt. Hood, Oregon (abstract), Geological Society of America, Abstracts With Programs, 9, p. 406.

Jaeger, J. C., 1964, Cooling and solidification of igneous rocks, in H. H. Hass and A. Poldervaart, eds., Basalts 2, Interscience, New York, p. 503-536.

Jaeger, J. C., 1964, Thermal effects of intrusions, Review of Geophysics, 2, p. 443-466.

Lachenbruch, A. H., Sass, J. H., Munroe, R. J., and Moses, T. H. Jr., 1976, Geothermal setting and simple heat conduction models for the Long Valley Caldera, Journal of Geophysical Research, 81, p. 769-784.

LaFehr, T. R., 1965, Gravity, isostasy, and crustal structure in the Southern Cascade Range, Journal of Geophysical Research, 70, p. 5581-5597.

Rikitaki, T., 1959, Studies of the thermal state of the earth, 2, Heat flow associated with magma intrusion, Bulletin of Earthquake Research Institute, Tokyo University, 37, p. 233-243.

Sass, J. H., Lachenbruch, A. H., Munroe, R. J., Green, G. W., and Moses, T. H. Jr., 1971, Heat flow in the western United States, Journal of Geophysical Research, 76, p. 6356-6431.

Schuster, J. E., Blackwell, D. D., Hammond, P. E., and Huntting, M. T., 1978, Heat flow studies in the Steamboat Mountain-Lemhi Rock area, Skamania County, Washington, Washington Division of Geology and Earth Resources, Information Circular 62.

REFERENCES (Con't.)

Simmons, G., 1967, Interpretation of heat flow anomalies, 2, Flux due to initial temperature of intrusives, Review of Geophysics, 5, p. 109-120.

Smith, R. L., and Shaw, H. R., 1975, Igneous-related geothermal systems, U. S. Geological Survey Circular 726, p. 58-83.

Thiruvathukal, J., 1968, Regional gravity of Oregon, Ph.D. thesis, Oregon State University, Corvallis, Oregon.

Wise, W. S., 1969, Geology and petrology of the Mt. Hood area: A study of High Cascade volcanism, Geological Society of America, Bulletin 80, p. 969-1006.

Yuhara, 1974, Morphological, hydrological and thermal characteristics of active volcanoes having no geothermal areas; and artificial hydrothermal systems for utilizing their latent internal heat: In Utilization of Volcano Energy; Colp, J. L. and Furnmato, A. S., eds., Sandia Labs Publ., Albuquerque, 23 pp.

OVERVIEW

Temperature Gradients

DOGAMI, in late 1978, successfully completed the drilling of eleven temperature gradient holes in the Mt. Hood area (Figure 1) to depths ranging from 76 to 152 m. Temperature gradients for the holes are shown in Figure 18 (Blackwell and Steele, 1979). Heat flow implications of these holes are discussed by the above authors. Those holes that were collared in the Columbia River Basalt or the Eagle Creek Formation were usable for heat flow determinations (1S/10E-9bc, 2S/6E-24ca, 3S/11E-1aa, and 2N/7E-31bd). The remainder of the holes that were collared in either andesite, alluvium, Pliocene volcanics, or plutonic rocks did not lend themselves to adequate heat flow analyses.

Based on the evaluation of the temperature-depth curves for the Mt. Hood area, it is apparent that holes collared in these materials need to be drilled much deeper than the heretofore depth of 152 m (500 ft). The quality of the data is affected by ubiquitous flows of water, lost circulation zones, indeterminate number of cinder and ash flows and/or soil or deeply weathered horizons. Thus, for holes not collared in the Columbia River Basalt or the Eagle Creek Formation, depth should be increased to at least a minimum of 305 m (1000 ft). The further upslope on the cone, the deeper the holes should be.

In order to better understand the heat flow regime of Mt. Hood, additional temperature gradient holes should be drilled

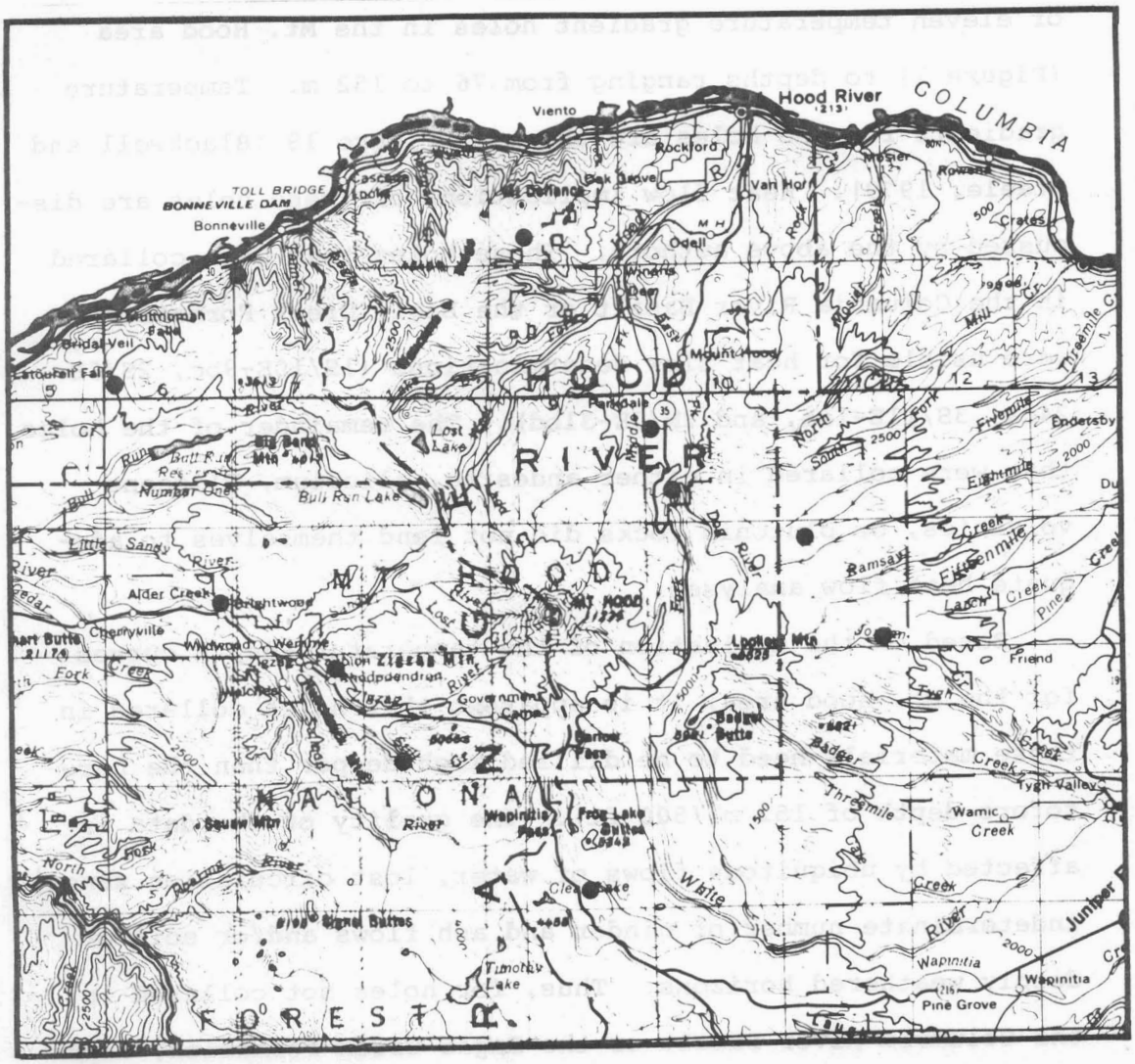

Figure 1. Location of temperature gradient holes, Mt. Hood area, Multnomah, Hood River, Clackamas and Wasco Counties. Scale - 1:500,000.

on the upper flanks of the cone and around the periphery or base of the volcano to fill in the gaps from the heat flow drilling recently completed. Northwest Geothermal Corp. has an ambitious drilling program with holes programmed to 500-2000 ft in depth for the southwesterly part of the Mt. Hood area. Further, the USGS plans to drill eight (8) hydrologic investigatory holes on or around Mt. Hood. Six holes are planned for the southern flank of the volcano; two holes on the northern flank. These holes, which are to be drilled to 500-2000 ft in depth, are to be equipped for temperature gradient measurements when the hydrologic studies are completed. It is entirely possible that the holes to be drilled by these two entities may suffice for the additional holes recommended.

The only geothermal anomaly discovered from the temperature gradient investigation was from a hole in Hood River Valley (1S/10E-9bc) northeast of Mt. Hood. The temperature-depth curve for this hole is shown in Figure 18 (Blackwell and Steele, 1979). This curve is characteristic of a shallow aquifer flow when the aquifer temperature is much above background temperature. Thus, water flowing in the aquifer heats the rock above and below the aquifer, resulting in the characteristic shape shown. Chemical analyses of the water from this hole suggest that the water may in fact be a geothermal fluid with a much higher geothermal temperature implied than is observed. This hole is immediately west of the Hood River fault northeast of the volcano and within a few kilometers east of a Holocene basaltic lava flow. Another temperature

gradient hole drilled approximately 3 miles to the south (1S/10E-29ca), also along the Hood River fault, did not display the same temperature relationship. Thus, it appears that the low-temperature water (24°C) is probably related to the intrusion that resulted in the lava flow. These results are of sufficient interest that additional geologic-geophysical studies should be carried out to investigate the geothermal implications of the anomaly. The proximity to major energy comsumption centers in Hood River Valley and The Dalles is also a favorable feature of the anomaly.

Temperature-depth relationships were also obtained from fifty (50) "free" holes, mostly water wells, as part of the Mt. Hood study. These holes were logged during 1977-79. The data were submitted to David Blackwell for heat flow modeling studies. Several anomalous temperature gradients were obtained from water wells near Powell Buttes, northeast of Bend, along the eastern margin of the High Cascade Range. For example, gradients in excess of 100°C/km were measured in two holes (16S/14E-16aa and 15S/14E-36aa) which are about 10 km apart. A bottom hole temperature of 37.5°C at 166.5 m and 31.7°C at 157 m were measured for the holes, respectively. According to Blackwell and Steele (1979), heat flow values for these two holes are in excess of 3.0 HFU. Additional studies including geologic mapping, spring sampling and associated water analyses as well as other "free" temperature gradient determinations, if available, should be initiated in order to more fully investigate the geothermal implications of this apparently anomalous area. In all probability,

drilling of temperature gradient holes would be required.

Old Maid Flat No. 1/2

The drilling history of this exploratory hole was made available to DOE by Northwest Geothermal Corporation and repetition is not warranted. The geology of this hole is discussed in the report by Beeson and Moran (1979) as well as by Blackwell and Steele (1979). Geophysical logs, including dual induction, compensated density, temperature, drift, fracture, and acoustic velocity, are available from the above company and from DOGAMI (Open File Report 0-78-6). Copies of these logs were previously forwarded to DOE.

According to Beeson and Moran (1979), the Columbia River Basalt has been ostensibly penetrated in this hole. This formation, which was the primary exploratory target, underlies the Old Maid Flat site at a depth interval from 618 m (2022 ft) to 991 m (3250 ft). Temperature in this interval ranges from about 46.5 to 79.4°C (Figure 2). Bottom hole temperature is approximately 82°C at 1220.4 m (4003 ft). Rocks in the interval from 991 m to total depth consist of andesitic volcanics which may be the equivalent of the John Day or Eagle Creek formations of lower Miocene to upper Oligocene age. However, it is also possible that this interval may represent the lower part of the Columbia River Basalt Group.

For a discussion of intra-hole fluid movement, see Blackwell and Steele (1979). To date, Northwest Geothermal Corp. has not undertaken any fluid sampling for geochemical analyses.

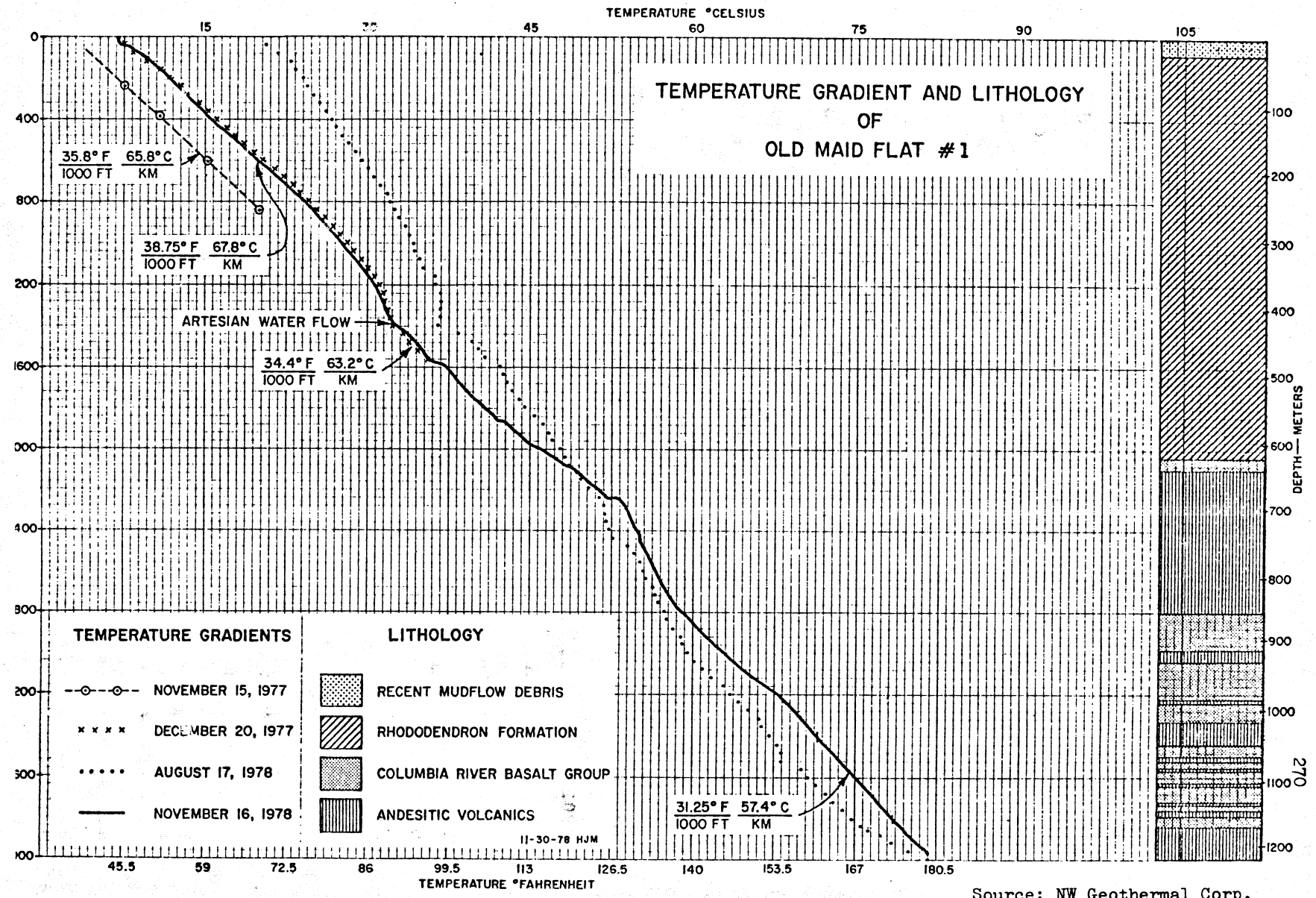

FIGURE 2

Source: NW Geothermal Corp.

Because of the heat flow implications (Blackwell and Steele, 1979) consideration should be given to the deepening of this hole to at least 1830 m (6000 ft). Northwest Geothermal Corp. should be encouraged to do the necessary fluid sampling as well as flow-testing either prior to or subsequent to the recommended deepening.

Timberline No. 2

The drilling history of this hole (3S/9E-7ab) was forwarded to DOE by others. The geology is discussed by White (1979) and the temperature-depth relationship is shown in Figure 21 (Blackwell and Steele, 1979). A subsequent temperature log of the hole by the USGS in late May 1979 indicates the temperature-depth relationship to be similar to that shown on the aforementioned figure.

This hole (target depth: 2000 ft) was originally drilled to 420.7 m (1380 ft) in depth and because of several re-drills due to either stuck drill pipe or twist-offs, the hole was completed at 226 m (741 ft). This hole represents the second attempt to drill at Timberline Lodge on Mt. Hood. The first, drilled in 1977, penetrated less than 100 ft of the planned 500-foot target depth.

One of the 2000 ft deep hydrologic holes to be drilled by the USGS this year (see above) is sited at Mt. Hood Meadows (3S/9E-3cc). This proposed hole is approximately the same distance from the center of the cone as is the Timberline hole and therefore should provide the data that would have been available if the Timberline hole had been drilled to the

target depth. Consideration should be given to drilling this hole to 3000 ft if conditions permit.

CONCLUSIONS

Notwithstanding the recommendation to deepen the Old Maid Flat hole, DOGAMI does not have sufficient data on hand to site a deep hole on or near Mt. Hood. Possibly when other data are made available from studies completed or in various stages of completion by the USGS and Lawrence Berkeley Laboratory that a firm recommendation can be made.

Provisions to carry out the several recommendations as indicated in the OVERVIEW should be engendered by DOE.

REFERENCES

Beeson, M. H., and Moran, M. R., 1979, Statigraphy and structure of the Columbia River Basalt Group in the Cascade Range, Oregon: PSU Grant No. 90-262-8126 from DOGAMI, unpublished report, 64 p.

Blackwell, D. D., and Steele, J. L., 1979, Heat flow modeling of the Mount Hood Volcano, Oregon: SMU Grant No. 86-09 from DOGAMI, unpublished report, 69 p.

White, G. M., 1979, Geology and geochemistry of Mt. Hood Volcano: OU Grant No. 50-262-8902 from DOGAMI, unpublished report, 54 p.